PREPARATION OF VACCINE FORMULATIONS FOR MELANOMA USING POTENT ADJUVANT CANDIDATE ASTRAGALOSIDE VII AND INVESTIGATION OF ANTI-TUMOR ACTIVITIES OF FORMULATIONS IN MOUSE CANCER MODELS

A Thesis Submitted to
the Graduate School of Engineering and Sciences of
İzmir Institute of Technology
in Partial Fulfillment of the Requirements for the Degree of

DOCTOR OF PHILOSOPHY

in Bioengineering

by
Nilgün YAKUBOĞULLARI ÖZEFE

July 2024
İZMİR

We approve the thesis of **Nilgün YAKUBOĞULLARI ÖZEFE**

Examining Committee Members:

Prof. Erdal BEDİR
Department of Bioengineering, İzmir Institute of Technology

Prof. Ayşe NALBANTSOY
Department of Bioengineering, Ege University

Prof. Güzide AKSU
Department of Internal Medicine, Ege University

Assoc. Prof. Ahu ARSLAN YILDIZ
Department of Bioengineering, İzmir Institute of Technology

Assist. Prof. Atakan EKİZ
Department of Molecular Biology and Genetics, İzmir Institute of Technology

24 July 2024

Prof. Erdal BEDİR
Supervisor
Department of Bioengineering
İzmir Institute of Technology

Assoc. Prof. Duygu SAĞ
Co-supervisor
Department of Medical Biology
Dokuz Eylül University

Assoc. Prof. Ceyda ÖKSEL KARAKUŞ
Head of the Department of Bioengineering

Prof. Mehtap EANES
Dean of Graduate School of
Engineering and Science

I would like to dedicate this dissertation to my dear grandmother, Remziye YAKUPOĞLU. Her proud spirit has accompanied me every step of this journey.

ACKNOWLEDGMENTS

I would like to express my sincere gratitude to my thesis committee and dissertation members Prof. Erdal Bedir, Prof. Ayşe Nalbantsoy, Prof. Güzide Aksu, Associate Prof. Ahu Arslan Yıldız and Assistant Prof. Atakan Ekiz for their guidance, comments and contributions to my thesis. I would like to thank my co-advisor Associate Prof. Duygu Sağ for her endless support and motivation.

I would like to express my gratitude to Prof. James Moon for giving me an opportunity to complete the final chapter of my thesis in the University of Michigan, USA. He opened his laboratory to me, shared his immense knowledge and provided constant support all the time. I would also like to thank Dr. Cheng Xu and Xingwu Zhou for their assistance and for sharing their experience with me.

I would like to express my very profound gratitude to my whole family. Thank you for your constant love, support, and courage. I am deeply grateful for everything you have done throughout my life.

I would like to express a special thanks to my husband Fatih Özefe. Your constant love, endless support and faith in my abilities have been my guiding light throughout the challenges that I met. I am grateful to you for the understanding you showed when I was overwhelmed, your determination to constantly motivate me, and for always standing by my side, no matter what. This accomplishment would not have been possible without you.

This thesis was financially supported by The Scientific and Technological Research Council of Türkiye (TUBITAK) (120S878) and Izmir Institute of Technology Research Fund (2020IYTE0098). I would like to thank TUBITAK 2214-A International Research Fellowship Programme for PhD Students (1059B142201226) for supporting me to complete the final chapter of my thesis in University of Michigan, USA. Thank you.

ABSTRACT

PREPARATION OF VACCINE FORMULATIONS FOR MELANOMA USING POTENT ADJUVANT CANDIDATE ASTRAGALOSIDE VII AND INVESTIGATION OF ANTI-TUMOR ACTIVITIES OF FORMULATIONS IN MOUSE CANCER MODELS

Cancer is a disease caused by the accumulation of point mutations in the genome and further progresses by structural alterations. One of the major categories in cancer immunotherapy is cancer vaccine, which activates body's immune system against cancer. As traditional therapies are not effective due to safety issues and non-proper immune system modulation, the application of nanomedicine-based approaches is a potential solution to address these problems. The formulations of immunostimulatory agents/adjuvants in a carrier material facilitate uptake by target cells, alter systemic exposure, provide a safer profile, and increase the therapeutic efficacy of immunotherapeutics. With this perspective, in the context of this thesis, a new adjuvant system (MA-NP) containing MonophosphoryllipidA/Astragaloside-VII in *Astragalus* polysaccharide-based nanocarrier was designed and developed. The *in vitro* and *in vivo* immunomodulatory properties and, subsequently, prophylactic and therapeutic efficacy of MA-NP in two murine melanoma models were investigated. Biocompatible, negatively charged, and 20-50 nm sized MA-NP with efficient uptake by dendritic cells was successfully prepared. MA-NP formulation including multi-peptides activated innate and adaptive immune cells, enhanced antigen-specific cytotoxic T lymphocytes primarily exhibiting central memory $CD8^+$ T cell response, induced functional IFN-γ^+CD8^+ T cells, increased intratumoral $CD4^+$, $CD8^+$ T cells and M1-like macrophages, dendritic cells, and potently inhibited tumor growth. Moreover, MA-NP eliminated established B16-F10 tumors when combined with anti-PD-1 treatment. These findings revealed a highly effective new saponin-based adjuvant system to be used in cancer vaccines and a promising combinatory therapy to improve cancer immunotherapy.

ÖZET

POTENT BİR ADJUVAN ADAYI OLAN ASTRAGALOZİT VII KULLANILARAK MELANOMAYA YÖNELİK AŞI FORMÜLASYONLARININ GELİŞTİRİLMESİ VE FORMÜLASYONLARIN ANTİ-TÜMÖR ETKİNLİKLERİNİN FARE KANSER MODELLERİNDE ARAŞTIRILMASI

Kanser, genomdaki nokta mutasyonların birikmesi sonucu ortaya çıkan ve yapısal değişikliklerle ilerleyen bir hastalıktır. Kanser immünoterapisinin ana kategorilerinden biri, vücudun kansere karşı kendi bağışıklık sistemini harekete geçiren kanser aşısıdır. Geleneksel tedaviler güvenlik sorunları ve bağışıklık sisteminin uygun olmayan modülasyonu nedenleriyle etkili olmadığından, nanotıp temelli yaklaşımların uygulanması bu sorunların çözümü için bir potansiyel oluşturmaktadır. Bir taşıyıcı malzeme içinde immünostimülatör ajanların/adjuvanların formülasyonları, hedef hücreler tarafından alımı sağlar, sistemik etkiyi değiştirir, güvenli bir profil sağlar ve immünoterapötiklerin terapötik etkinliğini arttırır. Bu bakış açısıyla bu tez kapsamında, *Astragalus* polisakkariti temelli bir nanotaşıyıcıya MPLA/Astragaloside-VII entegre edilerek yeni bir adjuvan sistemi (MA-NP) tasarlanmış ve geliştirilmiştir. MA-NP'nin *in vitro* ve *in vivo* immünomodülatör özellikleri ve ardından iki fare melanoma modelinde profilaktik ve terapötik etkinliği araştırılmıştır. Biyouyumlu, 20-50 nm boyutunda, negatif yüklü, dendritik hücreler tarafından etkin bir şekilde alınabilen MA-NP başarılı bir şekilde üretilmiştir. Çoklu peptitler ile formülize edilen MA-NP, doğal ve kazanılmış bağışıklık hücreleri aktive etmiş, öncelikli olarak merkezi bellek $CD8^+$ T hücre yanıtı gösteren antijen spesifik sitotoksik T hücre popülasyonunu arttırmış, fonksiyonel IFN-γ^+CD8^+ T hücrelerini indüklemiş, tümör içi $CD4^+$, $CD8^+$ T hücre, dendritik hücre ve M1 makrofajlarını arttırmış ve güçlü bir şekilde tümör büyümesini inhibe etmiştir. Ayrıca MA-NP ile oluşturulan nanoaşı, anti-PD1 antikorları ile birlikte farelere uygulandığında yerleşik B16-F10 tümörlerini ortadan kaldırmıştır. Bu bulgular, kanser aşılarında kullanılabilecek yeni bir saponin temelli adjuvan sistemini ve kanser immünoterapi yaklaşımını geliştirmek için umut verici bir kombine terapiyi ortaya koymaktadır.

TABLE OF CONTENTS

LIST OF FIGURES

Figure **Page**

Figure **Page**

Figure **Page**

Figure **Page**

LIST OF TABLES

Table **Page**

Table **Page**

ABBREVIATION

APC:	Antigen Presenting Cells
APS:	Astragalus Polysaccharide
AST-VII:	Astragaloside VII
BBD:	Box-Behnken Design
BMDCs:	Bone marrow derived dendritic cells
BSA:	Bovine Serum Albumin
BV:	Brilliant Violet
CTLs:	Cytotoxic T Lymphocytes
CXCL:	C-X-C Motif Chemokine Ligand
CXCR:	C-X-C Motif Chemokine Receptor
DAD:	Diode Array Detector
DAMPs:	Damage Associated Molecular Patterns
DCs:	Dendritic cells
DNS-Cl:	Dansyl cloride
DNA-MA-NP:	Dansyl integrated MPLA/AST-VII integrated nanoparticle
ELISA:	Enzyme-Linked Immunosorbent Assay
ELSD:	Evaporative Light Scattering Detector
FACS:	Fluorescence Activated Cell Sorting
FBS:	Fetal Bovine Serum
GM-CSF:	Granulocyte macrophage colony stimulating factor
HPLC:	High Performance Liquid Chromatography
IFN:	Interferon
IL:	Interleukin
LPS:	Lipopolysaccharide
MA-NP:	MPLA/AST-VII integrated nanoparticle
MHC:	Major Histocompatibility Complex
MPLA:	Monophosphoryl lipid A
MS:	Mass Spectroscopy
NK Cells:	Natural Killer Cells
NP:	Nanoparticle

OVA:	Ovalbumin
PADRE:	Pan DR T-helper epitope
PAMPs:	Pathogen Associated Molecular Patterns
PBS:	Phosphate Buffer Saline
PD-1:	Programmed Cell Death Protein 1
PRRs:	Pathogen Recognition Receptors
TCR:	T Cell Receptor
Th1:	T Helper 1 Cells
Th2:	T Helper 2 Cells
TLR:	Toll Like Receptor
TME:	Tumor microenvironment
Tregs:	T Regulatory Cells
Trp-2:	Tyrosinase-related protein 2

CHAPTER 1

INTRODUCTION

Cancer is a disease that comes forth from the accumulation of point mutations in the genome and further progresses by structural alterations.[1,2] In 2022, 20 million new cancer cases have arisen, and approximately 10 million cancer-related mortalities have been reported. According to a report released by the International Agency for Research on Cancer (IARC), over 35 million new cancer cases are projected in 2050.[3] To decrease global cancer burden and mortality rates, extraordinary efforts have been made to develop effective treatments.

Conventional cancer therapies, which are surgical interventions, radiotherapy, and chemotherapy, have several drawbacks such as toxicity, multidrug resistance, lack of specificity, and mainly harmful side effects.[4,5] Unlike conventional cancer therapies, immunotherapy is an encouraging treatment that modulates the immune system to fight against cancer cells. The concept of immunotherapy is not quite new. The idea of treating neoplastic disease using an immune system originated in the 19th century. First, Wilhelm Busch and Friedrich Fehleisen noticed the spontaneous tumor regression in people with a superficial skin infection, most caused by *Streptococcus pyogenes*. After this observation, William Coley hypothesized that this skin infection provided better results in patients with sarcoma. To prove that Coley treated patients with heat-inactivated *S. pyogenes* and *S. marcescens*, and obtained favorable responses in several cancers. However, using Coley's toxins for the treatment of cancer is overlooked with the discovery of radiotherapy and chemotherapy.[6,7]

In 20th century, Lewis Thomas and Sir Frank Macfarlane declared the "cancer immunosurveillance" hypothesis, describing immune system as able to recognize neoantigens and eradicate malignant cells to prevent carcinogenesis.[8] In addition to immunosurveillance, the tumors are capable of escaping immune recognition and elimination, promoting a more inclusive immunoediting hypothesis, which covers the host-protective and tumor-progressive functions of immune system. The three characteristic phases of cancer immunoediting are elimination, equilibrium, and escape

(Figure 1.1). In detail, the elimination phase demonstrates the concept of cancer immunosurveillance. The immune system and tumor coexist in the equilibrium phase, and cancer cells undergo alterations to overcome tumor-suppressive immune control. In the escape phase, cancer cells have surpassed immunological barriers in the equilibration phase by causing defects in antigen presentation machinery, upregulating negative regulatory pathways, and recruiting an immunosuppressive cell population.[1,9,10]

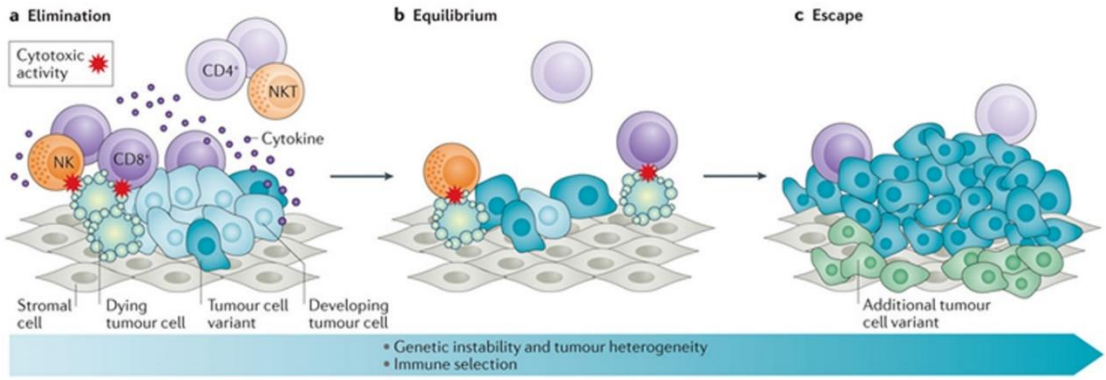

Figure 1.1. The three phases of cancer immunoediting.[9]

The clinical success stories related immunotherapy have shown that therapy induced immunity can control many escaped tumors.[11] Therefore, the number of patients using immunotherapy as their first choice for cancer treatments is increasing over time. Moreover, new combination therapies and druggable targets will take immunotherapy a step forward in cancer treatment.

1.1. The Major Categories of Cancer Immunotherapy

The cancer immunotherapy can be categorized as immune checkpoint inhibitors, adoptive cell therapy, oncolytic virus therapy and cancer vaccines according to emerging targets and approaches.

1.1.1. Immune Checkpoint Therapy

Immune checkpoints are evolutionarily conserved negative regulators of T cell activation and have a role in the co-inhibitory signaling pathways to regulate hyperactivation. The most used immune checkpoint inhibitors (ICIs) are cytotoxic T lymphocyte-associated molecule 4 (CTLA4), programmed cell death receptor 1 (PD1), and programmed cell death ligand 1 (PDL1). ICIs are designed to interrupt the co-inhibitory signaling pathway and support the eradication of malignant cells by immune cells.[1,8,12]

For the first time, James Allison et al. revealed that anti-CTLA4 antibodies provided anti-tumoral activity in mice with colon carcinoma and fibrosarcoma; even the mice were rechallenged with cancer cells, demonstrating the induction of long-term immunological memory. While CTLA4 monotherapy was shown efficacy in brain, ovarian, bladder, colon, and prostate cancers, it was not efficacious in SM1 mammary carcinoma and B16 melanoma. Although monoclonal antibody (mAb) targeting CTLA4 did not provide favorable responses in preclinical studies, FDA approved the first human IgG1κ anti-CTLA4 mAb, Ipilimumab, to be used in non-resectable stage III/IV melanoma in 2011. In clinical trials, Ipilimumab induced potent tumor necrosis with a 3.6-month increase in short-term survival.[8,13]

In parallel, PD1 was discovered as the mediator of apoptosis, but it was later understood its role in the negative regulation of immune responses. Contrary to CTLA4, demonstrating its regulatory effect on lymphoid tissue, PD1 reduces T cell activation in peripheral tissue. Moreover, PDL1, the ligand of PD1, is expressed in normal tissue and suppresses TCR-mediated lymphocyte proliferation when it binds to PD1. Tumor cells abnormally express PDL1 to enhance T cell exhaustion and facilitate tumor growth and invasion.[1,14]

The preclinical studies targeting PD1/PDL1 showed that the blocking PD1/PDL1 axis provided tumor cytolysis and limited metastasis. Following preclinical and clinical success, the humanized (pembrolizumab) and fully human (nivolumab) IgG4 anti-PD1 mAbs were approved by FDA to be used in refractory and unresectable melanoma in 2014. Further, in 2016, the first humanized IgG4 anti-PDL1 mAb (atezolizumab) was approved for the treatment of urothelial carcinoma.[15–17] Remarkable successes achieved

by mAbs targeting checkpoint inhibitors led to an immense investigation into discovering new mAbs and evaluating their efficacy in different cancer models. Despite their efficacy, checkpoint blockage therapy caused autoimmune reactions with loss of naive T cells and accumulation of overactive memory T cells, leading to invasion in peripheral organs and inflammatory damage.[8,18–20]

1.1.2. Adoptive T Cell Transfer Therapy

Adoptive T cell (ATC) therapy utilizes autologous or allogeneic T cells, which are isolated or genetically engineered, expanded ex vivo and infused into patients with cancer. For the first time, tumor-infiltrating lymphocytes were used in the treatment of metastatic melanoma. Lymphocytes isolated from cancer biopsy were expanded with IL-2, injected into the same patient, and showed therapeutic potency.[21] This study enlightened the use of genetically engineered T cells to target neoantigens by adoptive transfer therapy. T cell receptor (TCR) engineered lymphocytes limitedly respond to tumor antigens presented by MHC molecules rather than surface antigens on the tumor. To overcome MHC restrictions, chimeric antigen receptor (CAR) T cells are engineered. CAR T cells have antigen binding domains linked with signaling domains of TCR and different costimulatory molecules, providing direct cytotoxicity to target antigens on the surface of malignant cells.[22]

Besides efficacious therapeutic effects, the patients treated with ATC experienced cytokine release syndrome, having flu-like symptoms with life-threatening ones such as hypotension, high fever, coagulopathy, capillary leakage, and multisystem organ failure. Neurotoxicities are also observed following ATC treatment, including CAR T cell-related encephalopathy syndrome, mainly characterized by delirium and confusion. The patient-specific ATC design is necessary due to its side effects, but this approach has resulted in expensive and limited treatment along with challenging manufacturing processes.[23] Moreover, patients access limited certified laboratories to generate CAR-T cells, which are variable due to the lack of standard practices.

1.1.3. Oncolytic Virus Therapy

Traditional immunotherapy approaches to cancer treatment by enhancing immune response similar to those performed in bacterial or viral infections. Oncolytic viruses are one of the major categories in cancer immunotherapy, and they use the ability of replication-competent viruses to infect and lyse cancer cells. With this perspective, oncolytic herpes simplex virus type 1 (HSV1) is engineered to replicate in cancer cells and promote an anti-tumor immune response. The efficacy of the engineered virus known as Talimogene laherparepvec (T-VEC) was investigated in randomized clinical trials, and the results showed that T-VEC provided primary and point of durable response in patients having accessible and unresectable melanoma.[24] In 2015, T-VEC was approved by FDA for use in the treatment of recurrent melanoma after initial surgery. Following impressive clinical benefits obtained from melanoma, T-VEC has been investigated as a combination therapy in melanoma and a monotherapy in patients suffering from other cancer types. In addition to T-VEC, FDA approved a non-oncolytic adenovirus encoding IFNα-2b for treating Bacillus Calmette-Guering (BCG) unresponsive, non-muscle invasive bladder cancer in 2022.[25] Despite the potential of oncolytic virus therapy, the challenges including physical barriers in solid tumors, anti-viral immunity, immunosuppressive tumor microenvironment preventing virus delivery, and oncolysis should be tackled to improve the therapeutic benefits of oncolytic viruses.[26]

1.1.4. Cancer Vaccines

Cancer vaccines protect the body from cancer by inducing an effective immune response. The key time points in the development of cancer vaccines are given in Figure 1.2. This concept was first emphasized by William Coley with his observation about toxin-induced tumor regression. After a long period of time, Bacillus Calmette-Guérin vaccines were produced with an attenuated form of *Mycobacterium bovis* and treated the patients with bladder cancer.[8] In 1984, Hoover et al. used autologous tumor cells to investigate whether these cells would enhance the survival of patients suffering from

colorectal cancers. To do that, primary tumors resected from patients were enzymatically dissociated and injected into colorectal cancer patients. The encouraging results from the pilot trial led to scientists focusing on the tumor cells and their antigens.[27] In 1991, the first human tumor antigen, melanoma-associated antigen 1 (MAGE-1), was identified and brought a new perspective on using tumor antigens in cancer vaccines.[28] With this approach, Melacine was the first tumor lysate vaccine against melanoma, approved by the Canadian Health Protection Brand in 1999. This vaccine consists of whole tumor lysate and detoxified bacterial endotoxin adjuvant. Following treatment of melanoma patients with Melacine did not show significant survival of patients, but improved the life quality of patients compared to chemotherapy.[29]

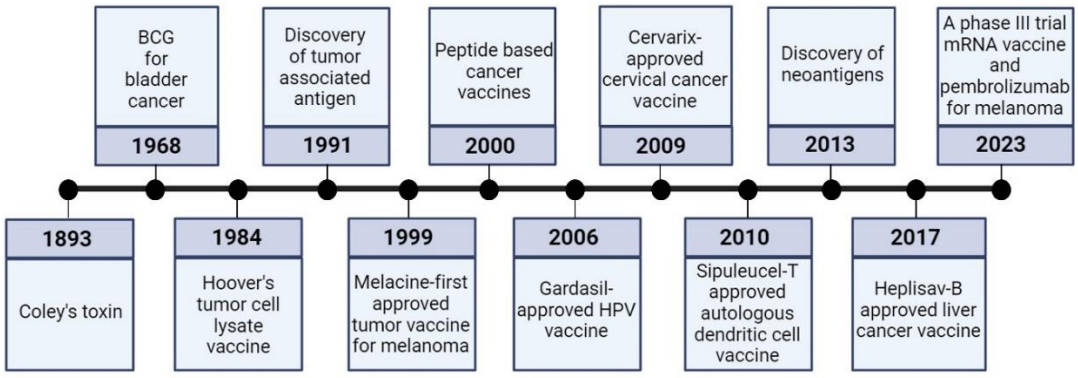

Figure 1.2.The key time points for cancer vaccine development.

After promising results from tumor cell lysate vaccines, peptide-based vaccines, which contain specific epitopes from antigens, emerged to promote immune response specifically to tumor antigens. Tumor antigens are categorized into tumor-associated antigens (TAA) and tumor-specific antigens (TSA). While TAA is an autoantigen expressed in normal tissues and overexpressed in cancer tissues, TSA is only expressed in cancer tissues by numerous somatic mutations. MAGE-1 is normally expressed in testis and melanoma, whereas human papillomavirus (HPV)-associated cervical and oropharyngeal cancers have high expression of E6 and E7 proteins.[4] These antigens could be used prophylactically to prevent tumor formation or therapeutically to eradicate tumors. Prophylactic cancer vaccines developed for HPV-induced cervical cancer

(Gardasil and Cervarix) and recently hepatitis B-caused liver cancer (Heplisav-B) represent significant milestones in the cancer vaccine development. The safety and immunogenicity profiles and long-term protections against HPV infections in women make these prophylactic vaccines outstanding.[30] The first approved autologous dendritic cell vaccine, sipuleucel-T, targets highly expressed TAA in prostate cancer cells. This therapeutic vaccine prolonged the survival of patients suffering from metastatic-resistant prostate cancer.[31]

Preclinical and clinical studies focusing on shared tumor antigens revealed some drawbacks due to tumor heterogeneity, poor immunogenicity, and immune tolerance. Moreover, cytotoxic T cell-mediated cellular immune response might be induced by cancer vaccines to eliminate malignant cells, whereas traditional antigens generally provide a humoral immune response. Therefore, further studies are carried out to discover efficacious tumor antigens. Neoantigens are not expressed in normal tissues and derived from non-synonymous cell mutations in tumor cells. Neoantigen vaccines are promising for stimulating cytotoxic T cells to promote effective anti-tumor immune response. The first mRNA-based neoantigen vaccine was injected into melanoma patients and effectively inhibited melanoma recurrence.[32] In recent years, the breakthrough therapy reported that personalized mRNA cancer vaccine combined with pembrolizumab decreased 44% of melanoma recurrence or death and did not increase the risk of side effects. Lastly, FDA granted accelerated approval of lifileucel, a tumor-derived autologous T cell immunotherapy, for unresectable or metastatic melanoma patients previously treated with anti-PD1.[4] These inspiring results are directed to combine different immunotherapies against cancer. Designing an optimal delivery platform, selecting optimal combinational therapy, avoiding immune escape, and inducing strong T cell response are still challenging and might need to be addressed.

1.2. Cancer Vaccine Adjuvants and Delivery Platforms

Rational vaccine design is challenging due to providing a potent immune response while meeting safety standards, leading researchers to develop subunit/peptide-based vaccines. Besides their safer profile, these vaccines are poorly immunogenic and need an

adjuvant. Adjuvants are chemical/biological compounds that enhance or augment a specific immune response to a particular antigen. With the help of vaccine adjuvants, cancer vaccines can be processed and presented in antigen-presenting cells (APCs), and tumor-antigen-specific T cells can recognize and kill cancer cells. Although the aluminum adjuvant was the first adjuvant approved by the FDA in 1939, only a few adjuvants have been accepted for use in human vaccines (Table 1.1).[33]

Table 1.1. The vaccine adjuvants approved by FDA.[33,34]

Adjuvant	Ingredient	Vaccines
Aluminum	Aluminum hydroxide, potassium aluminum sulfate	Anthrax, HPV (Gardasil 9), HepB (Engerix-B)
MF59	Squalene-based oil in water emulsion	Influenza (Fluad)
$AS01_B$	Monophosphoryllipid A (MPLA), QS-21	Zoster vaccine (Shingrix)
AS04	MPLA, aluminum salt	HPV (Cervarix)
CpG 1018	Cytosine phosphoguanine	Hep-B (Hepsilav-B)
Matrix-M	Saponin	COVID-19 vaccine (Novavax)
LNP	DSPC, cholesterol, PEG2000-DMA, ALC-0159, ALC-0315	COVID-19 vaccine (BioNTech/Pfizer)
LNP	DSPC, cholesterol, PEG2000-DMG, SM-102	COVID-19 vaccine (Moderna)

In cancer vaccines, adjuvants can be formulated with tumor antigens to deliver antigens, inducing strong and durable innate and adaptive immune responses. Earlier studies with traditional adjuvants did not provide an effective anti-tumor immune response against tumor antigens. Therefore, a number of new classes of adjuvants/ adjuvant systems have been designed and developed for cancer vaccines to deliver tumor antigens to APCs, increasing low immunogenicity of tumor antigens, breaking T cell tolerance, providing strong cytotoxic T cell and memory responses. Recently, molecular

pathogen recognition receptor (PRR) agonists, self-adjuvanting polymers, and lipid materials have been developed, evaluated in several cancer models and demonstrated superior therapeutic performance (Table 1.2). The ultimate objective of all self-assembled nanoparticulate-based cancer nanovaccines is to prime antigen-specific T cells, which are essential for an effective immune response against cancer.[4] Following injection of cancer nanovaccines into the body, these vaccines could passively traffic to lymph nodes or internalize by tissue-resident dendritic cells (DCs), resulting in activation and draining of DCs to the lymph nodes. Activated DCs upregulate co-stimulatory molecules (CD4, CD86, CD80) and present tumor antigens on MHC II molecules. In the lymph node, maturated DCs present tumor antigen to naive T cells and furtherly provide antigen-specific T cell activation. Activated T cells infiltrated into tumor tissue to eliminate cancer cells (Figure 1.3).

Table 1.2. PRR agonists formulated adjuvant systems for cancer immunotherapy. TLRs: Toll-like receptors, CDs: Cyclic dinucleotides, NLRs: Nod-like receptors.[33]

PRRs	Subsets	Agonists	Adjuvant Design	Cancer Model	References
TLRs	TLR3	dsRNA	DNA nanodevice	Melanoma Colorectal cancer	33
	TLR4	MPLA	Formulated nanodiscs with CpG	Melanoma Cervical cancer Colorectal cancer	35
	TLR7	1V209	Liposome	Breast cancer, Pancreatic ductal cancer	36
	TLR7/8	Resiquimod (R848)	Liposome Polymeric nanosuspension	Melanoma Colorectal cancer	37
CDs		cGAMP	Polymersomes	Melanoma	38
		cGAMP	PLGA NPs	Melanoma Pancreatic cancer	39
		ADU-S100 (CDA)	Mn^{2+}self-assembled lipid polymers	Melanoma Colorectal cancer	40
		ADU-S100 (CDA)	PEGlylated lipid and nanodiscs	Colorectal cancer Breast cancer Cervical cancer	41
NLRs	NOD2	Mifamurtide	Liposomal Vector	Melanoma	42

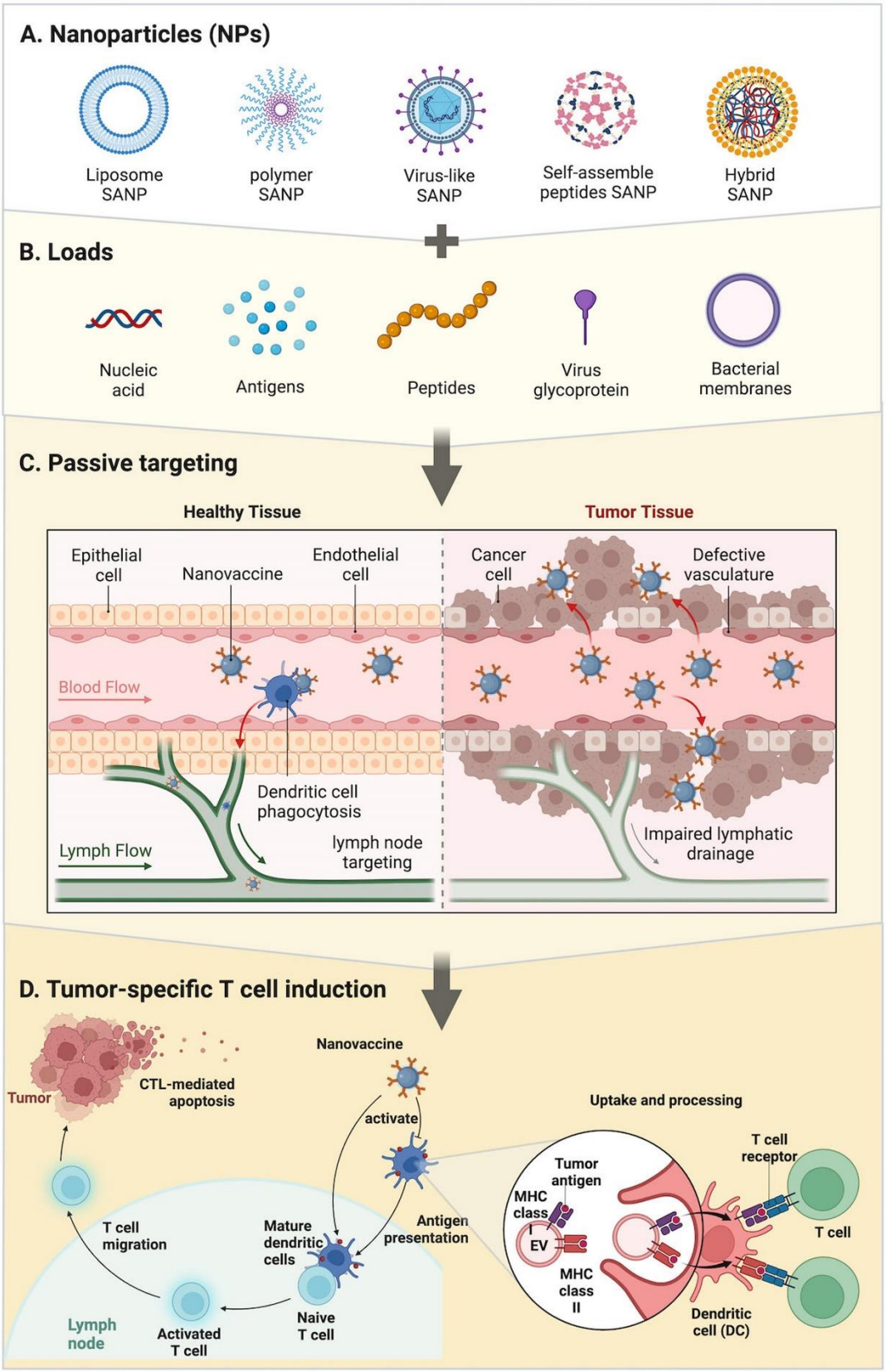

Figure 1.3. The preparation of nanoparticulated cancer nanovaccines and their mechanism of action in the body.[43]

1.3. Melanoma and Current Vaccine Development

Melanoma is a type of skin cancer originating in melanocytes, the cells responsible for pigment production in the body. The main cause of this cancer is exposure to ultraviolet light.[44] Skin cancer was the most diagnosed cancer group in 2020, where 325000 new malignant melanoma cases were estimated, and 57000 people died because of the disease. The number of newly diagnosed melanoma cases is projected to be 510000 in 2040.[45] The primary treatment for melanoma is surgical resection. On the other hand, chemotherapy is favorable for advanced melanoma, but overall survival has not improved. Melanoma is one of the cancers that respond reasonably to immune modulations. Several factors have been found for its sensitivity to immune system activation, including high tumor mutational load because of UV exposure, expression of cancer-testis antigens, and mimicking melanocyte lineage proteins with pathogen-associated antigens. Therefore, immunotherapeutic approaches have been widely recognized as effective treatments for melanoma. The approval of T-VEC and ICIs represents significant milestones for the development of new immunotherapeutics and combination therapies for melanoma.[46,47]

Extensive research efforts are underway to develop nanoparticulate cancer vaccines, highlighting a significant trend toward using nanotechnology to enhance cancer immunotherapy. In addition to TLR 2-5, 7, and 9 agonists, which are widely used in melanoma nanovaccines, ISCOMATRIX prepared with *Quillaja saponins*, QS-21, and adjuvants system developed with QS-21 and TLR agonists have been investigated for their anti-tumor potency in cancer vaccines. Silva et al. developed a saponin/MPLA nanoparticulate adjuvant system and investigated its immunomodulatory activities compared to ISCOMs and AS01.[48] This new adjuvant system provided a pro-inflammatory immune response by stimulating germinal center B cells and Tfh (Figure 1.4A). Sun et al. designed an adjuvant system by using STING (stimulator of interferon genes) agonist cyclic dinucleotide (CDN) and manganese (Mn^{2+}) ion, having the ability of metal ions could modulate immune response. In this study, the presence of Mn^{2+} ions enhanced the effects of STING agonist by 77-fold and provided a strong anti-tumor response (Figure 1.4B).[40] Park et al. aimed to prepare personalized vaccines by producing PEI-PEG based nanoparticular platform and integrating CpG and neoantigens. Following

injection with STING agonist into B16F10 mice, the developed nanovaccine provided CD8 T cell infiltration into the tumor microenvironment, eliminating tumor tissue and providing long-term memory response (Figure 1.4C).[49] Lynn et al. established a vaccine platform (SNP-7/8a) with charge-modified peptide-TLR-7/8a conjugates, which is self-assembled to 20 nm nanoparticles. These NPs were substantially taken by dendritic cells in lymph nodes, further promoted T cell immunity, and significantly decreased tumor growth in B16-F10 murine tumor model (Figure 1.4D).[37]

One of the other approaches in cancer vaccine development is the built-in adjuvant concept, which includes the self-assembly of peptide antigens corresponding to CD8 or CD4 T cell epitopes and adjuvants. In this perspective, Kakwere et al. produced 20 nm in sized, amphiphilic hyperbranched polymer-peptide bioconjugate based on Clec9a (for targeting dendritic cells), gp100 (melanoma antigen), Trp-2 (melanoma antigen) and PADRE (universal CD4 T cell epitope). The anti-tumor efficacy of nanovaccines was evaluated in B16-OVA tumor model, and the results showed that bioconjugate vaccines provided T cell infiltration into the tumor microenvironment in addition to increasing survival ratio of mice compared to unvaccinated counterparts (Figure 1.4E).[50] Recently, mRNA vaccines have become very popular due to the success of the COVID-19 pandemic. Ben-Akiva et al. engineered a polymeric NP platform containing poly(beta-amino ester) (PBAE) and CpG or poly I: C adjuvants to facilitate efficient mRNA delivery into DCs and investigate its potency as cancer vaccines. In B16-F10 model, mRNA encoding Trp2 and gp100 antigens were administrated into mice. The mice treated with this vaccine platform and anti-PD1 showed a decrease in tumor burden and increased median survival time (Figure 1.4F).[51] Overall, nanoparticulated peptide vaccines have shown promising results for use in clinical studies due to robust anti-tumor and immunomodulatory activities.

In the clinic, numerous completed or ongoing cancer vaccine trials for melanoma have been conducted, as outlined in Table 1.3. The clinical trials related to neoantigen encoding mRNA integrated with lipid nanoparticles and autologous DC vaccines have been continued. Moreover, peptide vaccines adjuvanted with TLR3 agonist (poly-ICLC) and Montanide, ISA-51 are also one of the ongoing trials. Allogenic tumor cell or lysate vaccines were investigated with BCG and Detox adjuvants when completed vaccine trials were evaluated. In peptide-based vaccines, tyrosinase, gp100, MART-1, MAGE-A3, and ganglioside (GM2) antigens were widely used with Montanide, ISA-51, QS-21 and QS-21 containing adjuvant system (AS15) (Table 1.3).[52]

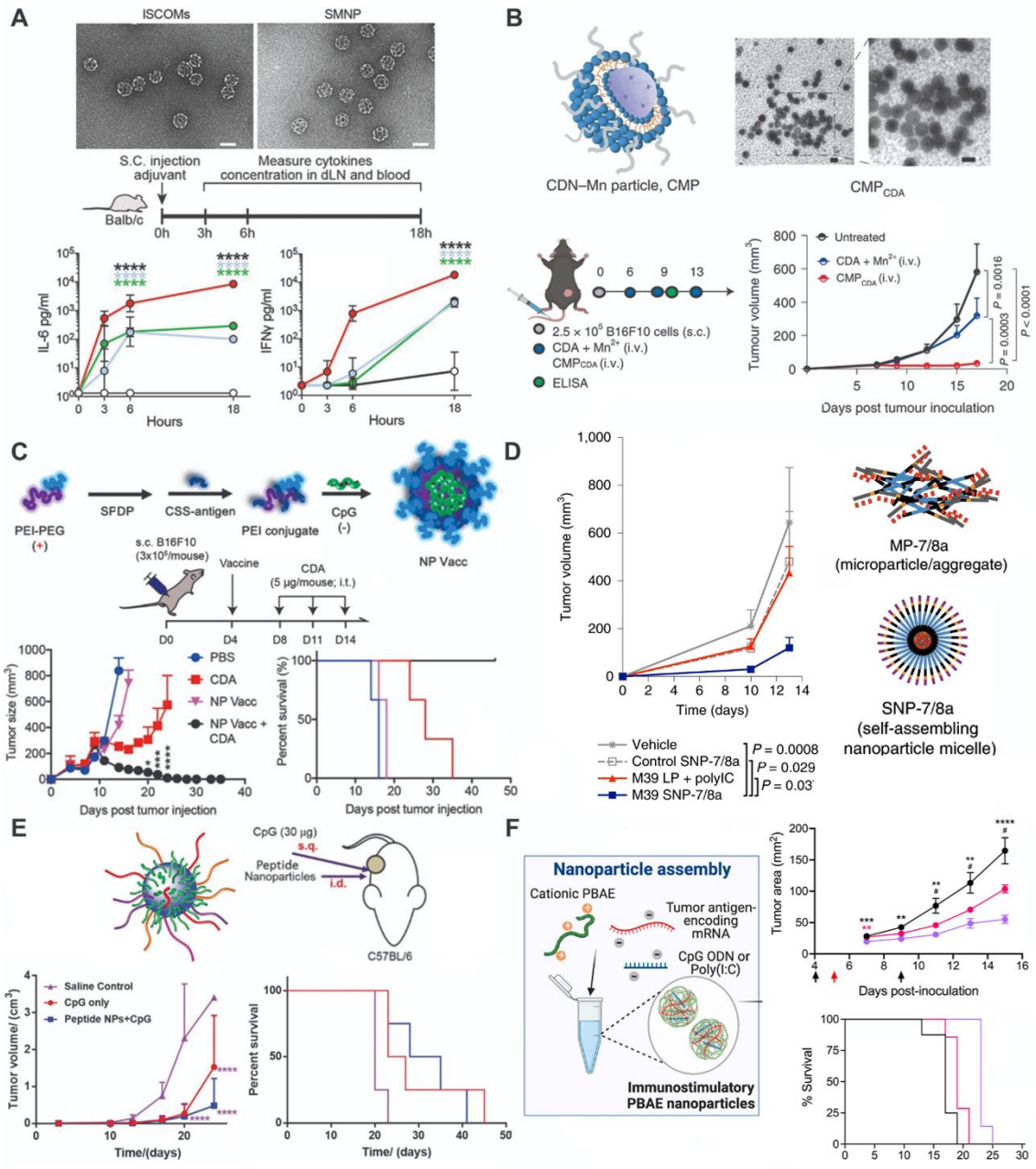

Figure 1.4. Developing cancer vaccine adjuvant platforms and evaluating their efficacy *in vivo* tumor models. (A) Saponin/TLR4 agonist adjuvant systems,[48] (B) immunotherapeutic potency of STING agonist and manganese nanoparticles,[40] (C) nanoparticulate vaccines with TLR9 agonist and STING agonists,[49] (D) a vaccine platform with charge-modified peptide-TLR7/8a conjugates,[37] (E) multi-peptide self-assembly nanovaccines and investigating anti-tumor activities with CpG adjuvant,[50] (F) lipophilic polymeric mRNA nanoparticles with CpG or poly (I:C).[51]

Table 1.3. Completed and ongoing cancer vaccine trials for melanoma.[4,52]

Vaccine/ Clinical trial	Vaccine Type	Target Antigen	Adjuvant	Status
NCT05933577	mRNA	Neoantigen mRNA	LNP	Ongoing
NCT03815058	mRNA	Neoantigen mRNA	LNP	Ongoing
NCT02410733	mRNA	NY-ESO-1, MAGE-A3, TPTE	LNP	Ongoing
NCT01302496	mRNA	MAGE-A3, MAGE-C2, tyrosinase, gp100	Autologous DC CD70, CD40 ligands, TLR4 agonist	Ongoing
NCT02897765	Peptide	Neoantigen	Poly-ICLC	Ongoing
NCT01846143	Peptide	pIRRS2, BRCA3	Montanide, IFA, ISA-51, Poly-ICLC	Ongoing
Peptide Vaccine	Peptide	Tyrosinase, gp100, MART-1	Montanide, ISA-51, GM-CSF	Completed
MDX-1379	Peptide	gp100	Montanide, ISA-51	Completed
Gp100:209-217 (210M)	Peptide	gp100	IL-2	Completed
GSK 1572932A	Peptide	MAGE-A3	AS15	Completed
GM2-KLH	Ganglioside	Ganglioside, GM2	QS-21, KLH	Completed
CancerVax (CANVAXIN)	Allogenic tumor cells	-	BCG	Completed
Melanoma Vaccine	Allogenic tumor cell	-	BCG	Completed
Melanicine	Allogenic tumor lysate	-	Detox	Completed

The vaccine formulations containing GM2-KLH (ganglioside-keyhole limpet hemocyanin), GD2-KLH (GD2 lactone), GD3-KLH (GD3-lactone) antigens, and QS-21 provided antibody response with flu-like side effects in phase I and II trials. Moreover, GM2-KLH and QS-21 vaccines also demonstrated antibody response in melanoma patients in phase III trials.

QS-21 is a natural product and the golden standard for saponin-based adjuvants. Saponins are plant- or marine-derived natural products and demonstrate several pharmacological properties. While the adjuvant activity of saponins has been extensively investigated, the primary focus for saponin-based adjuvants has been established with the triterpenoid glycosides extracted from the bark of *Quillaja saponaria*. One of the isolated compounds, QS-21, demonstrates effective antigen-specific antibody and $CD8^+$ T cell responses along with Th1-mediated cytokine productions. The mechanism of action studies revealed that QS-21 intercalates with cell membrane cholesterol, resulting in pore formation, enhancing cross-presentation of antigen, and inducing inflammasome activation.[53,54] Then, GSK developed adjuvant systems (AS0X) by combining traditional adjuvants with TLR agonists and QS-21. AS04 contains alum and MPLA and is approved for the vaccine against HPV (Cervarix). AS01, a liposomal formulation containing MPLA and QS-21, has been approved for malaria (Mosquirix) and shingles (Shingrix).[55] On the other hand, AS02 formulation was produced with MPLA and QS-21, but squalene-based oil-in-water emulsion was chosen as a delivery system.[56]

The strong immunomodulatory properties of AS01 and AS02 encouraged researchers to investigate their efficacy against cancer. AS02 adjuvant system combined with MAGE-A3 and applied to melanoma patients. This vaccine-induced humoral immunity, but no apparent clinical benefit was achieved. In a randomized phase II trial, AS15 adjuvant system, the form of AS01 combined with CpG, was formulated with MAGE-A3 and demonstrated robust humoral and CD4 T cell response and prolonged survival and clinical benefits. Unfortunately, the patients treated with this vaccine formulation did not show clinical benefit in follow-up trials.[57] Moreover, another nanoparticulate saponin adjuvant ISCOMATRIX formulated with NY-ESO-1 antigen and phase II trial for III-stage melanoma patients was conducted by Ludwig Institute.[58] The drawbacks of using QS-21 in adjuvant systems, including scarcity, heterogenicity, hydrolytic instability, and dose-limiting toxicity, have been limited its clinical advancement[55] and led to the researcher to find new potent and less toxic adjuvants and new formulations for cancer vaccines.

1.4. Astragaloside VII and its Potential as a Vaccine Adjuvant

Astragalus saponins have been extensively used in Chinese Traditional Medicine for their pharmacological properties, including immunomodulatory, anti-oxidant, anti-tumor, and anti-viral. While researchers have primarily focused on the anti-tumor activities of *Astragalus* saponins, there have been few studies reporting their potency as a vaccine adjuvant.[59] One compound in *Astragalus* saponins, Astragaloside VII (AST-VII), has gained attention due to its strong ability to induce IL-2 production in human whole blood.[60] As shown in Figure 1.5A, AST-VII is a cycloartane-type triterpenoid glycoside isolated from *Astragalus trojanus*. Preliminary *in vivo* studies have been conducted to reveal its potential as a vaccine adjuvant. Firstly, AST-VII was administrated into mice in combination with bovine serum albumin (BSA). AST-VII (120 μg) induced the production of BSA-specific antibodies comparable to Freund's adjuvant and remarkable IFN-γ production (Figure 1.5B).[61] When AST-VII was administrated with lipopolysaccharide (LPS), it enhanced the stimulation index in concanavalin A- (con A) and LPS-treated splenocytes and the production of IFN-γ, IL-2, and TGF-β. Moreover, the expression of activation markers (CD69, CD25) were investigated by immunohistochemistry and the results showed that AST-VII was able to upregulate these markers at lymph nodes (Figure 1.5C).[62]

Early *in vivo* studies demonstrated that AST-VII has the potential to be used as a vaccine adjuvant and further studies were conducted using viral antigens in vaccine formulations. Firstly, the adjuvant nanocarrier system (ANS) was developed by using AST-VII and *Astragalus* polysaccharide (APS), which is the root partner of AST-VII in the plant. AST-VII and ANS were formulated with seasonal influenza antigen (H3N2) and subcutaneously injected into mice. In this study, ANS substantially enhanced the stimulation index in splenocytes and increased H3N2-specific IgG and IgG1 responses along with AST-VII (Figure 1.5D).[63] In another study, AST-VII was formulated with TLR4 agonist and squalene-based oil in water (o/w) emulsion (ASE), and their efficacy was investigated in the Newcastle disease vaccine (NDV). AST-VII and ASE significantly increased HI titers and splenocyte proliferation, where only AST-VII was able to augment NDV-specific IgG, IgG1, and IgG2b titers (Figure 1.5E).[64]

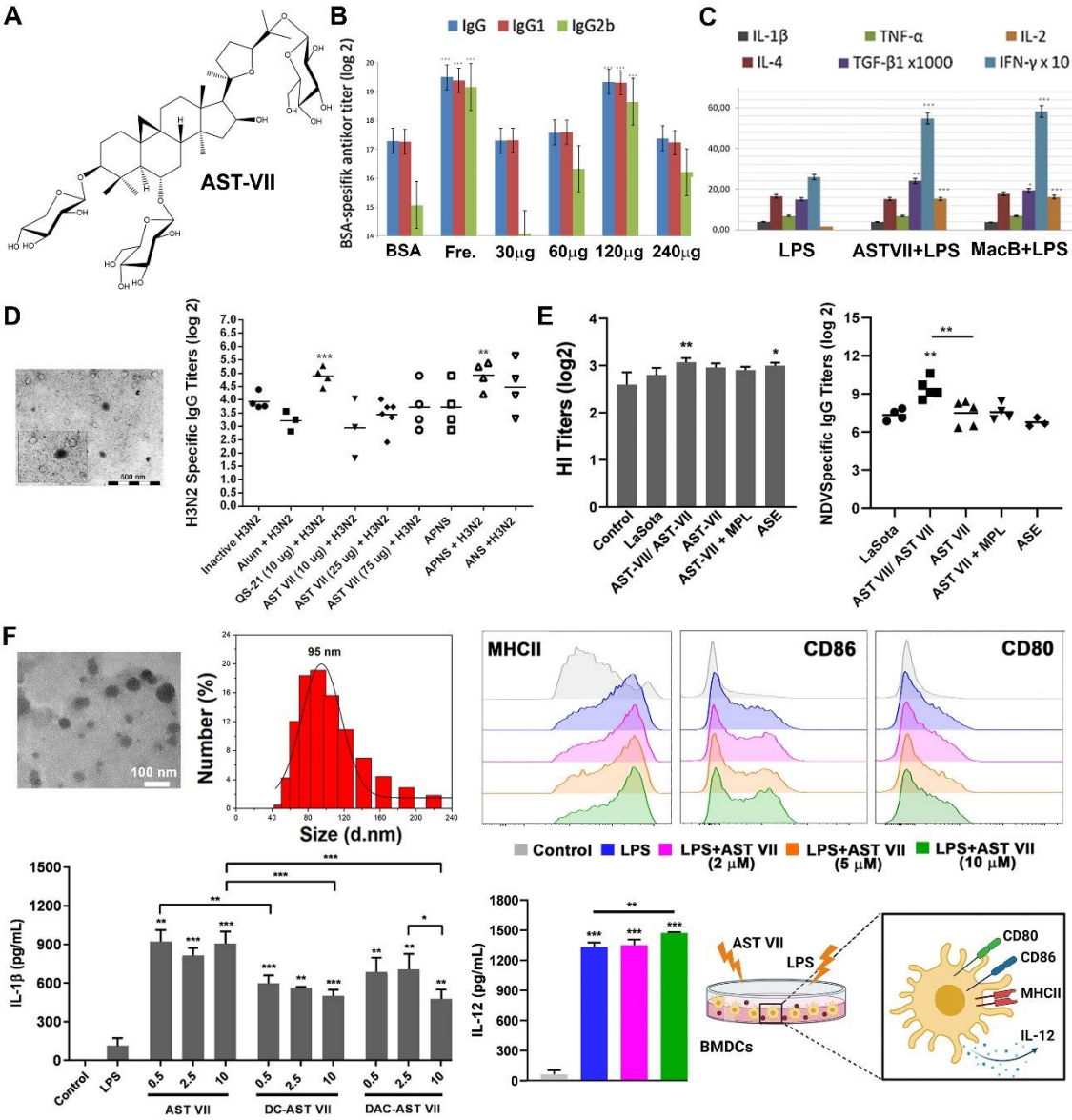

Figure 1.5. AST-VII and its potential as a vaccine adjuvant. (A) The chemical structure of AST-VII, (B) the effect of AST-VII on BSA-specific antibody production and IFN-γ/IL-4 secretion,[61] (C) the effects of AST-VII combination with LPS on splenocyte proliferation (SP), cytokine productions and activation status of immune cells by immunohistochemistry,[62] (D) development of adjuvant nanocarrier system for seasonal influenza vaccine and evaluation its efficacy in terms of SP and neutralizing antibody productions,[63] (E) development of new adjuvant systems combining TLR4 agonist and squalene o/w emulsion and investigation their adjuvant potential for Newcastle disease virus by SP and neutralizing antibody production,[64] (F) the mechanism of action studies of AST-VII and the characterization of self-assembling AST-VII molecules.[65]

Following the demonstration of AST-VII's efficacy as a vaccine adjuvant, an attempt was made to reveal its mechanism of action in dendritic cells. As saponins are amphiphilic compounds due to the presence of a water-soluble sugar chain and lipid-soluble aglycone,[66] they tend to form micelles or aggregates in aqueous solutions. Thus, firstly, the self-assembling ability of AST-VII was investigated. The results showed that AST-VII formed self-assembled structures in an aqueous solution above its critical micelle concentration (3.37 mM), and its immunomodulatory activity depended on its micelle formation concentration. When AST-VII was administrated alone to dendritic cells, there was no alteration in the activation status of cells. However, co-treatment with AST-VII and LPS resulted in a remarkable increase in the production of IL-1β and IL-12 and the upregulation of MHCII, CD86, and CD80 expressions on the surface of dendritic cells (Figure 1.5F).[65] These findings represent a substantial contribution to enhancing the applicability of AST-VII as a vaccine adjuvant.

Besides inducing cellular and humoral immune responses, a crucial aspect of adjuvant development is the accessibility and ease of production of the adjuvant itself. Many saponin-based adjuvants encounter challenges, including the low isolation yield from the plant material, inadequate purity, and inconsistent composition.[67] In contrast, AST-VII can be isolated with high purity and high yield, is stable, soluble in water, and demonstrates mild hemolytic activity at higher concentrations. These attributes position AST-VII as a favorable alternative to other saponin-based adjuvants.

1.5. Aims and Objectives of Thesis

The immune system modulation represents a critical therapeutic approach, particularly in the longstanding pursuit of vaccine development. In recent years, immunotherapy has emerged as a favorable treatment for many cancers. Thus, extensive preclinical and clinical studies have been conducted to develop new immunotherapies that effectively direct the immune system to the right place and time without inducing unacceptable toxicity. One of the approaches is engineering the delivery of immunotherapeutics by using nanomedicine. Formulation of immunotherapeutics in nanoparticles prepared by lipids or polymers prevents systemic exposure, promotes

accumulation in target tissues (tumors or draining lymph nodes), enhances uptake in innate immune cells, and activates cells to elicit desired immune response.[68,69] With this perspective, this thesis aims to design and develop new *Astragalus*-based nanoparticulate adjuvant systems and cancer nanovaccines and evaluate their anti-tumor and immunomodulatory activities in murine melanoma models.

The objectives of this thesis can be listed as:

(i) Design and development of new *Astragalus*-based nanoparticulate adjuvant systems composed of *Astragalus* polysaccharide, AST-VII, and TLR4 agonist by using statistical design of experiment tools,

(ii) Obtaining proper formulations of cancer nanovaccines with adjuvant systems and tumor antigens, SIINFEKL (CD8 T cell epitope for B16-OVA), Trp-2 (CD8 T cell epitope for B16F10) and PADRE (universal CD4 T cell epitope),

(iii) Investigating cytotoxic and immunomodulatory activities of developed adjuvant systems and nanovaccines, examining cellular uptake of adjuvant systems by dendritic cells *in vitro*,

(iv) Demonstrating *in vivo* immunogenicity of cancer nanovaccines by investigating vaccine-induced cellular and humoral immunity,

(v) Revealing anti-tumor and immunomodulatory activities of cancer nanovaccines in prophylactic and therapeutic murine melanoma models.

CHAPTER 2

MATERIALS & METHODS

2.1. Materials

Monophosphoryllipid A (MPLA) (Avanti Polar Lipids), lipopolysaccharide (LPS)(Sigma), and QS-21 (Desert King) were purchased. Astragaloside VII (AST-VII) was donated by Bionorm Doğal Ürünler, TR. Antigen peptides, including Trp-2 peptide SVYDFFVWL and PADRE peptide AKFVAAWTLKAA (SB-Peptide), $OVA_{257-264}$ peptide SIINFEKL (Anaspec) were purchased. HPLC grade solvents, acetonitrile, methanol, chloroform, and isopropanol were purchased from Merck. Dansyl chloride (Sigma Aldrich), Pur-A-Lyzer™ Midi Dialysis Kit (MWCO: 3.5 kDa) (Sigma Aldrich), ACK Lysing buffer, and brefeldin A (BioLegend) were purchased.

2.1.1. Materials for Bioactivity Studies

RPMI 1640 medium (Gibco), Fetal Bovine Serum (FBS)(Gibco), Dulbecco's Phosphate Buffer Saline (DPBS)(Gibco), Penicillin/Streptomycin (Gibco), MEM Non-Essential Amino Acids Solution (Thermo Fisher Scientific), 2-Mercaptoethanol (Aldrich), Trypsin-EDTA (Gibco) were purchased for *in vitro* cell culturing. Flow cytometry antibodies, including mouse ELISA antibodies including purified anti-mouse IL-1β, purified anti-mouse IL-6, purified anti-mouse IL-12p70, biotin anti-mouse IL-1β, biotin anti-mouse IL-6, biotin anti-mouse IL-12p70 (Biolegend), and mouse IFN-γ, IL-2, IL-10 and IL-4 ELISA kits (Invitrogen) were purchased. Thiazolyl blue tetrazolium bromide (MTT) (Acros) for *in vitro* cellular toxicity, DAPI (Biolegend), LysoTraker Red DND-99 (Invitrogen) for subcellular localization were purchased.

2.1.1.1. Flow Cytometry Antibodies

The panel for BMDCs maturation and activation: L/D Fixable Near-IR, anti-mouse PE/Cy7-CD11c (N418), APC-CD86 (GL-1), PE-CD80 (16-10A1), FITC-CD40 (3-23)(BioLegend), BV510-I-A/I-E (269)(eBioscience)

The panel for splenic T cell phenotyping: L/D Fixable Near-IR, anti-mouse FITC-CD45 (30-F11), PerCpCy5.5-TCRβ (H57-597), APC-CD8α (53-6.7), PE/Cy7-CD4 (RM4-5), APC-CD25 (PC61), PE-Foxp3 (MF-14)(BioLegend)

The panel for splenic innate cell phenotyping: L/D Fixable Near-IR, anti-mouse FITC-CD45 (30-F11), PerCP/Cy5.5-CD11b (M1/70), PE/Cy7-CD11c (N418), PE-F4/80 (BM8), APC-NK1.1(S17016D)(BioLegend)

The panel for tetramer staining in PBMCs: DAPI, anti-mouse PE-SIINFEKL, APC-CD8α (53-6.7), PE/Cy5-CD44 (IM7), APC/Cy7-CD62L (MEL14)(BioLegend)

The panels for T cell phenotyping in tumor microenvironment (TME):

(i) DAPI, anti-mouse FITC-CD45 (30-F11), AF700-CD3 (17A2), PE-Cy5-CD4 (GK1.5), APC-CD8α (53-6.7), BV711-CD25 (PC61), BV421-CXCR3 (CXCR3-173), PE-Cy7-PD1 (29F.1A12)(BioLegend)

(ii) DAPI, anti-mouse FITC-CD45 (30-F11), PE-CD3 (17A2), PE-Cy5-CD4 (GK1.5), APC-CD8α (53-6.7), BV711-CD25 (PC61), PE-Cy7-PD1 (29F.1A12)(BioLegend)

The panels for innate immune cell phenotyping in TME:

(i) DAPI, anti-mouse BUV805-CD45 (30-F11)(eBioscience), FITC-CD11c (N418), AF700-CD11b (M1/70), PE-F4/80 (BM8), APC-CD86 (GL-1)(BioLegend)

(ii) DAPI, anti-mouse FITC-CD45 (30-F11), PE-Cy7-CD11c (OX-42), AF700-CD11b (M1/70), PE-F4/80 (BM8), APC-CD86 (GL-1)(BioLegend)

The panel for splenic memory T cell phenotyping: DAPI, anti-mouse FITC-CD45 (30-F11), PE-CD3 (17A2), PE-Cy7-CD4 (RM4-4), APC-CD8α (53-6.7), PE/Cy5-CD44 (IM7), BV605-CD62L (MEL-14)(BioLegend)

2.1.2. Cells

B16-F10 melanoma (ATCC, CRL-6475) and DC2.4 dendritic cells (Sigma Aldrich, SCC142) were derived from C57BL/6 mice. Both cell lines were maintained at 37°C with RPMI-640 cell media supplemented with 10% fetal bovine serum (FBS), 1% penicillin/streptomycin and 50 μM β-mercaptoethanol, and additionally 1% non-essential amino acids for DC2.4 cell line. The cells were used after reaching 80% confluency.

2.1.3. Experimental Animals

Female C57BL/6 mice for *in vivo* immunogenicity assays were provided by International Biomedicine and Genome Center (IBG). The mice were housed in microisolator cages in a pathogen-free animal facility at IBG and maintained in groups of 5 under standard conditions of temperature 22 ± 1° C with regular 12 h light and 12 h dark cycles and free access to standard laboratory food and water. The Local Ethics Review Committee approved the experimental protocol for Animal Experimentation of IBG (2020-043).

Female C57BL/6 mice used for melanoma tumor models were conducted in accordance with the approval by the Institutional Animal Care and Use Committee at the University of Michigan (Ann Arbor, MI, USA).

2.1.4. Instruments

The following instruments were mainly used in the context of this thesis:

- Zetasizer Nano ZS (Malvern Panalytical)
- FT-IR (Perkin Elmer – Uatr Two)
- UV-Vis Spectroscopy (Peltier, Shimadzu-UV 2450)
- High-Pressure Liquid Chromatography (Agilent 1200)

- Flow Cytometry (FACSCanto, BD; Cytek Aurora)
- Fluorescence Microscopy (ZEISS – Observer Z1)
- Plate-reader (THERMO, Vario Skan Flash)
- Scanning Electron Microscopy (SEM) (FEI Quanta 250 FEG)
- Transmission Electron Microscopy (TEM) (JEOL JEM 1220)

2.2. Methods

2.2.1. Design and Development of MPLA and AST-VII Integrated Nanoparticulate Adjuvant Systems

The major active constituents found in *Astragalus* plants are polysaccharides and saponins.[59] Our preliminary studies conducted with *Astragalus* polysaccharide (APS) and AST-VII have shown promise that these compounds can be used in an adjuvant system.[59,63,64] Moreover, early mechanism of action studies revealed that AST-VII alone did not maturate and activate dendritic cells but cooperatively worked with TLR4 agonist, lipopolysaccharide (LPS), to enhance dendritic cell activation.[65] Therefore, we designed an adjuvant system where *Astragalus* polysaccharide is used as a delivery system, and AST-VII and monophosphoryllipid A (MPLA), TLR4 agonist and detoxified form of LPS, as immunostimulating agents co-integrated into the adjuvant system (Figure 2.1.).

2.2.1.1. Preparation of Nanoparticulate Adjuvant System

pH jump methodology, which involves a quick transient increase in pH up to 10-12, was followed to self-assemble building blocks into nanostructures.[70] A series of trial experiments were done to analyze the formation of nanostructures. Based on previous studies, *Astragalus* polysaccharide, MPLA and AST-VII concentrations in NPs were determined as 500 μg/mL, 100 μg/mL and 500 μg/mL, respectively.[62,71]

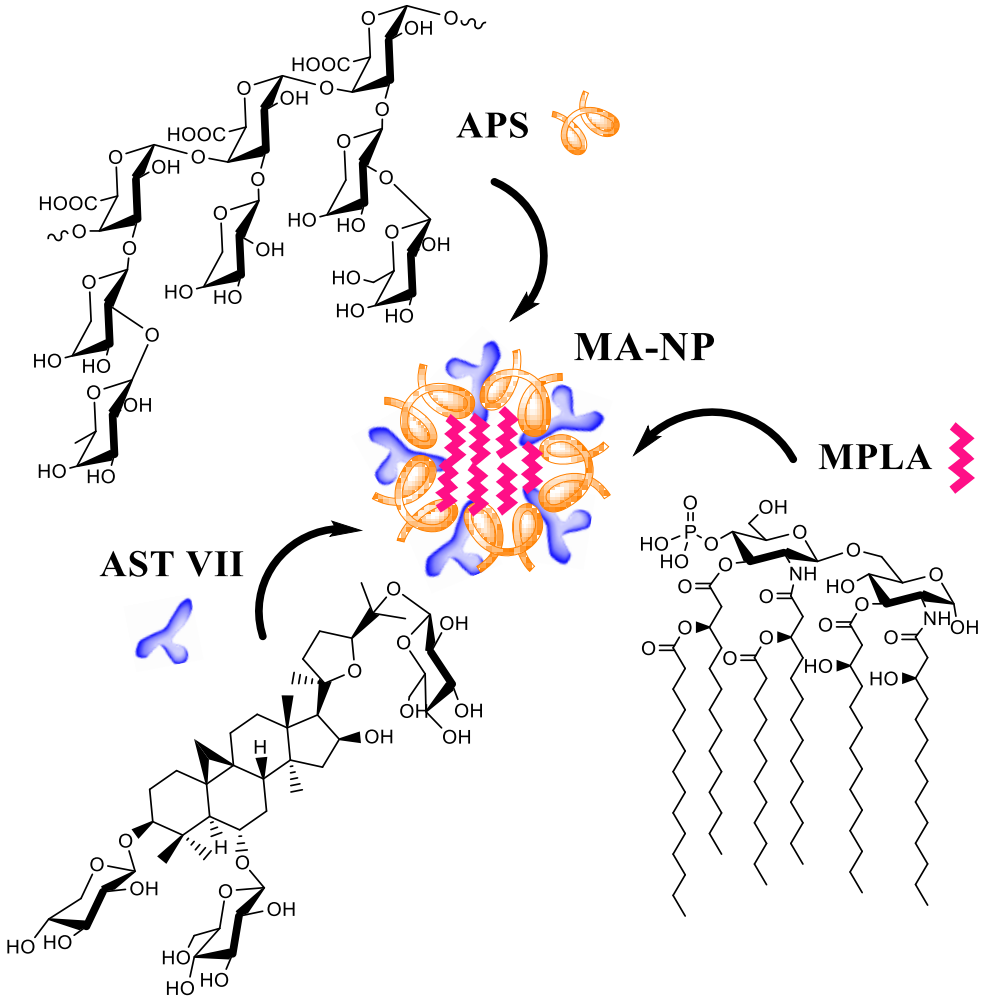

Figure 2.1. Design of MPLA/AST-VII integrated nanoparticulate (MA-NP) adjuvant system. APS: *Astragalus* polysaccharide, AST-VII: Astragaloside VII, MPLA: Monophosphoryllipid A.

Following the illustration for MA-NP preparation (Figure 2.2), **(i)** APS was dissolved in PBS (1X) at 60°C under continuous sonication. Afterward, **(ii)** MPLA and **(iii)** AST-VII were added with 10 min intervals of sonication. **(iv)** pH was jumped to 11 by adding 0.1 M NaOH, and then **(v)** pH was immediately adjusted to 5.5 by adding 0.1 M HCl. When the solution temperature reached to room temperature, **(vi)** the nanoparticles (NPs) were purified and collected by MWCO: 100 kDa centrifugal filters (Amicon, Millipore Sigma) (Figure 2.2).

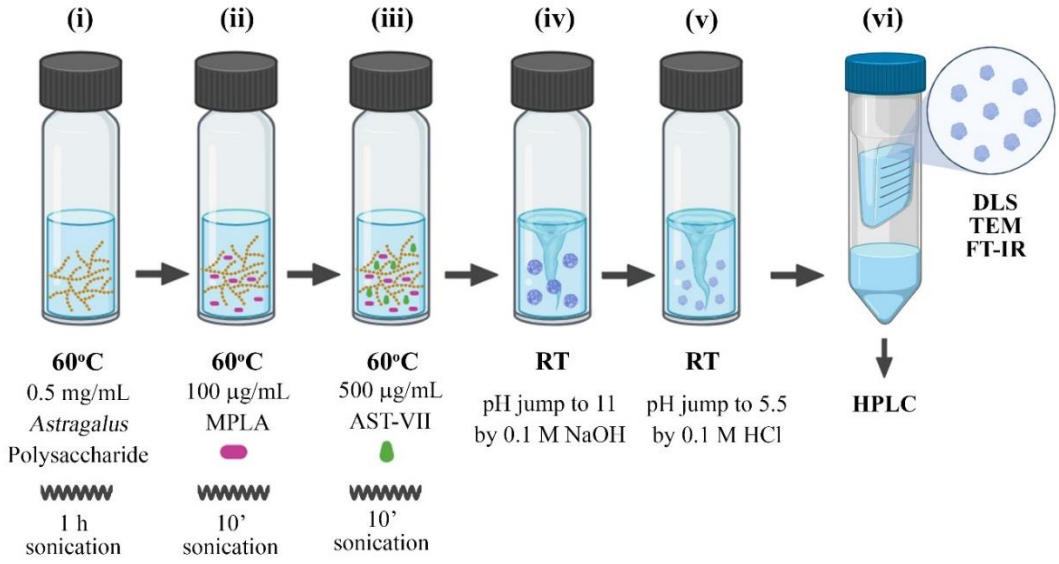

Figure 2.2.The schematic representation of MA-NP adjuvant system preparation.

Concentrated NPs were characterized in terms of their hydrodynamic particle size, zeta potential, and polydispersity index (PDI) by Zetasizer Nano ZS (Malvern Panalytical), their particle morphology by TEM (JEOL 1220) and SEM (Quanta 250), and the surface characteristics by FT-IR (Perkin Elmer – Uatr Two). The filtrate obtained from the centrifugal filter was analyzed by RP-HPLC (Agilent 1200). The entrapment efficiencies of AST-VII and MPLA were calculated by the following formula (2.1):

$$Entrapment\ efficiency\ (EE)(\%) = \frac{A-B}{A}\ x\ 100 \qquad (2.1)$$

A: Total concentration of immunomodulator in NPs

B: The concentration of free immunomodulator in the filtrate

2.2.1.2. Optimization of Medium pH

In MA-NP adjuvant system preparation methodology, pH was increased to 11 and immediately decreased to 5.5. As MPLA contains an ester bond in its chemical structure,

to understand whether the ester bond would be cleaved upon an increase in pH or not, MPLA was dissolved in PBS with varying pH conditions (5, 7, 9, 11) and then, the samples were analyzed by FT-IR.

2.2.1.3. Optimization of NPs Operation Parameters

To elucidate optimum operation conditions for NP formation, the roles of **(i)** pH jump time (Δjt), which corresponds to a time interval between pH value, **(ii)** duration of equilibrium time after pH jump (Δeq), and **(iii)** operation temperature (To)[70] must be investigated in terms of physicochemical properties of NPs such as particle size, zeta potential, and PDI.

Design-Expert® Software version 7.0 was used for NPs operation parameter optimization experiments. The upper and lower levels of numeric factors (temperature, pH jumping time, equilibration time) and related responses (particle size, zeta potential, and PDI) were selected and entered into BBD optimization tool (Iteration A) (Table 2.1).

Table 2.1. The upper and lower levels of numeric factors used in Iteration A.

Experimental Inputs				
Numeric Factors	**Symbols**	**Units**	**-1 level**	**+1 level**
Temperature	**A**	°C	25	45
pH jumping time	**B**	min	0	30
Equilibration time	**C**	min	0	30
Experimental Outputs				
Responses	**Symbols**	**Units**	**Constraints**	
Particle Size	Y_1	nm	20 – 50 nm	
Zeta Potential	Y_2	mV	minimize	
PDI	Y_3	-	minimize	

A Box-Behnken design (BBD) of 15 runs, three factors at two levels (3^2), with three replicates at the center point, was created to elucidate the roles of different factor variables on the NP formation and their physicochemical characteristics.

Fifteen runs obtained from BBD demonstrated each condition for NP formation (Table 2.2). NPs were prepared with APS (500 μg/mL), MPLA (10 μg/mL), and AST-VII (50 μg/mL) following operation conditions designed for each run. Then, the particle size, zeta potential, and PDI values of NPs were measured by Zeta-sizer, and the results for each response were subsequently analyzed in Design Expert software.

Table 2.2. The list of NP operation parameter conditions explored for Iteration A.

Run	Factor 1 A: Temperature (°C)	Factor 2 B: pH Jumping Time (min)	Factor 3 C: Equilibration Time (min)
4	25	15	30
6	25	0	15
9	25	30	15
14	25	15	0
1	35	15	15
2	35	30	0
3	35	0	0
5	35	15	15
7	35	30	30
12	35	15	15
15	35	0	30
8	45	30	15
10	45	0	15
11	45	15	30
13	45	15	0

A confirmation experiment was conducted to evaluate the reproducibility of the model designed for the NP formation with respect to operation parameters. In the confirmation experiment, BBD ensured the solutions to achieve 20 nm-sized NPs, to increase zeta potential and decrease PDI values. Based on these solutions, the most desirable solution was selected (Table 2.3), and further confirmation experiments were performed (n=3).

Table 2.3. The most desirable solution of the confirmation experiment obtained from NP operation parameters (Iteration A).

Temperature (°C)	**pH Jumping Time (min)**	**Equilibration Time (min)**	**Particle Size (nm)**	**Zeta Potential (mV)**	**PDI**	**Desirability**
38.04	2.31	30	20.3	-5.77	0.537	0.498

2.2.1.4. Optimization of Material Concentrations in NPs

As the concentration of each material in NPs affects the particle formation and its physicochemical characteristics, a BBD design, having 15 runs, three factors at two levels (32), and three replicates at the center point, was created to evaluate these effects on NP formation. The upper and lower concentration levels for each material were determined according to a literature search[62,71] (Table 2.4) and entered into BBD optimization tool (Iteration B) in Design-Expert® Software version 7.0.

Three responses were chosen as particle size, zeta potential, and entrapment efficiency (EE) of AST-VII, and the software created a recipe containing 15 runs (Table 2.5). NPs were produced according to the concentrations of materials given in Table 2.5 following optimized operation conditions (38°C, pH jumping time: 2.31 min, equilibration time: 30 min). Prepared NPs were analyzed by Zeta-sizer for particle physicochemical characteristics and by RP-HPLC for quantification of AST-VII and MPLA.

Table 2.4. The numeric factors and related min and max values used for Iteration B.

Experimental Inputs				
Numeric Factors	**Symbols**	**Units**	**-1 level**	**+1 level**
APS Concentration	A	μg/mL	500	2000
MPLA Concentration	B	μg/mL	0	100
AST-VII Concentration	C	μg/mL	0	1200
Experimental Outputs				
Responses		**Symbols**	**Units**	**Constraints**
Particle Size		Y_1	nm	20 – 50 nm
Zeta Potential		Y_2	mV	minimize
Entrapment Efficiency AST-VII		Y_3	%	maximize

Table 2.5. The list of NP material concentration variations explored for Iteration B.

Run	**Factor 1 A: APS Concentration (μg/mL)**	**Factor 2 B: MPL Concentration (μg/mL)**	**Factor 3 C: AST VII Concentration (μg/mL)**
4	2000	0	600
5	1250	0	0
12	500	0	600
15	1250	0	1200
1	1250	50	600
2	2000	50	1200
3	1250	50	600
7	500	50	1200
9	500	50	0
10	1250	50	600
13	2000	50	0

(cont. on next page)

Table 2.5. (cont.).

6	1250	100	1200
8	500	100	600
11	2000	100	600
14	1250	100	0

Following the recipe given above, each response (particle size, zeta potential, EE% AST-VII) entered BBD, and further, a confirmation experiment was conducted to evaluate the reproducibility of the models designed for the material concentrations driving NP formation. In the confirmation experiment, BBD provided the solutions to obtain 20-50 nm-sized NPs, increase zeta potential, and maximize the entrapment efficiencies of AST-VII. The preferable solutions were selected with respect to the desirability score (Table 2.6), and further confirmation experiments were performed following the instructions in the solutions (n=3).

Table 2.6. The recipe of solutions designed for the confirmation experiments of material concentration in NPs.

Solution #	APS Concentration (μg/mL)	MPLA Concentration (μg/mL)	AST-VII Concentration (μg/mL)	Particle Size (nm)	EE% AST VII	Desirability
1	2000	31	1200	20	55.47	0.971
6	500	84	1200	35	54.23	0.949

2.2.1.5. Preparation of blank NP, MPLA NP, and AST-VII NP

The adjuvant systems prepared only APS (blank NP), MPLA loaded NPs (MPLA NP), and AST-VII loaded NPs (AST-VII NP) were prepared according to operation conditions and material concentrations optimized for MA-NPs (Table 2.7). APS (2 mg)

was dissolved in PBS (1X) at 60°C under continuous sonication for 1 hour. Based on the presence/absence of MPLA or AST-VII, MPLA (31 μg/mL) and AST-VII (1200 μg/mL) were added into the particular adjuvant system and sonicated for 15 min. pH of the solution was jumped to 9 by adding 0.1 M NaOH, and then adjusted to 5.5 by 0.1 M HCl. When the solution temperature reached room temperature, NPs were collected by an Amicon centrifugal filter (MWCO: 100 kDa). All NPs were characterized in terms of their hydrodynamic particle size, zeta potential by Zeta-sizer, and the entrapment efficiencies of AST-VII and MPLA by RP-HPLC.

Table 2.7. The material concentrations for the preparation of blank NP, MPLA NP, and AST-VII NP.

Adjuvant Systems	**APS Concentration**	**MPLA Concentration**	**AST-VII Concentration**
Blank NP	2000 μg/mL	-	-
MPLA NP	2000 μg/mL	31 μg/mL	-
AST-VII NP	2000 μg/mL	-	1200 μg/mL

2.2.2. Integration of Antigens into Adjuvant Systems

2.2.2.1. Integration of SIINFEKL Peptide

To determine the antigen adsorption capacity of MA-NP adjuvant system, CD8 T cell epitope of $OVA_{257-264}$ peptide, SIINFEKL (Anaspec), was chosen as a model antigen. One mg MA-NP adjuvant system was dissolved in PBS at different pHs (3, 5, 7, 9). SIINFEKL peptide at the various concentrations (5, 10, 20 μg) was added into the solution and incubated for two hours at room temperature with continuous shaking at 350 rpm. At the end of incubation, the solution was centrifuged using MWCO 100 kDa centrifugal filters (Amicon, Millipore Sigma) at 4000 rpm and 4C° for 20 min. The zeta potential of

MA-NPs and SIINFEKL adsorbed MA-NPs were analyzed by Zeta-sizer. The filtrate was concentrated with a speed vacuum with no temperature. The amount of free SIINFEKL in the filtrate was measured by BCA assay (Takara) according to the manufacturer's instructions.

2.2.2.2. Integration of Trp-2 and PADRE Peptides

To develop prophylactic/therapeutic vaccines for melanoma, Tyrosinase-related protein 2 (Trp-$2_{180\text{-}188}$, SVYDFFVWL) and pan DR T-helper epitope (PADRE, AKFVAAWTLKAAA**)** (SB Peptide) peptides were used. As in the literature, 10-50 μg Trp-2 and PADRE peptides were injected into mice,[50,72–74] and two different peptide concentrations (30 and 50 mg) were selected. Moreover, the integration of peptides on MA-NP was performed on the various pH levels (3 and 5) in terms of the net charge of peptides in the particular pH range. One mg MA-NP adjuvant system was dissolved in PBS at different pHs (3, 5). Trp-2 and PADRE peptides at different concentrations (30 and 50 μg) were added into the solution and incubated for two hours at room temperature with continuous shaking at 350 rpm. The solution was centrifuged using an Amicon centrifugal filter (MWCO: 100 kDa) at 4000 rpm and 4° for 20 min. The zeta potential of MA-NPs and Trp-2 and PADRE adsorbed MA-NPs were analyzed by Zeta-sizer. The amount of free Trp-2 and PADRE in the filtrate was measured by HPLC-DAD and BCA assay according to the manufacturer's instructions.

2.2.3. Characterization of Nanoparticulate Adjuvant Systems

2.2.3.1. Particle Size and Zeta Potential Characterization

The particle size and zeta potential of nanoparticulate adjuvant systems were measured using Malvern ZetaSizer Nano-ZS (Malvern Panalytical) with a detector angle

of 173°. Zeta potential measurements were carried out using disposable capillary cells. Standard deviations were calculated from several independent experiments that measured at least three replicates.

2.2.3.2. Transmission and Scanning Electron Microscopy

The morphology of nanoparticulate adjuvant systems was examined under scanning electron microscopy (SEM) (FEI Quanta 250 FEG) and transmission electron microscopy (TEM) (JEOL JEM 1220) with an acceleration voltage of 100 V. In TEM analysis, a drop of samples was placed onto a formvar/carbon-coated copper grid and allowed to dry before imaging. For SEM analysis, the samples were coated with a thin gold layer, and imaging was performed.

2.2.3.3. Fourier Transform Infra-Red Spectroscopy (FT-IR)

Liquid samples were analyzed using an FT-IR spectrometer (Perkin Elmer – Uatr Two) equipped with an ATR accessory. The samples were placed on the ATR, and the solvent was slowly evaporated to form a thin film before scanning. The number of scans was set at 64 and recorded at a resolution of 4 cm^{-1} at room temperature.

2.2.3.4. Reversed Phase-High Performance Liquid Chromatography (RP-HPLC)

The quantification of AST-VII in the NPs was assessed by RP-HPLC (Agilent 1200). To quantify AST-VII, the samples and AST-VII standards were dissolved in ultrapure water (UPW) and analyzed on a Chromolith RP-C18 column (4.6 mm x 100 mm; particle diameter: 2 μm) using a constant flow rate (0.75 mL/min, 25 °C). Gradient

conditions of A flow [UPW] and B flow [acetonitrile (ACN)] were followed as shown in Table 2.8. AST-VII was detected using a DAD (diode array detection) detector in the 203, 210, and 254 nm wavelengths.

Table 2.8. RP-HPLC methodology to quantify AST-VII.

Retention time (min)	**Flow rate (mL/min)**	**A (%) UPW**	**B (%) ACN**
0.00	0.75	70	30
1.50	0.75	70	30
11.50	0.75	45	55
13.00	0.75	45	55
13.01	0.75	70	30
15.00	075	70	30

The amount of MPLA in the filtrate of NPs was assessed by RP-HPLC by modifying the published procedure.[75] To quantify MPLA, samples and MPLA standards were dissolved in HPLC grade methanol and analyzed on Chromolith RP-C18 column (4.6 mm x 100 mm; particle diameter: 2 μm) using a constant flow rate (0.5 mL/min, 25 °C). Gradient conditions of Buffer A [95% methanol (MeOH), 5% ultrapure water (UPW), 0.1% TFA] and B [100% isopropanol (IPA), 0.1% TFA] were followed as shown in (Table 2.9). MPLA was detected using an evaporative light scattering detector (ELSD)(65°C, gain: 11).

The quantification of Trp-2 and PADRE peptides in adjuvant systems was analyzed by RP-HPLC. The samples obtained from peptide adsorption studies and Trp-2 and PADRE standards were dissolved in UPW containing 0.1 % TFA and subsequently analyzed on Phoneix RP-C18 column (4.6 mm x 150 mm; particle diameter: 300 A) using a constant flow rate (1 mL/min, 25°C). Gradient conditions of A flow [ACN] and B flow [UPW] were followed, as shown in Table 2.10. Peptides were detected using a DAD detector at a wavelength of 210 nm.

Table 2.9. RP-HPLC methodology to quantify MPLA.

Retention time (min)	Flow rate (mL/min)	A (%): 95 % MeOH + 5 % UPW + 0.1 % TFA	B (%): 100 % IPA + 0.1 % TFA
0	0.5	95	5
5	0.5	60	40
7	0.5	20	80
16	0.5	20	80
17	0.5	95	5

Table 2.10. RP-HPLC methodology to quantify Trp-2 and PADRE peptides.

Retention time (min)	Flow rate (mL/min)	A (%) ACN	B (%) UPW
0	1	1	99
20	1	50	50
30	1	50	50

2.2.3.5. *In vitro* Release of Antigens

The *in vitro* antigen (Trp-2 and PADRE) release from antigen-adsorbed MA-NP was investigated in terms of time (0-96 h) and pH (5.5 and 7.4). One mg nanovaccine was dissolved in 1 mL PBS and mixed well. The solutions were placed in a dialysis bag (Spectra/Pore membrane MWCO:14 kDa, 16 mm flat width, Spectrum Medical Industries) and incubated in PBS (pH 5.5 and pH 7.4), stirring continuously at 37°C for 96 h. At certain time points, 1 mL aliquots of dialysis solution were taken and replaced by 1 mL fresh buffer at 37°C. The antigen release in the samples was measured using a BCA assay to calculate the cumulative antigen release (%) over time.

2.2.4. Investigation of *in vitro* Cytotoxic and Immunomodulatory Activities of NPs

2.2.4.1. Assessment of *in vitro* Cytotoxicity of Adjuvant Systems

Blank NP, AST-VII NP, MPLA NP, and MA-NPs were dissolved in PBS and filtered through a 0.22 μm syringe filter. DC2.4 ($1x10^5$ cells/mL) and B16-F10 cells ($2x10^4$ cells/mL) were plated into 96-well tissue culture plates and incubated with adjuvants systems (0.032, 0.063, 0.125, 0.25, 0.5, 1 mg/mL) for either 24 or 48 hours at 37°C in a 5 % CO_2 incubator. After the end of the incubation period, MTT reagent was added to the media at a final concentration of 0.5 mg/mL, and the cells were incubated for 4 hours at 37 °C in a 5% CO2 incubator. The formazan crystals were dissolved in DMSO, and the absorbance at 570 nm and 650 nm was measured by Multiskan™ GO Microplate Photometer (Thermo Scientific).

2.2.4.2. Cellular Uptake and Subcellular Localization of MA-NP in Dendritic Cells

Dansyl chloride (DNS-Cl) was integrated into MA-NP (DNS-MA-NP) to track particles in dendritic cells. MA-NP was dissolved in dH_2O, and the pH of the solution was adjusted to 9 by adding 0.1 M NaOH. DNS-Cl was mixed with MA-NP and sonicated for one hour. The pH of the solution was adjusted to 5 by adding 0.1 M HCl. Free DNS-Cl was removed using a dialysis membrane (MWCO: 3.5 kDa) against PBS for four days. The integration of DNS-Cl onto MA-NP was analyzed using UV-Vis spectroscopy.

For cellular uptake studies, DC2.4 cells were incubated with DNS-MA-NP (0.1 mg/mL) for different periods (30 min to 24 h) at 37°C. Cells were washed thrice with PBS and imaged using a fluorescence microscope (ZEISS – Observer Z1).

To visualize the subcellular localization of DNS-MA-NP, DC2.4 cells were incubated with DNS-MA-NP (0.1 mg/mL) for six h at 37°C. Then, the cells were

incubated 50 nM Lysotracker Red DND-99 for 30 min with to stain endolysosomal compartments. Then, the cells were fixed with 4 % paraformaldehyde for 15 minutes, stained with 300 nM DAPI for 10 minutes, and visualized by fluorescence microscope.

2.2.4.3. Investigating DC Maturation and Activation

To investigate pro-inflammatory cytokine production, DC2.4 cells (10^5 cells/mL) were treated with blank NP, MPLA NP, AST-VII NP, and MA-NP (0.063 – 0.25 mg/mL) or MPLA (0.4 μg/mL) and AST-VII (6.75 μg/mL) for six hours (IL-1β) or 48 h (IL-6, IL-12). The cell supernatants for each well were collected and stored at -20°C for ELISA.

Bone marrow-derived dendritic cells (BMDCs) were used and prepared as described previously to assess DC maturation and activation.[76] BMDCs ($2.5x10^5$ cells/mL) were treated with blank NP (0.1 mg/mL), MA-NP (0.1 mg/mL), MPLA (0.4 μg/mL) + AST-VII (6.75 μg/mL) and MPLA (0.4 μg/mL) + QS-21 (2 μg/mL) for 24 h. At the end of incubation, the cells were stained with anti-mouse CD40, CD86, CD80, and MHCII, and their expression levels were analyzed by flow cytometry (Cytek Aurora).

2.2.5. Evaluation of *in vivo* Immunogenicity of NPs

To evaluate *in vivo* immunogenicity of nanovaccines, female C57BL/6 mice (6-8 weeks old) were vaccinated following the immunization schedule given in Figure 2.3.

Briefly, mice were subcutaneously (s.c) injected with vaccination groups (Table 2.11) on day 0 (D0) and D7. Two weeks after the boosting immunization (D21), mice were anesthetized with an intraperitoneal injection of ketamine/xylazine cocktail (kx mouse cocktail 0.1mL/20g mouse; 87.5 mg/kg ketamine and 12.5 mg/kg xylazine). The blood was collected using cardiac puncture methodology. The blood samples were centrifuged at 1500 rpm for 15 min, and the mice sera were stored at -20°C for subsequent ELISA analysis. After that, the mice were sacrificed by cervical dislocation, and the spleens for each mouse were collected for immunophenotyping and ELISA analysis.

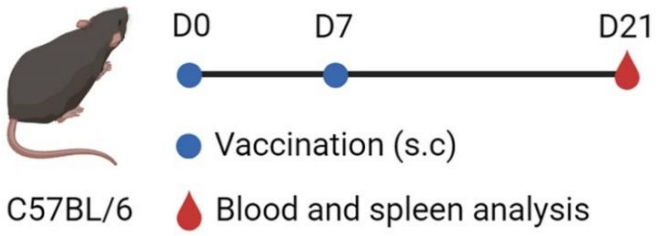

Figure 2.3. The immunization schedule for *in vivo* immunogenicity assessment of Trp-2 and PADRE loaded NPs.

Table 2.11. The vaccination groups for *in vivo* immunogenicity study (n = 7-8).

Group Name	Description	Dose/mouse
PBS	Negative Control	-
Trp-2 + PADRE	MultiAntigen (MultiAgs)	38 μg Trp-2 + 34 μg PADRE/mouse
MA-NP	Peptide free NP	1 mg NP/mouse (contains 3 μg MPLA, 86 μg AST-VII)
MA-NP: MultiAgs	MultiAgs loaded NP vaccine	1 mg NP/mouse (contains 3 μg MPLA, 86 μg AST-VII and 38 μg Trp-2 + 34 μg PADRE)
Blank NP :MultiAgs	MultiAgs loaded delivery system	1 mg NP/mouse (contains 38 μg Trp-2 + 34 μg PADRE)
MPLA+AST-VII +MultiAgs	Soluble vaccine	3 μg MPLA + 86 μg AST-VII + 38 μg Trp-2 + 34 μg PADRE
MPLA+QS-21 +MultiAgs	Positive Control	3 μg MPLA + 3 μg QS-21 + 38 μg Trp-2 + 34 μg PADRE

2.2.6. Investigating Anti-tumor Activities of MA-NP in Murine Melanoma Models

2.2.6.1. Prophylactic Murine B16-OVA Model

To reveal the efficacy of MA-NP adjuvant system in B16-OVA model, $OVA_{257-264}$ peptide (SIINFEKL) was adsorbed on MA-NP. Female C57BL/6 mice (6-8 weeks old) were vaccinated following the immunization schedule given in Figure 2.4.

Briefly, mice (n=5) were subcutaneously (s.c) injected with vaccination groups (Table 2.12) on days 0 (D0) and D7. One week after each vaccination, the blood samples were collected by submandibular bleeding, and peripheral blood mononuclear cells (PBMCs) were analyzed following tetramer staining. On D14, mice were subcutaneously challenged with B16-OVA cells ($5x10^5$ cells) on the right-side flank. Tumor growth and body weight were monitored every other day. The tumor volume was measured by digital capillary and calculated by the formula: tumor volume= length*$width^2$*0.52.[74] Animals were euthanized when the tumor masses reached 1.5 cm in diameter or when animals became moribund with severe weight loss or ulceration. Tumor masses and spleen samples were collected at D33 to analyze immune cell populations.

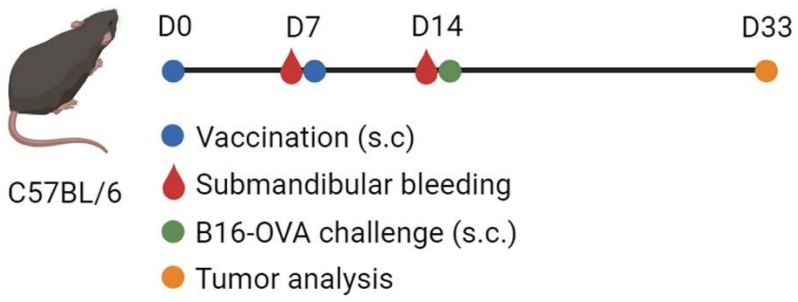

Figure 2.4. The immunization schedule for the prophylactic murine B16-OVA model.

Table 2.12. The vaccination groups for the prophylactic B16-OVA murine melanoma model.

Group Name	Description	Dose/mouse
PBS	Negative Control	-
SIINFEKL	Antigen	10 μg/mouse
MA-NP	SIINFEKL adsorbed NP vaccine	1 mg NP/mouse (contains 3 μg MPLA, 86 μg AST-VII and 10 μg SIINFEKL)
MPLA+AST-VII +SIINFEKL	Soluble Form	3 μg MPLA + 86 μg AST-VII + 10 μg SIINFEKL
MPLA+QS-21 +SIINFEKL	Positive Control	3 μg MPLA + 3 μg QS-21 + 10 μg SIINFEKL

2.2.6.2. Prophylactic Murine B16-F10 Model

To investigate the efficacy of multiAgs adsorbed MA-NP in B16-F10 model, female C57BL/6 mice (6-8 weeks old) were vaccinated following the immunization schedule given in Figure 2.5. Briefly, mice (n=5) were subcutaneously (s.c) injected with the vaccinations group (Table 2.13) on days 0 (D0) and D7.

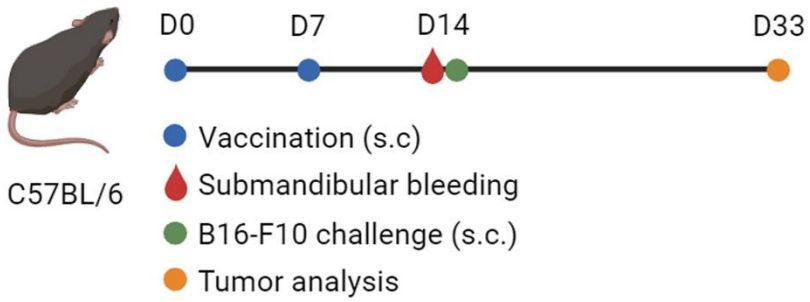

Figure 2.5. The immunization schedule for the prophylactic murine B16-F10 model.

Table 2.13. The vaccination groups for prophylactic B16-F10 murine melanoma model.

Group Name	Description	Dose/mouse
PBS	Negative Control	-
MA-NP	Trp-2 and PADRE adsorbed NP vaccine	1 mg NP/mouse (contains 3 μg MPLA, 86 μg AST-VII and 34 μg Trp-2 and 34 μg PADRE)
MPLA+AST-VII +Trp-2+PADRE	Soluble Form	3 μg MPLA + 86 μg AST-VII + 34 μg Trp-2 and 34 μg PADRE
MPLA+QS-21 +Trp-2+PADRE	Positive Control	3 μg MPLA + 3 μg QS-21 + 34 μg Trp-2 and 34 μg PADRE

The blood samples were collected by submandibular bleeding on D14, and peripheral blood mononuclear cells (PBMCs) were analyzed for functional assessment of T cells. One week after the last immunization (D14), mice were subcutaneously challenged with B16-F10 cells (10^5 cells) on the right-side flank. Tumor growth and body weight were monitored every other day. The tumor volume was measured by digital capillary and calculated by the following formula: tumor volume= length*width^2*0.52.[74] Animals were euthanized when the tumor masses reached 1.5 cm in diameter or when animals became moribund with severe weight loss or ulceration. Tumor masses and spleen samples were collected at D33 to analyze immune cell populations.

2.2.6.3. Therapeutic Murine B16-F10 Model

The efficacy of multiAgs adsorbed MA-NP and combinatory immunotherapy with anti-PD1 was investigated in the therapeutic murine B16-F10 model. Female C57BL/6 mice (6-8 weeks old) were vaccinated following the immunization schedule given in Figure 2.6.

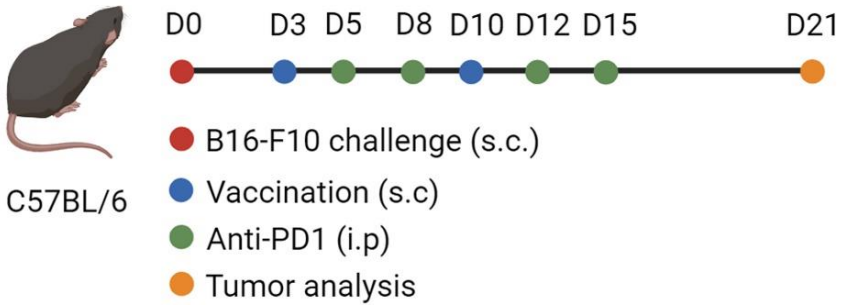

Figure 2.6. The immunization schedule for the therapeutic murine B16-F10 model.

For therapeutic murine melanoma model, B16-F10 cells (10^5 cells) were subcutaneously inoculated to mice (n= 5) on the right-side flank (D0). Three days after tumor inoculation, PBS, MA-NP: MultiAgs and MPLA+QS-21+MultiAgs vaccination groups were subcutaneously administered into mice at one-week intervals (D3 and D10) (Table 2.14). For combinatory immunotherapy, anti-mouse PD-1 (100 μg/mouse) antibody was intraperitoneally injected on days 2 and 5 after each vaccination of MA-NP: MultiAgs (D5, D8, D12, D15).[74]

Table 2.14. The vaccination groups for therapeutic B16-F10 murine melanoma model. ICI: Immune checkpoint inhibitor.

Group Name	Description	Dose/mouse
PBS	Negative Control	-
MA-NP: MultiAgs	Trp-2 and PADRE adsorbed NP vaccine	1 mg NP/mouse (contains 3 μg MPLA, 86 μg AST-VII, 34 μg Trp-2, 34 μg PADRE)
MPLA+QS-21 +MultiAgs	Positive Control	3 μg MPLA + 3 μg QS-21 + 34 μg Trp-2 and 34 μg PADRE
Anti-PD1	ICI therapy	100 μg/mouse
MA-NP:MultiAgs+ anti-PD1	Combinatory therapy	1 mg MA-NP/mouse + 100 μg anti-PD1/mouse

Tumor growth and body weight were monitored every other day following tumor inoculation. Animals were euthanized when the tumor reached 1.5 cm in diameter or when they became moribund with severe weight loss or unhealing ulceration. Tumor masses and spleen samples were collected at D21 to analyze immune cell populations.

2.2.7. Tetramer Staining Assay

PBMCs were analyzed for the percentages of SIINFEKL-specific $CD8^+$ T cells using tetramer staining assay as described previously[77]. The blood samples collected via submandibular bleeding were incubated with lysing buffer to remove red blood cells. After centrifuging samples at 1500xg for 5 min, the cell pellet was suspended in FACS buffer. After washing, PBMCs were incubated with mouse CD16/32 antibody for 10 min at RT, H-2Kb OVA Tetramer-SIINFEKL-PE for 30 min on ice, and CD8-APC, CD44-PE-Cy5, CD62L-APC-Cy7 antibodies for 20 min on ice, respectively. Following washing two times with FACS buffer, the final pellet was dissolved in FACS buffer containing DAPI and then analyzed by flow cytometry.

2.2.8. Functional Assessment of T cells

To assess the functionality of primed $CD8^+$ T cells, PBMCs were stimulated *ex vivo* with 5 μM Trp-2 and 5 μM PADRE peptides in the presence of brefeldin A solution for 6 h at 37°C[78]. The cells were stained with APC-CD8 antibody following cell surface staining protocol, then fixed, permeabilized and stained with PE-IFN-γ antibody using intracellular staining protocol. Then, IFN-γ^+CD8^+ T cell populations were analyzed by flow cytometry.

2.2.9. ELISA

The cytokine concentrations of mouse IL-1β, IL-6, IL-12, and IFN-γ, IL-2, IL-10, and IL-4 ELISA kits were measured in accordance with the manufacturer's instructions. Briefly, to analyze IL-1β, IL-6, and IL-12p70, Nunc-Immunoplates were coated with capture antibodies in a coating buffer and incubated overnight at 4°C. After the washing steps, the plate was blocked by assay buffer for one hour at RT. The samples and standards were diluted, added to the appropriate well, and then incubated for two hours at RT. The detection antibody for the corresponding cytokine was added and incubated for one hour. Avidin-HRP as a secondary antibody was added and incubated for 30 min. After washing, a TMB substrate was added, and the plate was incubated for 15 minutes in the dark. At the end of the incubation period, the reaction was stopped by adding 2 N H_2SO_4. The absorbance at 450 nm and 570 nm was measured with Varioskan.

2.2.10. Flow Cytometry

For cell surface or intracellular staining, cells were suspended in FACS buffer (PBS, 1% BSA, 0.025% NaN_3). The cells were blocked with CD16/32 blocking antibody for 10 min and stained with a cell surface staining cocktail for 30 min at 4°C in the dark. A Live/Dead Fixable Near IR viability kit or DAPI was used to analyze cell viability. For intracellular staining, cells were fixed with 4% paraformaldehyde for 15 min and permeabilized with Foxp3 Staining Buffer Set after the cell surface staining. Then, cells were stained with PE anti-mouse Foxp3 for 30 min at 4°C in the dark. The cells were run using BD FACS Canto or Aurora Cytek spectral analyzer. The data were analyzed with FlowJo software version 10.

CHAPTER 3

RESULTS & DISCUSSION

3.1. Design and Development of MPLA and AST-VII Integrated Nanoparticulate (MA-NP) Adjuvant Systems

3.1.1. Pre-experiments for Adjuvant System Preparation

Pre-experiments were conducted following the conditions in Table 3.2 to determine the formation of nanoparticles using APS, MPLA, and AST VII. After NPs were prepared, their physicochemical properties were characterized by using Zetasizer and TEM.

Table 3.1. The conditions followed in the pre-experiments for particle formation.

Rxn materials		**Rxn conditions**					
Compounds	**Concentration**	**Trial 1 (T1)**			**Trial 2 (T2)**		
APS	500 μg/mL	**Temperature**	**pH**	**pH**	**Temperature**	**pH**	**pH**
MPLA	100 μg/mL	**(°C)**	**at 9**	**at 5**	**(°C)**	**at 9**	**at 5**
AST-VII	500 μg/mL	RT	30 min	30 min	45	0	25 min

The hydrodynamic particle sizes were measured as 45.6 ± 13 nm and 32 ± 9.5 nm for T1 and T2, respectively (Figure 3.1A). The hydrodynamic particle size decreased by increasing the operation temperature to 45°C and decreasing the pH jumping time (at pH

9). The negatively charged NPs were obtained -8.4 ± 0.99 mV and -7.5 ± 0.41 mV for T1 and T2, respectively (Figure 3.1B). The presence of carboxylic acid groups of galacturonic acids in APS and phosphate groups in MPLA contribute to the negative characteristic of MA-NP adjuvant system. The operation conditions in the pre-experiment did not have a statistically significant effect on the zeta potential of NPs. The PDI values were in the interval of 0.7 and 0.9, indicating a polydispersity index higher than 0.5, attributed to heterogeneous size distribution (Figure 3.1C). The morphology of NPs dominantly existing on the TEM grid was shown in Figure 3.1D, spherical-shaped nanoparticulate structures with defined borders were observed.

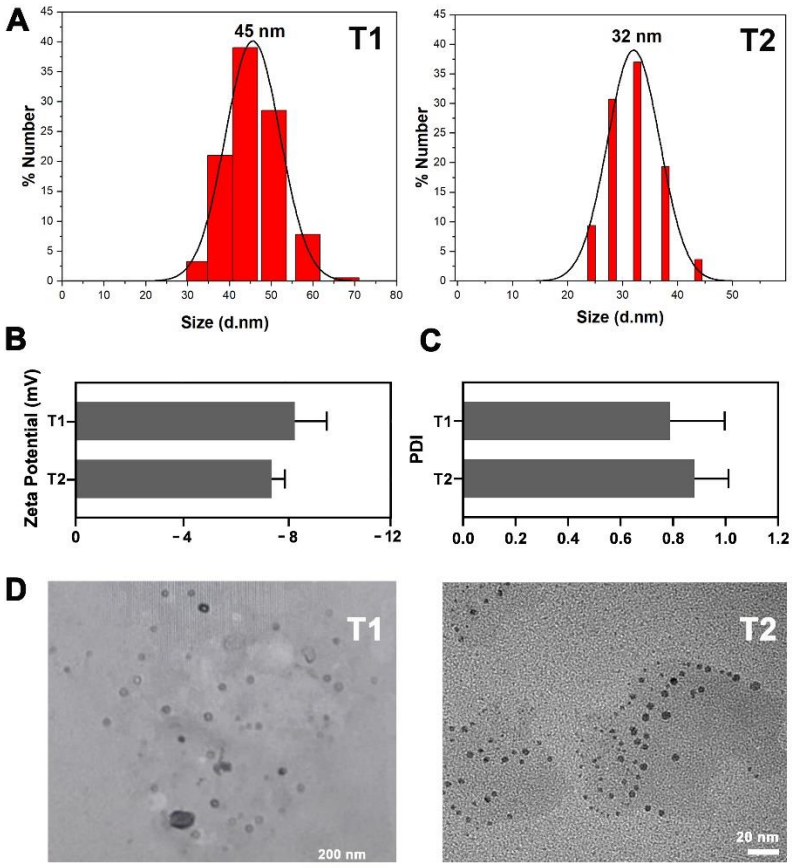

Figure 3.1. The characterization of adjuvant systems prepared using different experimental setups. (A) the hydrodynamic particle size of T1 and T2 (B) zeta potentials (mV), (C) PDI, (D) TEM images of T1 (left) and T2 (right).

These data indicated that the nanoparticulate adjuvant systems were successfully prepared. However, the operation conditions and material concentrations needed to be optimized to prepare homogeneously distributed 20-100 nm in-sized NPs.

3.1.2. Optimization of Medium pH

pH jump methodology was used to prepare MA-NP adjuvant system, which includes increasing the pH of the medium to 11 and immediately decreasing the pH to 5. As MPLA contains an ester bond in its chemical structure, the stability of MPLA in different medium pH was investigated to decide the optimum medium pH. For this purpose, MPLA was dissolved in PBS with different medium pH's, and then the samples were analyzed by FT-IR. The stretching vibrations corresponding to C=O of the ester groups were observed at 1737 cm^{-1} in the solution with pH 5, 7, 9, and 10 (Figure 3.2).

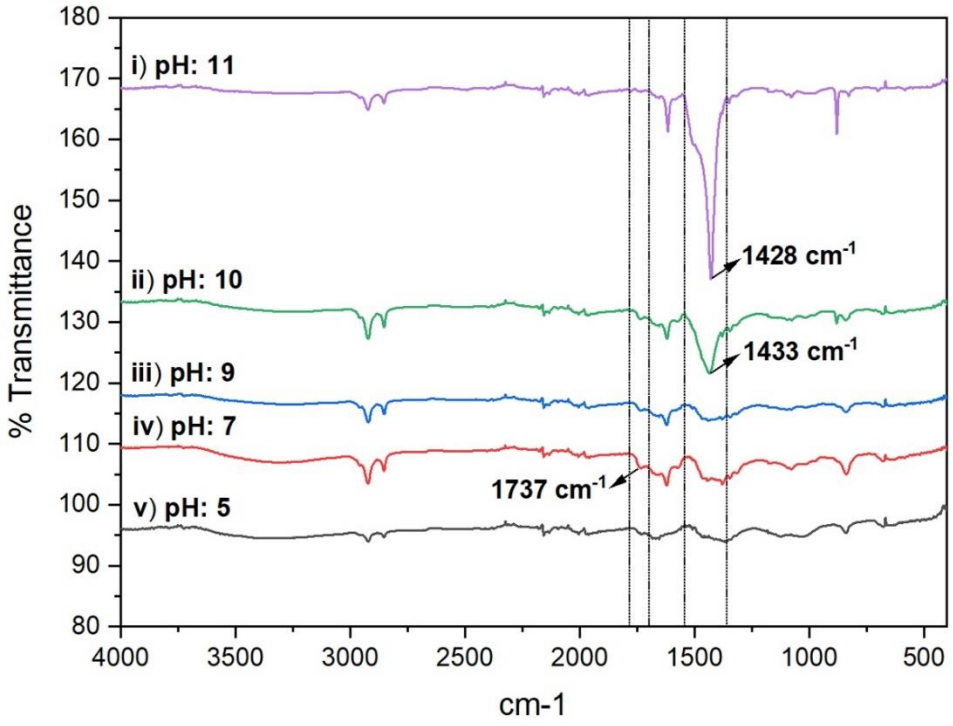

Figure 3.2. The FT-IR spectrum of MPLA with different medium pH (5 to 11).

When the pH of the solution was higher than 9, the intensity of the peak at 1737 cm^{-1} decreased, and another peak appeared at 1428-1433 cm^{-1} (Figure 3.2). This peak intensity increased parallel to the increase in the pH solution. In literature, the symmetric carboxylate stretch band is reported to appear at 1423 cm^{-1}.[79] Therefore, the peak observed at 1428-1433 cm^{-1} was assigned as a symmetric carboxylate stretch of sodium myristate (C14).

Based on these results, the ester bonds in MPLA started to cleave in an aqueous solution at pH > 9, causing the formation of sodium myristate (C14) in the solution. Therefore, the solution of pH was jumped to 9 and then decreased to 5 in the NPs preparation methodology.

3.1.3. Optimization of NP Operation Parameters

In the adjuvant market, new adjuvant/adjuvant systems and immunostimulators are needed to develop efficient immunotherapies for cancer or infectious diseases. Besides new immunostimulators, there is also a need to model the immune system by replacing empirical adjuvant screening with statistical design of experiments (DoE) to improve the efficiency of adjuvant selection and development processes.[80] DoE provides an optimal set of experiments by giving multiple input parameters, allowing the use of empirical data to extrapolate toward the larger output space.[80,81] Box-Behnken design (BBD) defines an experimental domain in the optimization process by providing minimum and maximum values for each factor.[82]

To investigate the effect of operation parameters (temperature, pH jumping time, and equilibration time) on the physicochemical properties of MA-NP adjuvant system, iteration A was conducted with 15 runs, three factors at two levels (3^2), with three replicates at the center point. The desirable NPs should have the following physicochemical characteristics: (i) particle size diameter of 20-100 nm for optimal circulation time,[83] (ii) negatively charged NPs, (iii) PDI smaller than 0.5.

3.1.3.1. Particle Size

NPs were prepared following the operation conditions given in iteration A, and NPs were collected by Amicon centrifugal filter (MWCO: 100 kDa) for further particle size analysis by Zeta-sizer. The hydrodynamic particle sizes were 10-30 nm in all 15 runs (Figure 3.3). ANOVA and 2FI models were used to evaluate the main and pairwise interaction effects in iteration A.

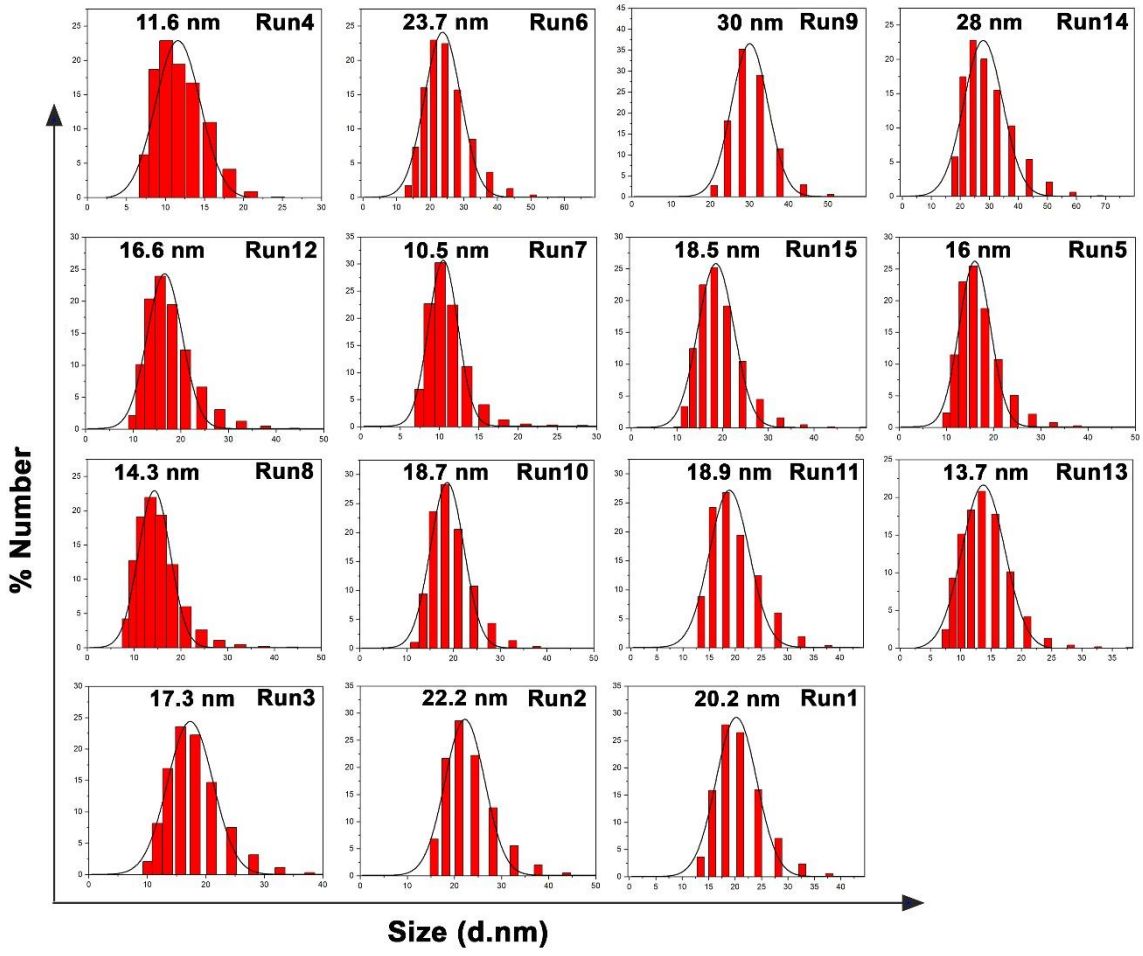

Figure 3.3. The particle size distributions obtained from the experiments following Iteration A. Represented distribution graphs demonstrated average of triplicate measurements.

In ANOVA table (Table 3.2), p-value for the reduced 2FI model is lower than 0.05, indicating the model was significant. Lack of fit value compares the variation between actual data and the predicted value to the variation between replicates. The "Lack of Fit-F value" of 0.8433 implied that lack of fit was not significant relative to pure error, which was desirable in the model. The predicted R2 of 0.8050 was in reasonable agreement with the adjusted R2 of 0.8754, showing good predictive power with observed values of each run by the model.

Table 3.2. ANOVA results analyzed by response surface reduced 2FI model for NP particle size (nm) iteration A.

Source	**Sum of Squares**	**df**	**Mean Square**	**F Value**	**p-value Prob > F**	
Model	269.73	5	53.95	19.27	0.0003*	**significant**
A-Temperature	26.99	1	26.99	9.64	0.0146*	
B-pH jumping time	17.63	1	17.63	6.30	0.0364*	
C-Equilibration time	58.86	1	58.86	21.03	0.0018*	
AxC	116.64	1	116.64	41.67	0.0002*	
BxC	41.60	1	41.60	14.86	0.0048*	
Lack of Fit	12.07	6	2.01	0.39	0.8433	**not significant**
Pure Error	10.32	2	5.16			

Notes: R-Squared=0.9233 ; Adj R-Squared = 0.8754 ; Pred R-Squared = 0.8050

The influence of temperature (T) and equilibration time (Δeq) on the particle size was exhibited by response surface plots (Figure 3.4A). In this model, the main factors (temperature, pH jumping time, and equilibration time) and their pairwise interactions (temperature x pH jumping time and pH jumping time x equilibration time) had a statistically significant effect on the particle size of NPs (Table 3.2, Figure 3.4A). Moreover, the observed particle size was a good fit with the resultant model of the data (Pearson correlation r = 0.96) (Figure 3.4B).

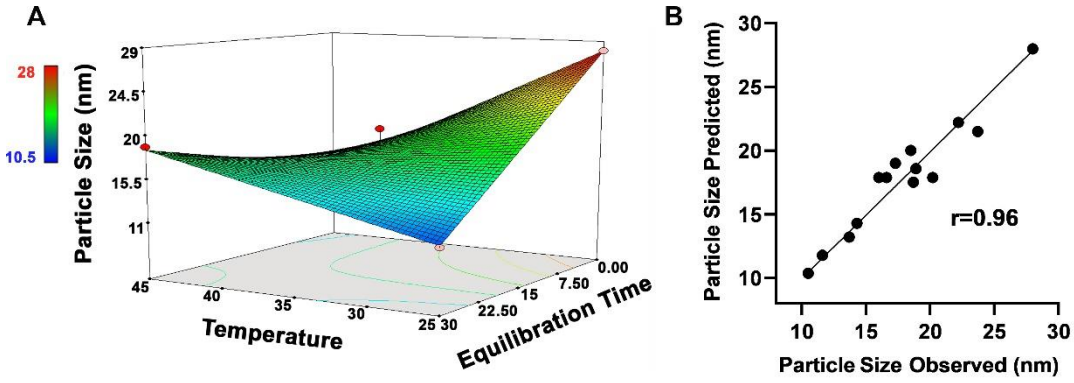

Figure 3.4. Response surface and regression analysis for particle size (iteration A). (A) Response surface plot for particle size (nm). Pink points indicate the local maxima and minima for particle size. Red points indicate the desired points for particle size (20 nm). (B) The 14-point model accurately predicts particle size with respect to observed values.

3.1.3.2. Zeta Potential

NPs were prepared following Iteration A, and the zeta potential of each run was measured by a Zeta-sizer. All NPs had a zeta potential of -4 and -8 mV (Figure 3.5). These negative characteristics of NP are due to carboxylic groups on galacturonic acid at the structure of APS and ionized phosphate groups at the structure of MPLA.

To evaluate main and pairwise interaction effects, ANOVA and quadratic models were applied to zeta potential values obtained from iteration A. In ANOVA table (Table 3.4), the quadratic model was significant, and the lack of fit value of 0.8823 was not significant relative to pure error. The predicted R^2 of 0.8934 was in reasonable agreement with the adjusted R^2 of 0.9409, indicating the powerful model for zeta potential is applicable.

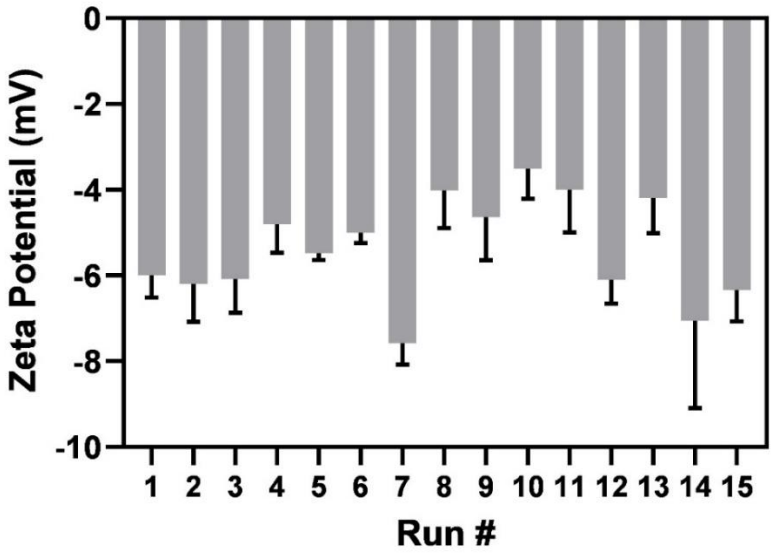

Figure 3.5. The zeta potentials (mV) of different runs from the experiments performed following iteration A.

Table 3.3. ANOVA results analyzed by response surface reduced quadratic model for zeta potential (mV).

Source	Sum of Squares	df	Mean Square	F Value	p-value Prob > F	
Model	11.31	6	1.89	32.81	0.0002*	**significant**
A-Temperature	1.43	1	1.43	24.94	0.0025*	
B - pH jumping time	0.00067	1	0.00067	0.012	0.9175	
C- Equilibration time	0.0044	1	0.0044	0.076	0.7919	
AxB	0.19	1	0.19	3.29	0.1195	
A^2	7.71	1	7.71	134.17	<0.0001*	
C^2	0.23	1	0.23	3.94	0.0945	
Lack of Fit	0.12	4	0.030	0.26	0.8823	**not significant**
Pure Error	0.23	2	0.11			

Notes: R-Squared=0.9704 ; Adj R-Squared = 0.9409 ; Pred R-Squared = 0.8934

Only temperature had a quadratic effect on the zeta potential of NPs (Figure 3.6A). Moreover, the observed and predicted values for zeta potential were also well-fitted (Pearson correlation r = 0.98) (Figure 3.6B).

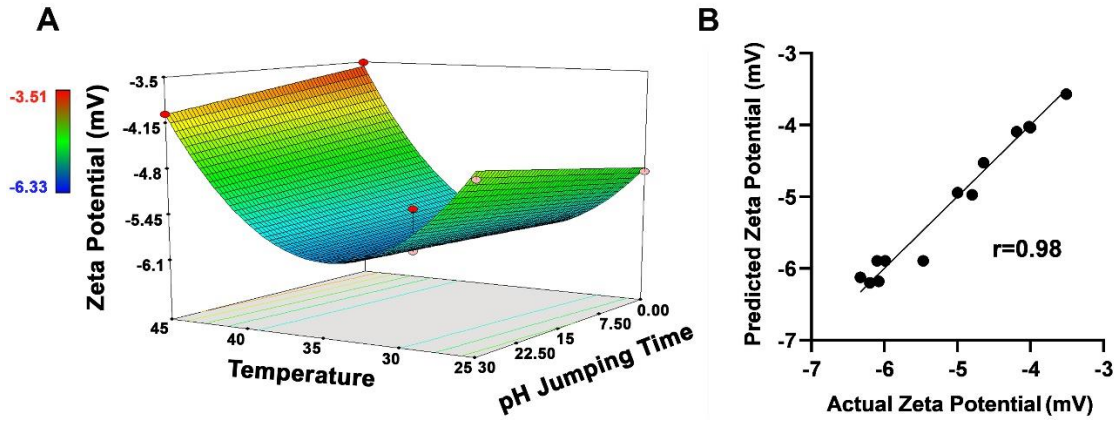

Figure 3.6. Response surface and regression analysis for zeta potential (iteration A). (A) Response surface plot corresponding zeta potential (mV). Pink points indicate the local maxima and minima for particle size. Red points indicate the desired points for zeta potentials. (B) The 13-point model accurately predicts zeta potential of NPs with respect to observed values.

3.1.3.3. PDI

NPs prepared following iteration A demonstrated PDI values ranging from 0.5 to 1, indicating heterogeneous size distributions (Figure 3.7).

The ANOVA and quadratic effects were applied to PDI values. In ANOVA table (Table 3.4), the quadratic model was significant, and the lack of fit value of 0.8612 was not significant relative to pure error. The predicted R^2 of 0.8293 was in reasonable agreement with the adjusted R^2 of 0.8889, indicating the model for PDI is applicable.

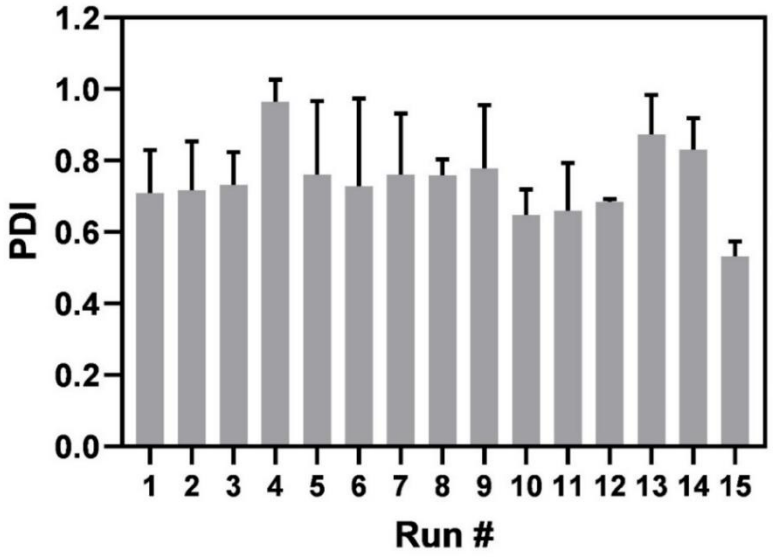

Figure 3.7. PDI of different runs from the experiments performed following Iteration A.

Table 3.4. ANOVA results analyzed by response surface reduced quadratic model for PDI.

Source	Sum of Squares	df	Mean Square	F Value	p-value Prob > F	
Model	0.084	7	0.012	14.72	0.0046*	**significant**
A-Temperature	0.0034	1	0.0034	4.12	0.0981	
B - pH jump time	0.0077	1	0.0077	9.39	0.0280*	
C- Equilibration time	0.014	1	0.014	17.59	0.0085*	
AxC	0.0045	1	0.0045	5.47	0.0664	
BxC	0.0036	1	0.0036	4.45	0.0888	
A^2	0.013	1	0.013	15.63	0.0108*	
B^2	0.0094	1	0.0094	11.49	0.0195*	
Lack of Fit	0.0011	3	0.00037	0.24	0.8612	**not significant**
Pure Error	0.003	2	0.0015			

Notes: R-Squared=0.9537 ; Adj R-Squared = 0.8889 ; Pred R-Squared = 0.8293

In this model, pH jumping time and equilibration time showed main effect on PDI, while temperature and pH jumping time had quadratic effects (Table 3.4, Figure 3.8A). In addition to the response surface plot, predicted and actual PDI values were in a good assignment (Pearson correlation r = 0.97) (Figure 3.8B).

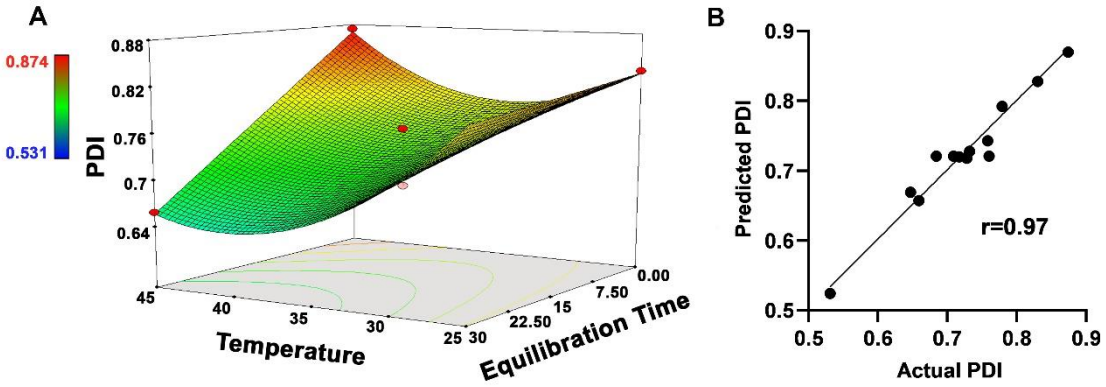

Figure 3.8. Response surface and regression analysis for PDI (iteration A). (A) Response surface plot corresponding PDI. Pink points indicate the local maxima and minima for particle size. Red points indicate the desired points for PDI. (B) The 13-point model accurately predicts PDI values with respect to observed values.

3.1.3.4. Confirmation Experiment for Iteration A

To validate the robustness and accuracy of the developed prediction models, a confirmation experiment was performed following the solution for iteration A, setting the particle size to 20 nm, maximizing zeta potential, and minimizing PDI values. For this purpose, NPs were prepared at 38°C under continuous sonication with 2.31 min for pH jumping time and 30 min for equilibration time in triplicates. Then, NPs were analyzed for their physicochemical properties by Zeta-sizer.

Twenty-three nm-in-sized, negatively charged, and polydisperse NPs were achieved (Table 3.5). As the mean of particle size and zeta potential values were in the interval of 95% predictive interval (PI) low and 95% PI high, the prediction models for

particle size and zeta potential were a good fit with experimental data, except for PDI, resulting polydisperse population due to coagulative properties of polymeric material (APS).[84] Overall, the optimum operation parameters for obtaining 20 nm-sized NPs were 38°C for operation temperature, 2.31 min for pH jumping time, and 30 min for equilibration time. pH jumping time and equilibration time were also consistent with the operation parameters for forming lipid nanoparticles.[70,85]

Table 3.5. Model predictions and experimental values of particle size (nm), zeta potential (mV) and PDI values for the NP operation parameters. PI: Predictive Interval.

	Particle Size (nm)	**Zeta Potential (mV)**	**PDI**
Run 1	32.7 ± 14.7	-6.39 ± 0.77	0.684
Run 2	11.7 ± 6.4	-5.95 ± 1.49	0.659
Run 3	23.7 ±7.7	-5.98 ± 0.29	0.899
Mean	**22.7 ± 9.6**	**-6.11 ± 0.25**	**0.747**
95% PI low	15.58	-6.49	0.45
95% PI high	25.05	-5.05	0.63

3.1.4. Optimization of Material Concentrations in NPs

After the optimization of operation conditions for NP preparation, the effects of material concentrations on NP formation were investigated and optimized through BBD analysis tool. Fifteen runs, three factors at two levels (3^2), with three replicates at the center point, were set up and analyzed in terms of particle size, zeta potential, and entrapment efficiency (EE) of AST VII (iteration B). The entrapment efficiency of MPLA was excluded from the model due to out of the detection limit of MPLA in RP-HPLC.

3.1.4.1. Particle Size

NPs were prepared following the conditions given in iteration B, and each run was separated by an Amicon centrifugal filter (MWCO: 100 kDa) for further particle size analysis by Zeta-sizer. Seven to 25 nm, 5 to 53 nm, and 18 to 116 nm-sized NPs were prepared in the conditions of no MPLA, MPLA with 50 μg/mL, and MPLA with 100 μg/mL, respectively (Figure 3.9).

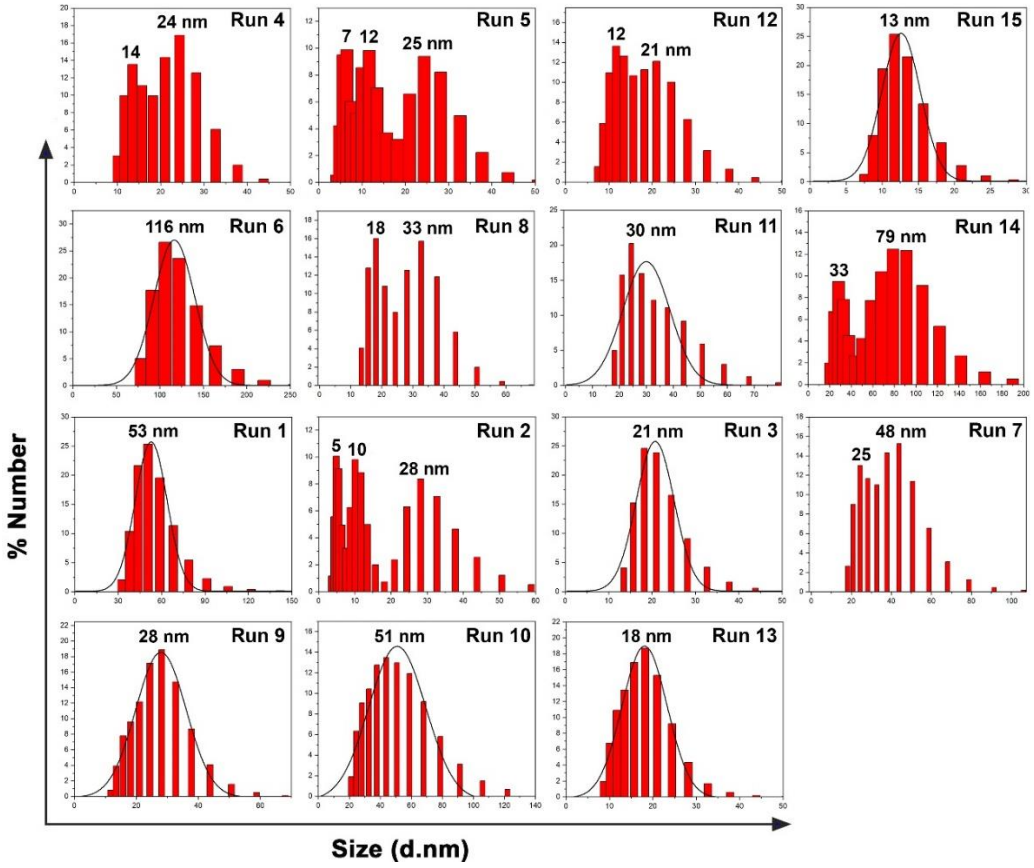

Figure 3.9. The particle size distributions obtained from the experiments following iteration B. Represented distribution graphs demonstrated the average of triplicate measurements.

The linear model was selected to give the highest-order polynomial where additional terms are not significant, and the model was not aliased. In the ANOVA table (Table 3.6), the *p*-value for the reduced linear model is 0.0034, lower than 0.05, showing the mathematical model for particle size was significant. The "Lack of Fit-F value" of 0.6139 implied no significant lack of fit value, which was desirable in the model.

Table 3.6. ANOVA results analyzed by response surface linear model for NP particle size (nm) in Iteration B.

Source	Sum of Squares	df	Mean Square	F Value	p-value Prob > F	
Model	0.0038	1	0.0038	12.73	0.0034*	**significant**
B–MPLA Concentration	0.0038	1	0.0038	12.73	0.0034*	
Lack of Fit	0.0033	11	0.0003	0.96	0.6139	**not significant**
Pure Error	0.0006	2	0.0003			

Notes: R-Squared=0.4947 ; Adj R-Squared = 0.4558 ; Pred R-Squared = 0.3632

In this model, only MPLA concentration had a statistically significant effect on the particle size of NPs (Table 3.6, Figure 3.10A). Despite the variations in the actual and predicted particle size (Pearson correlation r = 0.78) (Figure 3.10B), the modest predictive model for particle size (adjusted R^2 = 0.46) could be derived to predict the responses. In the preparation steps, the fluidity of the hydrophobic tails of MPLA increases at the applied temperature (60°C), which facilitates the lipid structures to curl into the core of APS-based nanoparticles.[70] Increasing the concentration of MPLA provided a chance to curl more MPLA into the core of nanoparticles, resulting an increase in the particle size of NPs.

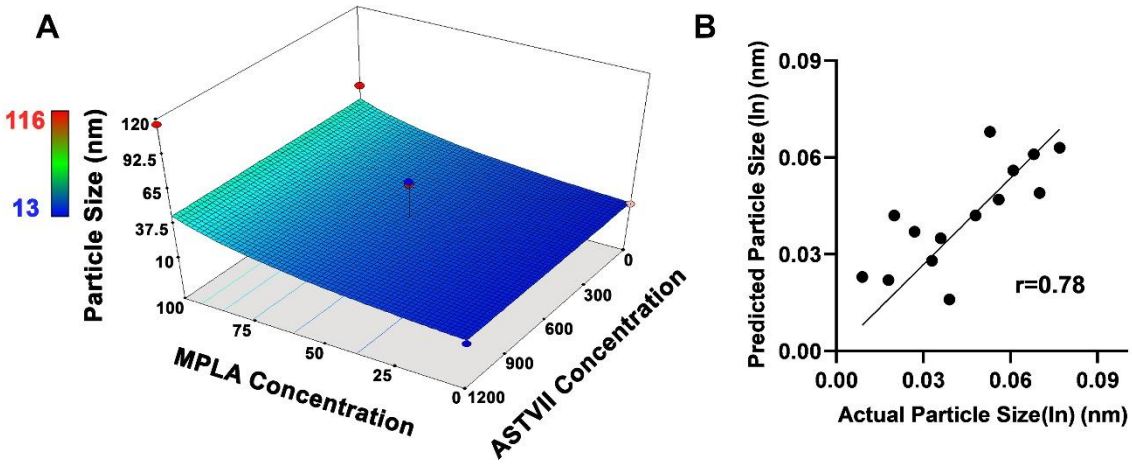

Figure 3.10. Response surface and regression analysis for particle size (iteration B). (A) Response surface plot corresponding particle size (nm). (B) The 14-point model accurately predicts particle size with respect to observed values.

3.1.4.2. Zeta Potential

NPs were prepared following iteration B and the zeta potential of each run was measured by Zeta-sizer. NPs showed varying zeta potentials from -8 to -11 mV (Figure 3.11).

ANOVA and linear model were used to evaluate the main and interaction effects of each factor in iteration B. In the ANOVA table (Table 3.7), the p-value for the reduced linear model is 0.0026 and the lack of fit values (0.1894) was desirable in this model.

In this model, only MPLA concentration had a statistically significant effect on the zeta potential of NPs (Table 3.7, Figure 3.12A). Because of the amphiphilic nature of phospholipids,[86] the hydrophobic lipid tails can intercalate with the inner core of APS-based NPs and extend their phosphate head groups to the external surface of the NPs. Therefore, increasing the concentration of MPLA in the solution resulted in an increase of NP's zeta potential. Moreover, the linear model for zeta potential provided modest prediction (adjusted R2 = 0.54) with moderately fitted response in actual and predicted zeta potential (Pearson correlation r = 0.76) (Figure 3.12B).

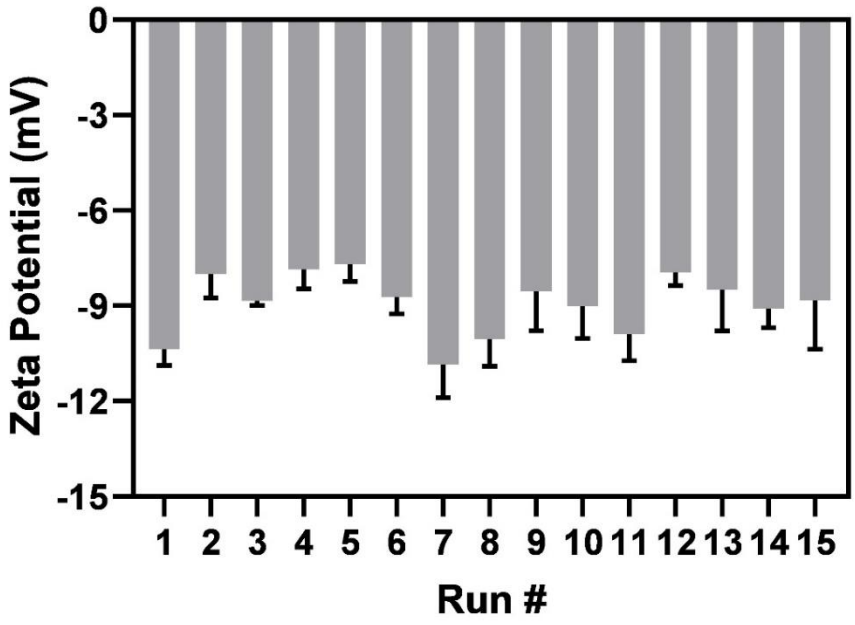

Figure 3.11. The zeta potentials (mV) of different runs from the experiments performed following iteration B.

Table 3.7. ANOVA results were analyzed using a response surface reduced linear model for zeta potential (mV) in iteration B.

Source	Sum of Squares	df	Mean Square	F Value	p-value Prob > F	
Model	3.66	1	3.66	14.96	0.0026*	**significant**
B – MPL Concentration	3.66	1	3.66	14.96	0.0026*	
Lack of Fit	2.67	10	0.27	16.51	0.1894	**not significant**
Pure Error	0.016	1	0.016			

Notes: R-Squared=0.5762 ; Adj R-Squared = 0.5377 ; Pred R-Squared = 0.3764

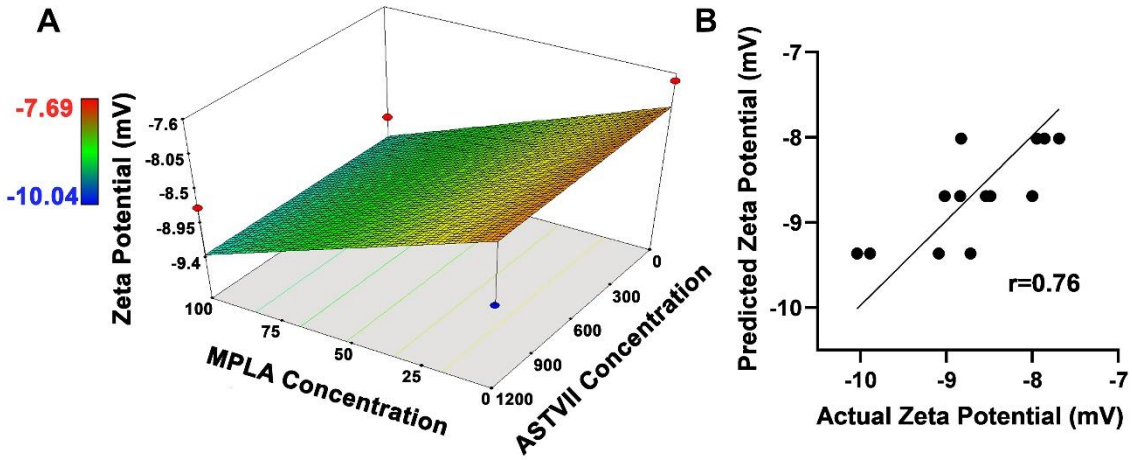

Figure 3.12. Response surface and regression analysis for zeta potential (iteration B). (A) Response surface plot for zeta potential (mV). (B) The 13-point model accurately predicts zeta potential with respect to observed values.

3.1.4.3. PDI

Some of the nanoparticles prepared in accordance with iteration B demonstrated lower PDI values than 0.05, indicating homogeneous size distributions (Figure 3.13). When the PDI values were analyzed by ANOVA in BBD design, there was no direct correlation between the main and interactive factors in iteration B. Therefore, BBD did not produce a model, and PDI was excluded from the response in the confirmation experiment.

3.1.4.4. Quantification of AST-VII and MPLA in NPs

NPs were prepared following iteration B, centrifuged using Amicon centrifugal filters (MWCO: 100 kDa), and finally, the sample filtrate was collected to quantify AST-VII and MPLA by RP-HPLC through indirect methodology.

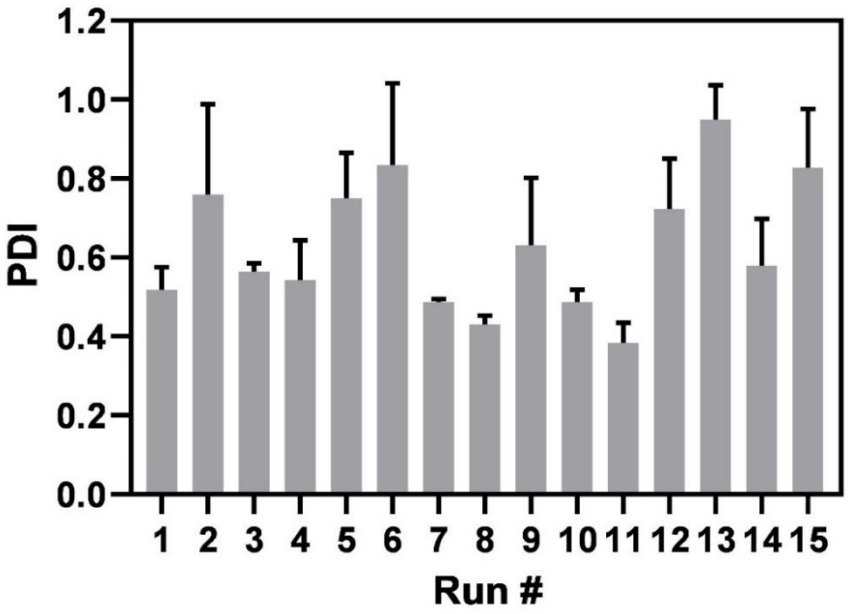

Figure 3.13. PDI of different runs from the experiments performed following Iteration B.

To detect AST-VII, the Chromolith RP-C18 column was used with the following gradient flow of mobile phases, ultrapure water, and acetonitrile, and subsequently, AST-VII was detected using a DAD detector in the 203, 210, and 254 nm wavelengths. In the HPLC chromatograms, AST-VII eluted as a single peak with a retention time of 5.32 min, while the peak seen at 2.1 min was assigned as a solvent peak (UPW) (Figure 3.14). In the HPLC chromatogram, the peak area for AST-VII was estimated, and the entrapment efficiencies (EE %) of AST-VII for each run were calculated (Figure 3.15). The considerable EE for AST-VII was achieved in Run 4 (APS: 2000 μg/mL, No MPLA), Run 2 (APS: 2000 μg/mL; MPLA: 50 μg/mL) and Run 6 (APS: 1250 μg/mL; MPLA: 100 μg/mL) as 57.2 %, 52.9%, and 53.5 %, respectively.

To investigate the main and interaction effects of each factor on the EE of AST-VII, ANOVA and 2FI models were used. The insignificant terms were excluded from the 2FI model, and the model was modified. In the ANOVA table, the model was significant ($p = 0.0009$), and AST-VII concentration, the pairwise interaction between APS and MPLA has shown a statistically significant effect on the EE (%) of AST-VII (Table 3.8) (Figure 3.16A). Moreover, the predicted and actual values for EE of AST-VII were fitted (Pearson correlation $r = 0.86$) (Figure 3.16B) in the robust predicted model (adjusted $R2 = 0.79$). By keeping APS concentration constant, increasing MPLA concentration in NP

also increased the entrapment efficiency of AST VII. AST-VII is also an amphiphilic compound, so MPLA may provide a lipophilic core to integrate more AST-VII into NP by interacting with the aglycone backbone of AST-VII.

Triterpenoid and steroidal saponin could form a stable complex with cholesterol in the cell membrane and generally cause hemolysis.[87] Inspired by this phenomenon, the lipophilic structures were integrated into the nanoparticle formulations when saponins were involved in the NP structures. Consistent with our previous results, AST-VII integrated APS nanocarriers could not protect its structure without a lipophilic compound, resulting in the nanoparticle's dissipation. These results also implied the importance of MPLA in MA-NP formation.

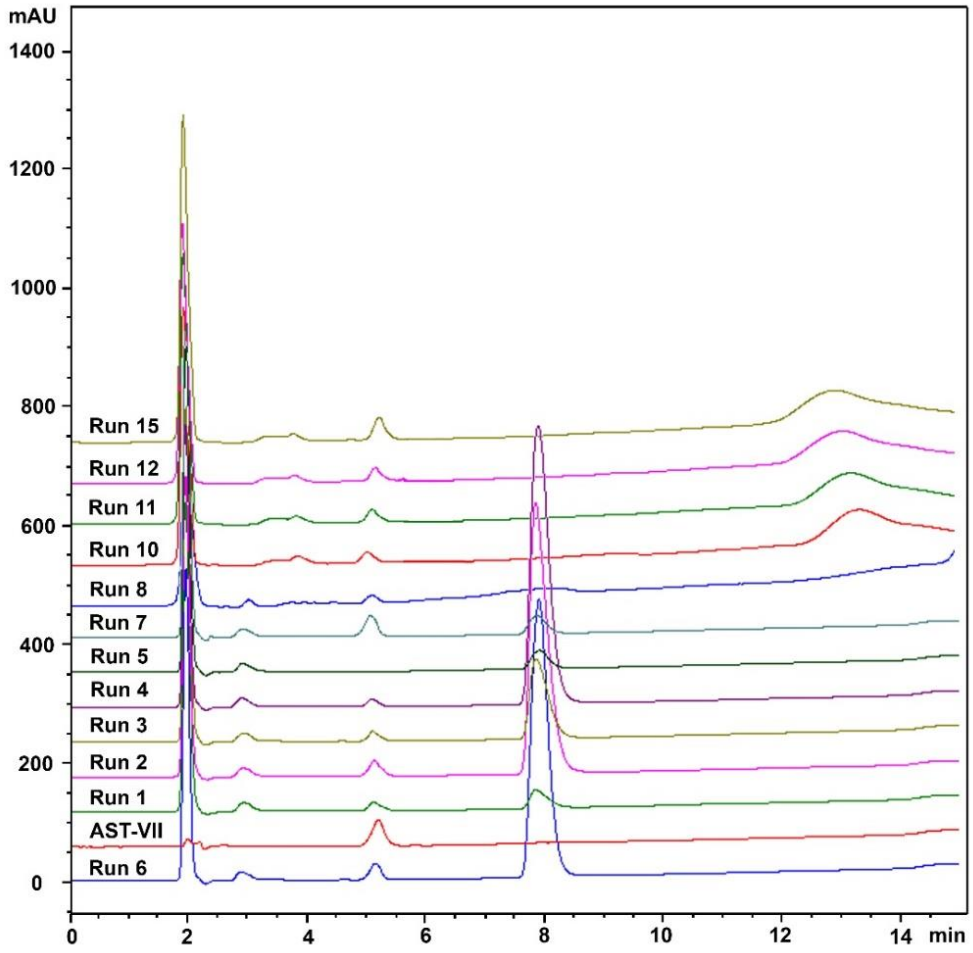

Figure 3.14. HPLC-DAD chromatograms of MA-NP adjuvant systems were prepared following iteration B and AST-VII standard (1000 ppm) at 210 nm.

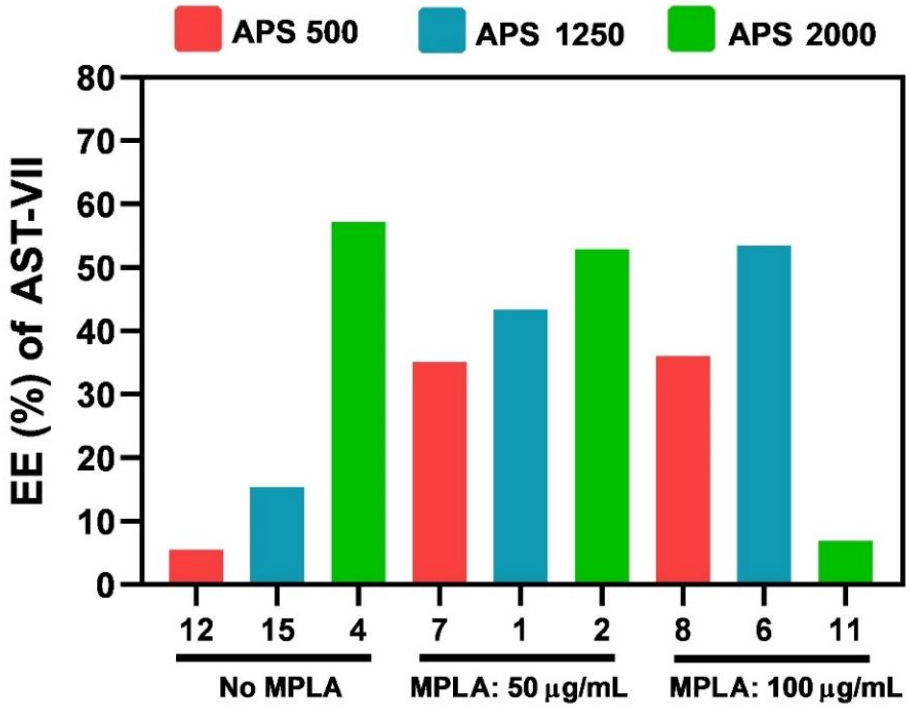

Figure 3.15. The entrapment efficiency (EE %) AST-VII in MA-NP adjuvant systems prepared following iteration B.

Table 3.8. ANOVA results were analyzed using the response surface reduced 2FI model for EE (%) of AST-VII in Iteration B.

Source	Sum of Squares	df	Mean Square	F Value	p-value Prob > F	
Model	5863.67	4	1465.92	12.89	0.0009*	**significant**
A- APS Concentration	203.41	1	203.41	1.79	0.2140	
B- MPLA Concentration	40.99	1	40.99	0.36	0.5631	
C- ASTVII Concentration	4015.47		4015.47	35.30	0.0002*	
AxB	1632.97	1	1632.97	14.36	0.0043*	
Lack of Fit	385.61	7	55.09	0.17	0.9672	**not significant**
Pure Error	638.19	2	319.10			

Notes: R-Squared=0.8514 ; Adj R-Squared = 0.7853 ; Pred R-Squared = 0.7675

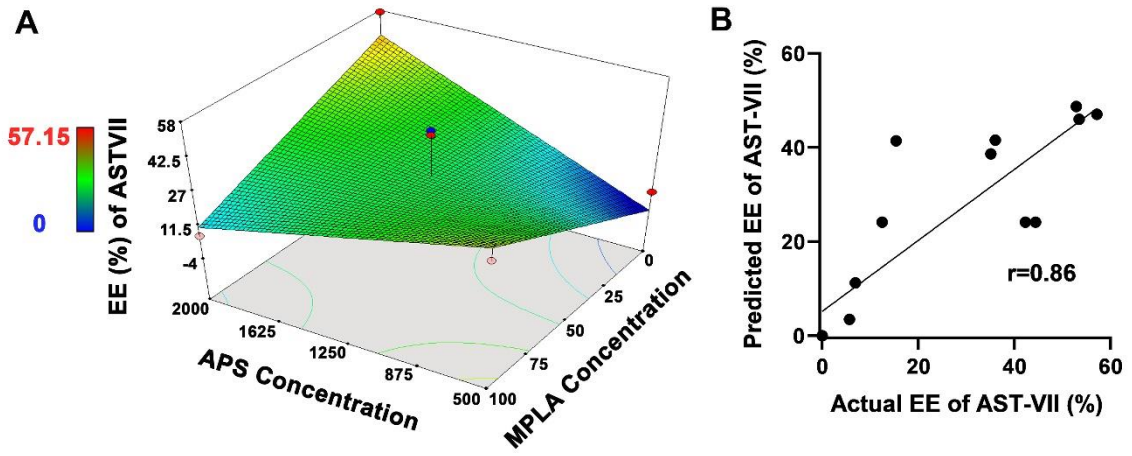

Figure 3.16. Response surface and regression analysis for EE of AST-VII (iteration B). (A) Response surface plot for EE (%) of AST-VII. (B) The 13-point model accurately predicts EE of AST-VII with respect to observed values.

Besides quantifying AST-VII, the DAD detector was also used to detect MPLA, but MPLA did not detect below the 100 µg/mL concentration. An ELSD (Evaporative Light Scattering Detector) detector was used in the RP-HPLC system to quantify MPLA in low concentrations. ELSD is compatible with most solvents and chromatographic techniques employing gradient elution; it is sensitive and capable of detecting any compound as long as it is less volatile than the mobile phase. Moreover, the ELSD detector has high sensitivity and applicability for different classes of lipophilic compounds.[88]

MPLA standard (250 ppm) and Run 1 obtained from iteration B, a representative MA-NP sample, were analyzed in RP-HPLC-ELSD. The peak that appeared in 3.44 min both in MPLA and Run 1 samples was assigned as the solvent peak, which is PBS (Figure 3.17). The corresponding peak for MPLA was seen in 13.1 min. However, no peak corresponding to MPLA was observed in Run 1 or the other runs.

An attempt was made to degrade MA-NP to release MPLA for further quantification in RP-HPLC. For this purpose, two different methodologies were followed. MA-NPs were dissolved in acetonitrile or 1 % acetic acid containing UPW and extracted with chloroform for analysis in HPLC-ELSD. Unfortunately, the MPLA peak did not appear in HPLC-ELSD chromatograms.

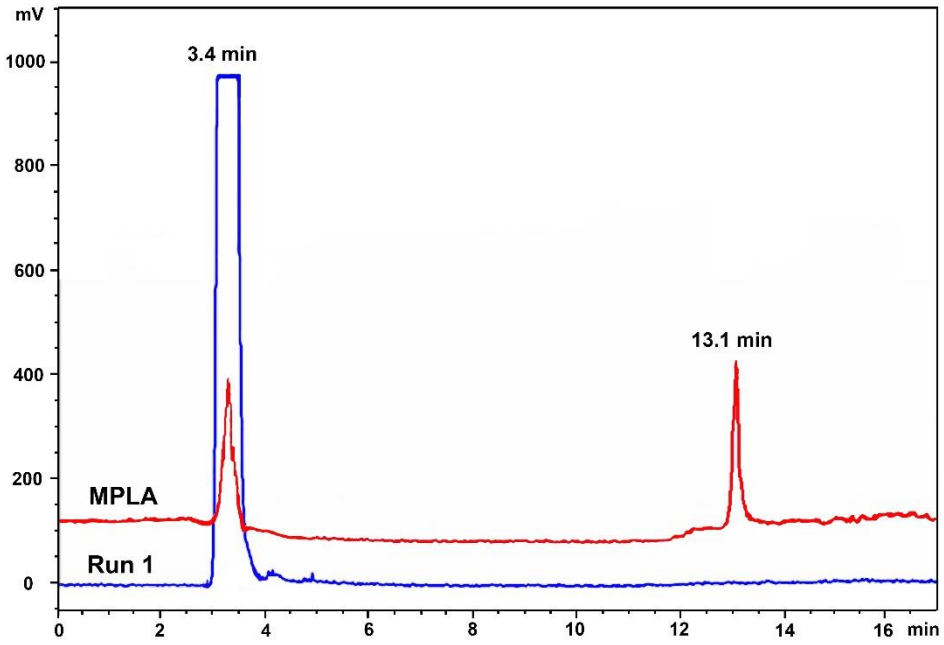

Figure 3.17. HPLC-ELSD chromatograms of Run 1 prepared following iteration B and MPLA standard (250 ppm) at 65°C drift tube temperature and gain 11.

The failure in the detection of MPLA using NP disruption methodology led to think that the very low amount of MPLA in the samples might fall below the detection limit of ELSD. Therefore, the spiking methodology was followed. Spiking in analytical chemistry refers to adding a known amount of a known substrate to a sample.[89] To evaluate the performance of the methodology, 25 ppm of MPLA standard was added into 25 ppm MPLA, and the spiked standard was analyzed in RP-HPLC-ELSD. After HPLC analysis, the amount of MPLA in the spiked MPLA standard (final 50 ppm) was calculated as 47.1 ppm based on HPLC-ELSD chromatograms. The recovery (%) was calculated according to the formula given below (3.1). The corresponding recovery was 88.4 %, which is in the acceptable range (80-120 %)(Table 3.9).[89] It was decided to apply the spiking methodology in NP samples for further MPLA quantification.

$$Recovery\ (\%) = \frac{C\ spiked\ sample - C\ unspiked\ sample}{C\ add} \qquad (3.1)$$

Table 3.9. Calculation for the recovery (%) of spiked MPLA standard.

After spike	C spiked	C unspiked	C add	Recovery (%)
MPL 25 ppm +25 ppm (50 ppm)	47.1 ppm	25 ppm	25 ppm	88.4

3.1.4.5. Confirmation Experiment for Iteration B

The confirmation experiment was conducted to obtain 20-50 nm in sized, negatively charged particles with a maximum EE % of AST-VII. NPs were prepared with given material concentrations (Table 2.6) and optimized operation conditions. After preparation and collection of NPs, the physicochemical properties of NPs were evaluated by Zeta-sizer, and the entrapment efficiency of AST-VII was analyzed by RP-HPLC-DAD.

Thirty-two nm and 40 nm-sized NPS were obtained following the methodology given in solution 1 (Sol 1) and solution 6 (Sol 6), respectively (Figure 3.18A). Negatively charged NPs (-19.3 for Sol1, -18.7 for Sol6) were obtained, demonstrating that the zeta potential of NPs was maximized (Figure 3.18B). The EE of AST-VII were 47.5 % and 39 % for Sol 1 and Sol 6, respectively (Figure 3.18C). NPs prepared in Sol 1 (C_{APS}: 2000 μg/mL, C_{MPLA}: 31 μg/mL) provided a statistically significant increase in the entrapment of AST-VII than NPs prepared in Sol 6 (C_{APS}: 500 μg/mL, C_{MPLA}:84 μg/mL).

The model predictions and experimental values for each response are given in Table 3.11. Based on these results, the average values of particle size and the EE % AST VII were 95% PI low and 95% PI high in both optimal conditions and maximizing the zeta potential of NPs. Overall, Sol1 was chosen for optimal conditions in NP preparation as it showed smaller particle size, higher zeta potential, and EE % of AST-VII compared to Sol 6.

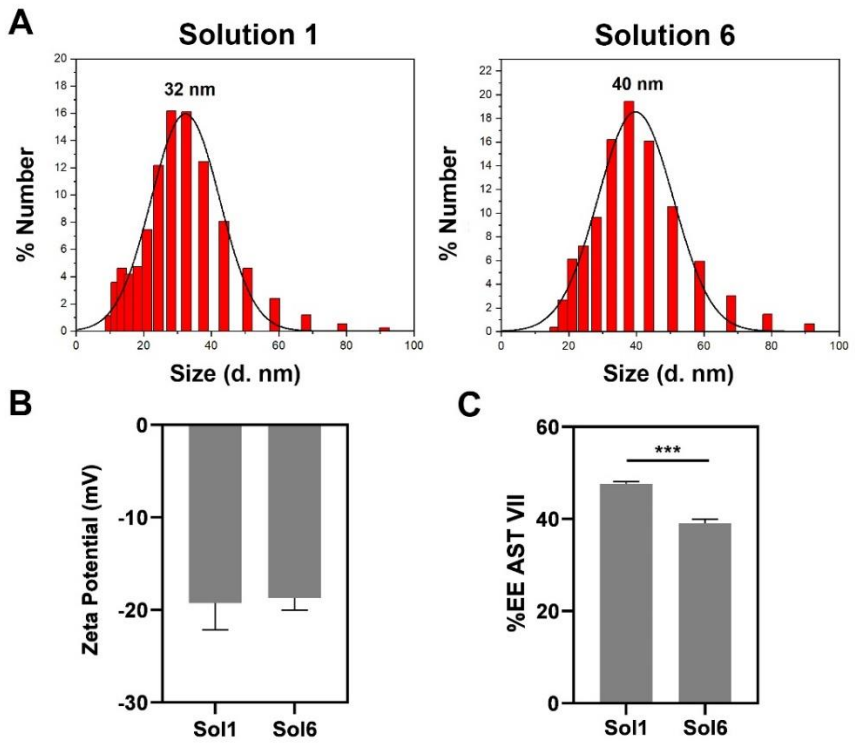

Figure 3.18. The physicochemical characterization of NPs prepared in iteration B. (A) The particle size distribution and (B) zeta potential of NPs prepared with Solution 1 (Sol1) and Solution 6 (Sol6 (C) EE (%) of AST-VII in NPs analyzed by RP-HPLC-DAD. Statistically significant differences between Sol1 and Sol6 were analyzed using the Student's-test. ***$p \leq 0.001$.

Table 3.10. Model predictions and experimental values of particle size (nm), zeta potential (mV), and EE % AST-VII for iteration B. PI: Prediction Interval.

	Particle Size	**Zeta Potential**	**EE % ASTVII**
Solution 1	**32 ± 20.3 nm**	**-19.3 ± 2.9 mV**	**47.55 ± 0.55**
95% PI low	11.93	-9.57	18.46
95% PI high	73.50	-7.30	92.48
Solution 6	**40 ± 22.3 nm**	**-18.7 ± 1.3 mV**	**39 ± 0.92**
95% PI low	24.43 nm	-10.32	15.55
95% PI high	62.93	-8	92.92

To quantify MPLA in Sol1, the spiking methodology was applied. As the recovery of spiked MPLA standard (88.4 %) was in the acceptable recovery range, 25 ppm MPLA was added to the samples. The samples were analyzed by RP-HPLC-ELSD, and the amount of MPLA was estimated based on the ELSD area in the HPLC chromatogram. Finally, the EE of MPLA in Sol1 was calculated as 99.22 %.

3.1.5. Preparation of Blank NP, MPLA NP, and AST-VII NP

Blank NP, MPLA NP, and AST-VII NP were also prepared following a methodology optimized for MA-NP adjuvant system and subsequently characterized for their physicochemical properties. According to DLS analysis, 10-27 nm in sized NPs, blank NP (23 ± 21 nm), AST-VII NP (9.4 ± 6.5 nm), MPLA NP (27.4 ± 25 nm) and MA-NP (21 ± 20 nm), were obtained (Figure 3.19A). The incorporation of MPLA into NPs increased the particle size, while the addition of AST-VII into NPs decreased the particle size of NPs.

There was no statistically significant difference in the zeta potential of NPs (-19 to -20 mV) in terms of whether a single immunostimulating agent (MPLA or AST-VII) was present or not in NPs. However, the integration of both MPLA and AST-VII into NPs significantly decreased the zeta potential (-16 mV) (Figure 3.19B). Moreover, the EE of AST-VII in AST-VII NP and MA-NP was calculated as 8.4 % and 67.2 %, respectively (Figure 3.19C). As clearly indicated that MPLA and AST-VII interaction affected the entrapment of AST-VII into NPs in the Box-Behnken model, the absence of MPLA resulted in a decrease in the EE of AST-VII. Consistent with BBD model, the presence of MPLA in NPs by interacting with AST-VII provided the entrapment of AST-VII into NPs more effectively than NPs prepared without MPLA. Therefore, MPLA in NPs maximized the EE of AST-VII. Lastly, the morphology of each NP was examined by scanning electron microscopy (SEM). All NP adjuvant systems produced spherical-elliptical structures (Figure 3.19.D). Overall, all NP combinations were successfully prepared following optimized conditions and characterized.

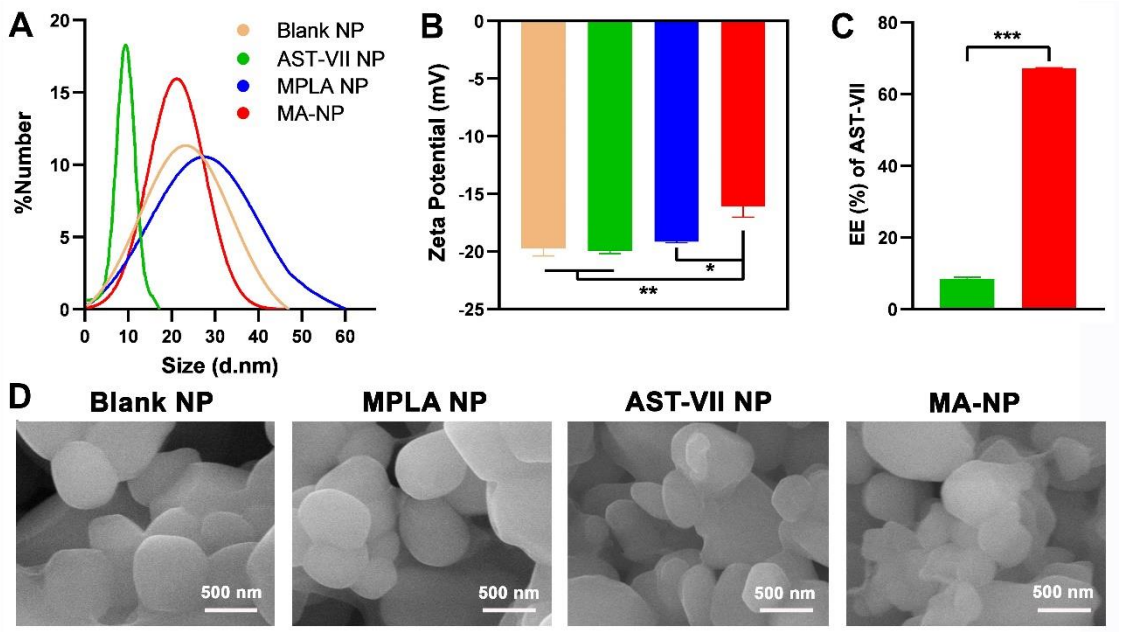

Figure 3.19. The physicochemical characterization of blank NP, MPLA NP, AST-VII NP, and MA-NP. (A) The particle size distributions and (B) zeta potentials of NPs were analyzed by Zeta-sizer, (B) Entrapment efficiency (EE) (%) of AST-VII in AST-VII NP and MA-NP was calculated in terms of the peak area in HPLC-DAD chromatograms, (D) the morphology of NPs were examined by SEM. Data are shown as the mean ± SEM of two independent experiments. Data were analyzed by one-way ANOVA (C) with Tukey's multiple comparison test and Student-t test (D) *p ≤ 0.05, **p ≤ 0.01, ***p ≤ 0.001.

3.1.6. Integration of Antigens into Adjuvant Systems

Therapeutic and prophylactic cancer vaccination aims to activate and augment anti-tumor T cell immunity by providing antigenic and costimulatory signals to professional antigen-presenting cells (APCs).[90] Free soluble vaccines exhibited limited efficiency due to the rapid clearance of free antigens upon *in vivo* administration and poor co-delivery of antigens and adjuvants to APCs. At this point, NP-based delivery systems provide improved pharmacological properties, targeted delivery, and controlled and localized release of immunomodulatory agents and antigens for the efficient modulation

of specific immune cells.[91] In light of this information, MA-NP adjuvant systems combined with several peptide antigens such as $OVA_{257-264}$ peptide, tyrosinase-related protein 2 ($Trp\text{-}2_{180-188}$), and pan DR T-helper epitope (PADRE) to furtherly evaluate their anti-tumor activities.

3.1.6.1. Integration of $OVA_{257-264}$ Peptide

$OVA_{257-264}$ peptide, SIINFEKL, which is CD8 T cell epitope[92] was used as a model antigen to evaluate the antigen adsorption capacity of MA-NP adjuvant system as well as the anti-tumor efficacy of MA-NP adjuvant systems in murine B16-OVA model.

SIINFEKL peptide is neutrally charged in physiological pH (Figure 3.20). Considering the positively and negatively charged state of SIINFEKL in an acidic and alkaline environment (Figure 3.20), an antigen adsorption experiment was conducted at various pH levels (3,5,7,9).

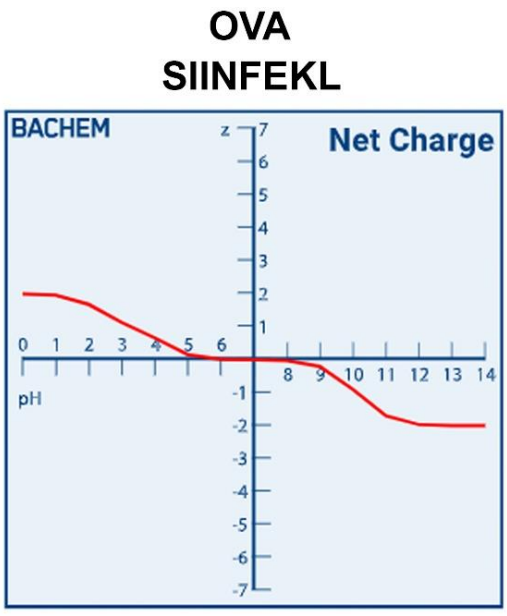

Figure 3.20. pH vs net charge isotherms for $OVA_{257-264}$ (SIINFEKL) peptide.[93]

Moreover, the effect of antigen concentration on the adsorption capacity of MA-NP was also investigated with respect to different peptide concentrations (5, 10, and 20 μg). Following incubation of MA-NP adjuvant system with SIINFEKL peptide, the entrapment efficiency of SIINFEKL in MA-NP was measured by BCA assay.

Considerable entrapment efficiencies were obtained in PBS solution at pH 3 with SIINFEKL concentration at 5 μg (76 %) and 10 μg (74 %) (Figure 3.21). When the SIINFEKL concentration was kept constant, there was a statistically significant increase in the entrapment efficiency of SIINFEKL at pH 3 compared to other pH levels. Even if SIINFEKL concentration was increased to 20 μg, the EE % of SIINFEKL decreased compared to other SIINFEKL concentrations at the pH 3.

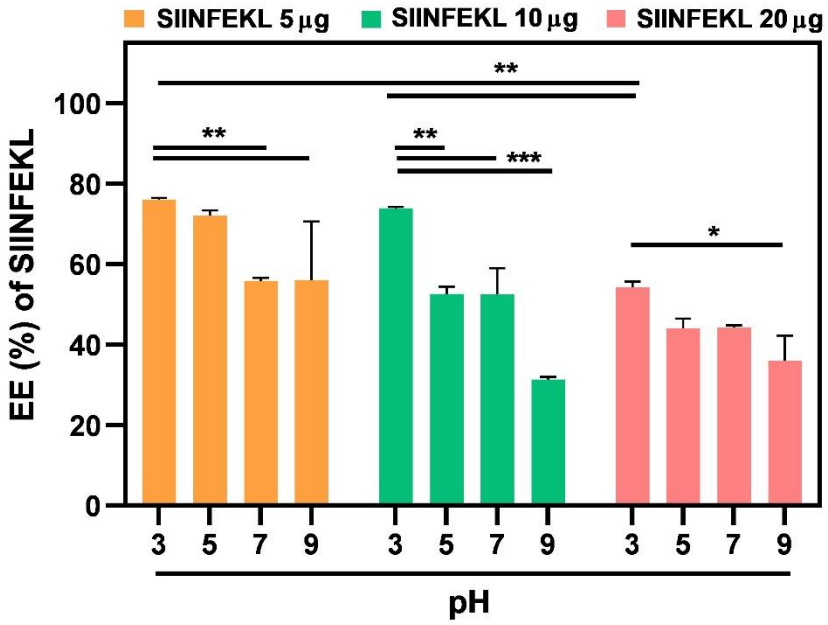

Figure 3.21. The entrapment efficiency (EE) (%) of SIINFEKL in MA-NPs in terms of different pH (3,5,7,9) and peptide concentrations (5, 10, and 20 μg). Data are shown as the mean ± standard deviation of triplicates. Statistically significant differences between groups were analyzed by Two-way ANOVA and Tukey's multiple comparisons test. *$p \leq 0.05$, **$p \leq 0.01$, ***$p \leq 0.001$.

As SIINFEKL at pH 3 has a positive net charge, and MA-NPs were negatively charged, promoting electrostatic interaction between SIINFEKL and MA-NPs.

Consequently, the adsorption of SIINFEKL at pH 3 surpassed that at other pH levels due to the attraction of oppositely charged materials.

In order to obtain more information about the location of the SIINFEKL peptide, the zeta potential measurements were performed as a function of the peptide concentration and pH of the solution. If the peptide is preferentially located inside the particles or if the positively charged peptide is fully neutralized by the negative surface charges of NPs, a more minor change in the zeta potential towards more positive values is to be expected.[94] Blank MA-NPs demonstrated a negative charge in all pH levels. As the highest EE of SIINFEKL was obtained at pH 3, the zeta potential of SIINFEKL adsorbed MA-NPs was compared, and the addition of SIINFEKL peptide at pH 3 resulted in a slight decrease in the zeta potential of MA-NPs (-7.5 to -6.5 mV) towards a positive way (Figure 3.22).

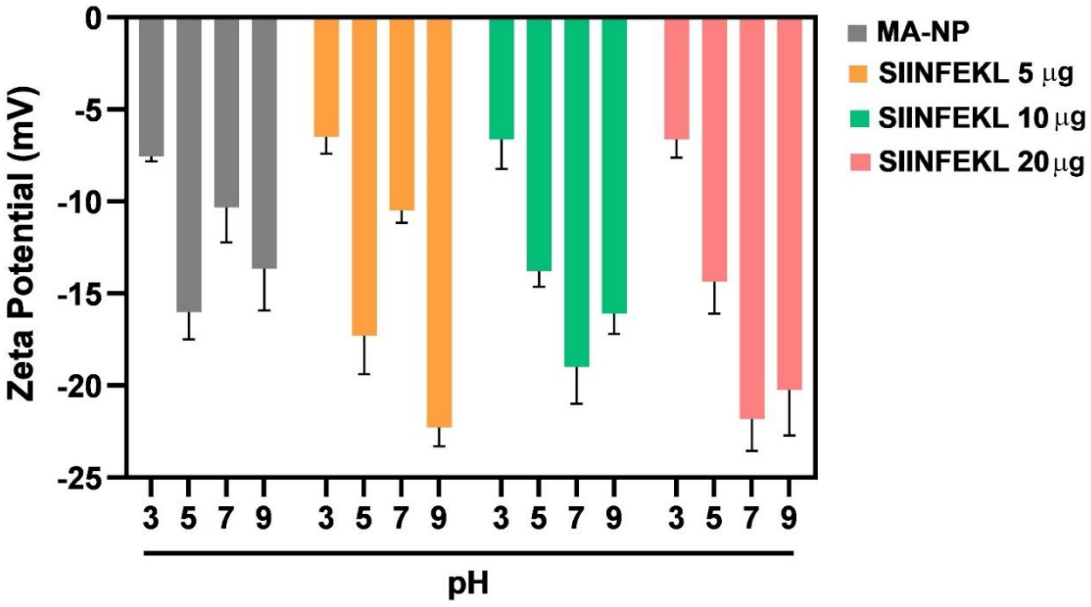

Figure 3.22. The zeta potential of peptide-free MA-NPs and SIINFEKL (5, 10 and 20 µg) adsorbed MA-NPs in different pH levels (pH 3,5,7,9).

It can be concluded that the physical adsorption of SIINFEKL peptide onto negatively charged MA-NPs resulted in the neutralization of negative charges on the surface of MA-NPs. Moreover, when the zeta potential of SIINFEKL (5 µg) adsorbed on

MA-NPs at pH 9 was investigated, the zeta potential was increased to -22.3, possibly due to the contribution of negatively charged SIINFEKL peptide at pH 9. The lowest SIINFEKL adsorptions in MA-NPs were obtained in pH 9, concluding the importance of opposite charges between MA-NPs and peptides for the physical adsorption.

3.1.6.2. Integration of Trp-2 and PADRE Peptides

To provide multi-epitope T cell responses against B16-F10 melanoma model, multiple antigens (multiAgs), melanoma-associated tyrosinase-related protein 2 (Trp-$2_{180\text{-}188}$) (SVYDFFVWL) for CD8 T cell epitope and pan DR T-helper epitope (PADRE**)** (AKFVAAWTLKAAA) for CD4 T cell epitope,[73] were selected and loaded on MA-NP adjuvant system.

The peptide adsorption optimization studies by SIINFEKL peptide demonstrated that the opposite charges between nanoparticle and antigen affected the adsorption efficiency of antigen onto NPs. The zeta potential results showed that all adjuvant systems, including blank NP, MPLA NP, AST-VII NP, and MA-NP, were negatively charged. The Trp-2 peptide is negatively charged at the physiological pH, whereas PADRE peptide is positively charged (Figure 3.23). In light of this information, the peptide adsorption studies on MA-NP were carried out in different Trp-2 and PADRE concentrations (30 and 50 μg) and pH levels (3 and 5).

To evaluate the efficiency of antigen adsorption, free Trp-2 and PADRE peptides were analyzed by RP-HPLC-DAD. In the RP-HPLC-DAD chromatograms, the peaks corresponding to Trp-2 and PADRE were not detected in the MA-NPs solution (Figure 3.24), as the concentrations of the peptides were out of the detection limit of HPLC device. Therefore, a BCA assay was carried out to determine the total antigen concentration in MA-NP.

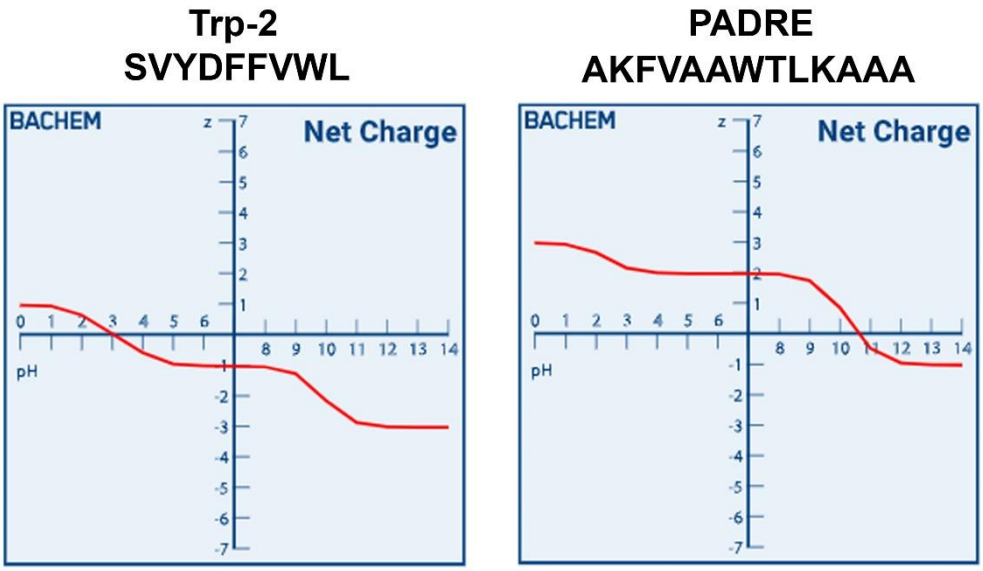

Figure 3.23. pH vs. net charge isotherms for Trp-2 and PADRE peptides.[93]

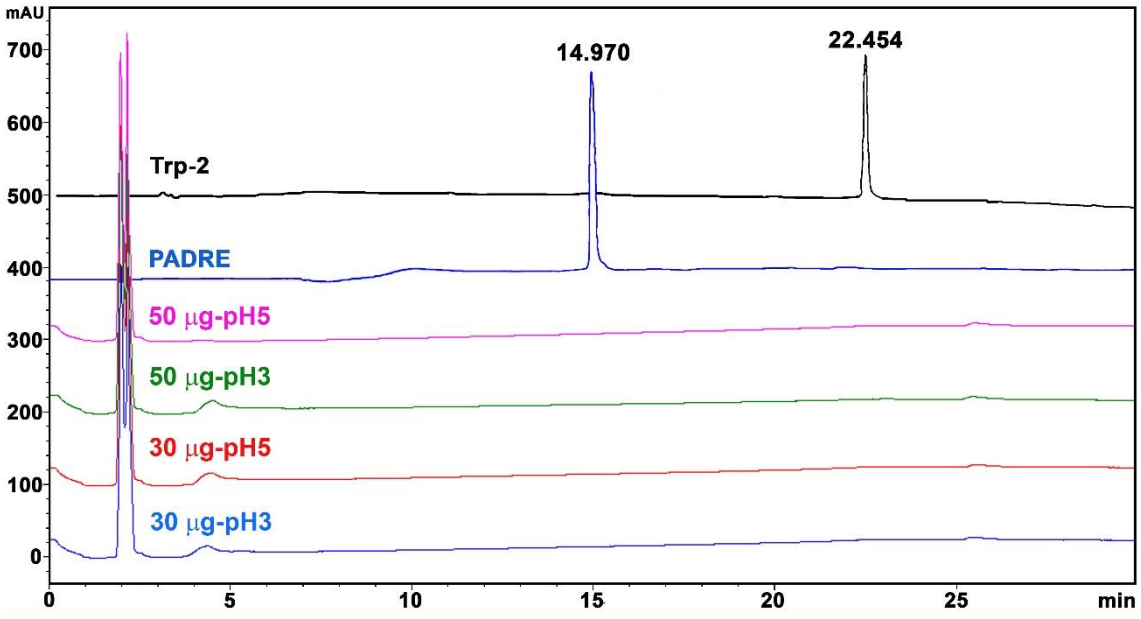

Figure 3.24. RP-HPLC-DAD chromatograms of antigen (Trp-2 and PADRE) adsorbed on MA-NP at different antigen concentrations (30 and 50 μg) and pH levels (3 and 5), Trp-2 and PADRE standards (1000 ppm) at 210 nm.

Based on BCA results, there were no statistically significant differences in the entrapment efficiency of total antigen where the antigen concentration was kept constant. In the case of constant pH (pH 3), MA-NP incubated with 50 μg peptide concentration provided higher entrapment efficiency (73.5 %) compared to 30 μg peptide concentration (60.7 %) (Figure 3.25). Therefore, 50 μg peptide concentration and pH 3 were chosen as optimum conditions for Trp-2 and PADRE integration onto MA-NP.

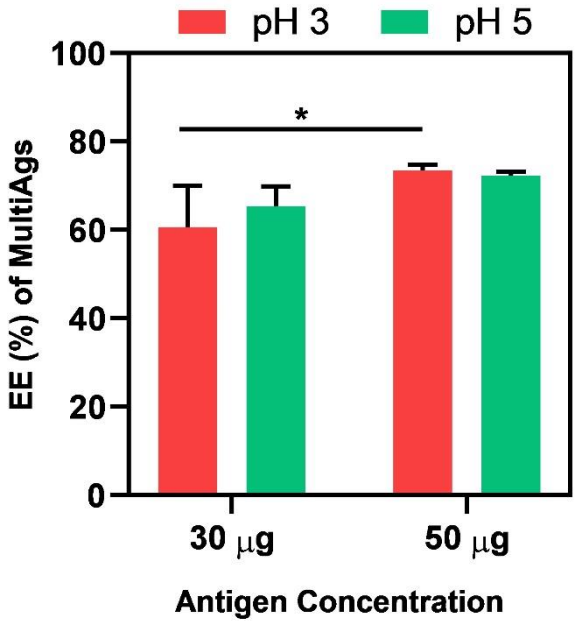

Figure 3.25. The entrapment efficiency (EE) of total antigen (Trp-2+PADRE) adsorbed on MA-NPs at different antigen concentrations (30 and 50 μg) and pH levels (3 and 5). The data was presented as mean ± SEM. The statistically significant differences were shown by Two-way ANOVA Tukey's multiple comparison test. *$p \leq 0.05$.

To prove the physical adsorption of peptides on MA-NP, the zeta potential of peptide-free and peptide-adsorbed MA-NPs was analyzed by Zeta-sizer. Following peptide adsorption, the zeta potential of peptide-adsorbed MA-NPs prepared with 30 μg and 50 μg peptide concentrations at pH 3 were decreased to -3.2 and -2.6 mV from -7.5 (Figure 3.26). In the case of antigen adsorption at pH 5, the zeta potential of peptide-adsorbed MA-NPs prepared with 30 and 50 μg peptide concentrations was -8.7 and -8.4

mV, where free MA-NPs showed -16 mV. Overall, Trp-2 and PADRE peptides neutralized the zeta potential of MA-NPs during the adsorption process at pH 3 due to the net charges of each peptide, which were 0 for Trp-2 and +2 for PADRE. Based on these results, Trp-2 and PADRE peptides were successfully adsorbed onto MA-NP adjuvant system.

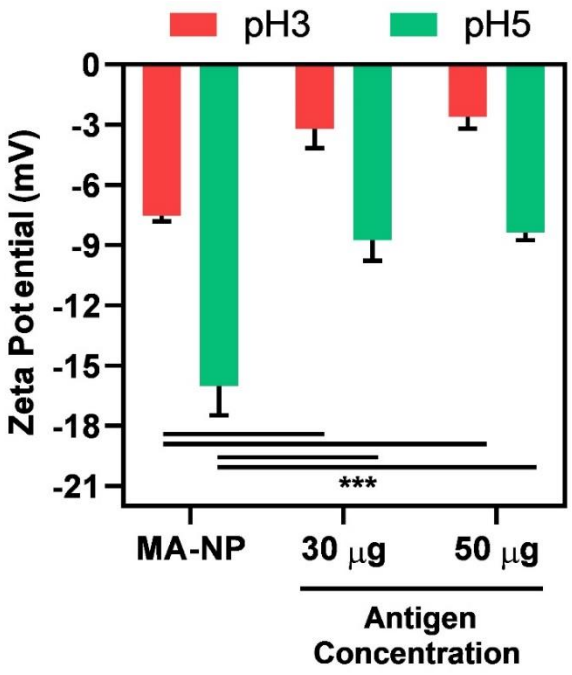

Figure 3.26. The zeta potential of multiAgs-adsorbed on MA-NP adjuvant system at different antigen concentrations and pH levels The data was presented as mean ± SEM. The statistically significant differences were shown by Two-way ANOVA, Sidak's multiple comparison test. ***$p \leq 0.001$.

Following optimization of adsorption conditions for Trp-2 and PADRE peptides, these peptides (50 μg) were loaded on other adjuvant systems at pH 3. Blank NP and MPLA NP demonstrated 85% EE of total antigen, while integration of AST-VII into NPs resulted a decrease in the EE % of total antigen (Figure 3.27). Comparing the zeta potential of multiAgs-free NPs, all adjuvant systems loaded with multiAgs demonstrated a statistically significant decrease in their zeta potential, indicating successful adsorption of multiAgs on the NPs (Figure 3.28).

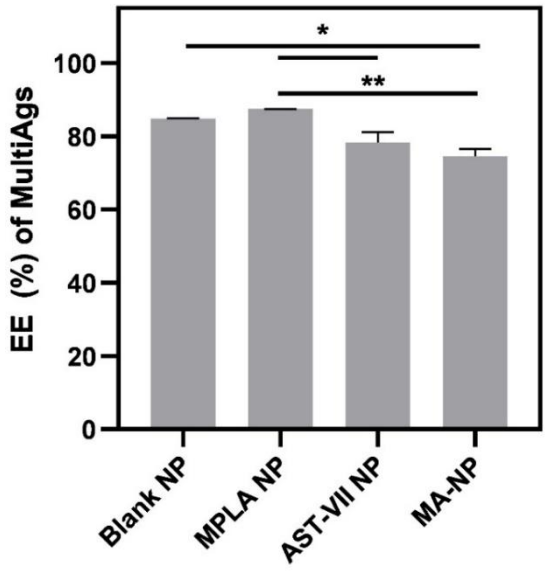

Figure 3.27. The entrapment efficiency of multiAgs-adsorbed NPs. The data was presented as mean ± SEM. The statistically significant differences were shown by One-way ANOVA, Tukey's multiple comparison test. *$p \leq 0.05$, **$p \leq 0.01$.

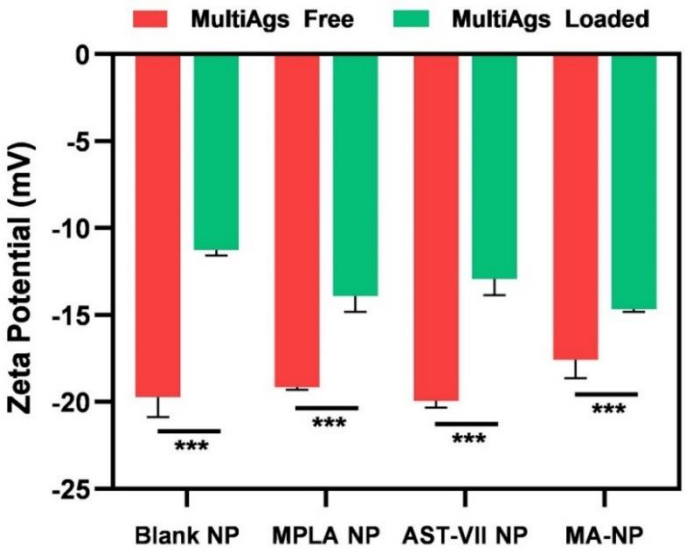

Figure 3.28. The zeta potential (mV) of multiAgs-loaded NPs. The data was presented as mean ± SEM. The statistically significant differences were shown by One-way ANOVA, Tukey's multiple comparison test. ***$p \leq 0.001$.

3.1.6.2.1. *In vitro* Antigen Release Study

The *in vitro* release profile of antigens from MA-NP was investigated by dialysis at pH 5.5 and pH 7.4 against PBS at 37°C over a period of 96 h. There was a burst release of antigen from MA-NP adjuvant system up to 20 % against pH 5.5 and pH 7.4 in 2 h dialysis. Then, the antigen release slowed but gradually increased over time (Figure 3.29). pH of the buffer did not statistically alter the antigen release with respect to time. These results showed that MA-NP adjuvant system started to release antigens in early times and sustained the release of antigens over time, which is essential to obtain long-term immunity.[95]

Following injections of multiAgs-adsorbed MA-NP into mice, 20% of antigens were released to skin tissue. However, within 24 h, multiAgs-adsorbed MA-NPs could be drained to lymph nodes,[96] where 80% of antigens could be presented to T cells for priming.

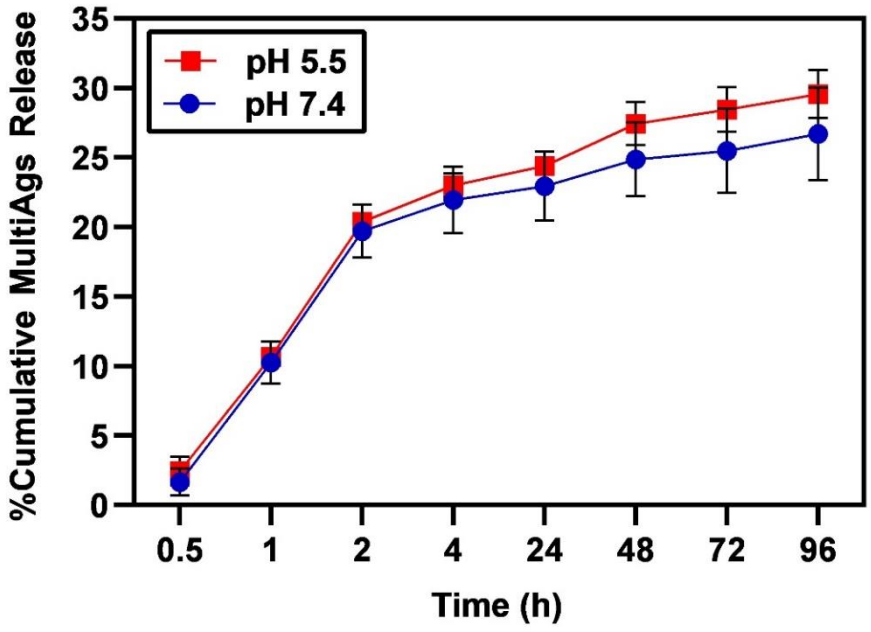

Figure 3.29. The time and pH-dependent release of multiAgs adsorbed on MA-NP against PBS at 37°C.

3.2. Investigating *in vitro* Cytotoxic and Immunomodulatory Activities of Adjuvant Systems

3.2.1. Assessment of *in vitro* Cytotoxicity of Adjuvant Systems

The materials used in biological systems must have low or no cellular toxicity; thus, the adjuvant systems and multiAgs-loaded vaccines were evaluated for their toxicity against DC2.4 dendritic and B16-F10 melanoma cell lines *in vitro*. DC2.4 and B16-F10 cells were treated with serial dilutions of NPs solutions (1 to 0.032 mg/mL) and incubated for 24 h or 48 h. At the end of the incubation period, the cell viability was assessed via an MTT cell viability assay. DC2.4 cells incubating with NPs for 24 h showed inconsistent cell viability with respect to NP concentration (Figure 3.30A).

On the other hand, following 48 h incubation period, the dose-dependent response to NP treatment was achieved in DC2.4 cells. In this incubation period, the relative cell viability for all NPs was higher than 65% at the concentration of 0.032-0.125 mg/mL (Figure 3.30B). In B16-F10 cells, the treatment with NPs did not demonstrate toxicity in either 24 h or 48 h incubations (Figure 3.30C-D). The cell viability after treatment with NPs was approximately 70% following 48 h incubation, excluding blank NP (1 mg/mL) and MA-NP (0.063 mg/mL) treatments.

Nanoparticulate adjuvant systems showed higher than 60% cell viability at the concentrations $\leq$ 0.25 mg/mL. Therefore, subsequent cellular viability studies were conducted with multiAgs (Trp-2+PADRE peptides) loaded NPs at 0.016 – 0.25 mg/mL concentrations. MultiAgs loaded NPs were applied to DC2.4 and B16-F10 cells and incubated for 24 and 48 h. MultiAgs loaded NPs demonstrated cell viability $\geq$ 80% on DC2.4 cells at 24 h and 48 h incubation periods (Figure 3.31A-B).

At 48 h, multiAgs loaded AST-VII NPs provided less viability in DC2.4 cells than other NPs, especially at 0.25 mg/mL. In the case of B16-F10 cells, no toxicity was observed following the treatment with multiAgs loaded NPs in either 24 or 48 h incubations (Figure 3.31C-D). Only MPLA NP (0.016 mg/mL) decreased the cell viability by around 60% in B16-F10 cells at 48 h incubation. AST-VII NP without antigen demonstrated higher cellular viability in dendritic cells than other NPs, especially in 48

h. On the other hand, AST-VII NPs formulated with multiAgs led to a decrease in the cellular viability compared to multiAgs free form and other multiAgs-loaded NPs.

Overall, these results demonstrated that nanoparticulate adjuvant systems and their multiAgs-loaded vaccines did not show cellular toxicity at particular concentrations and could be used safely in the applications of biological systems.

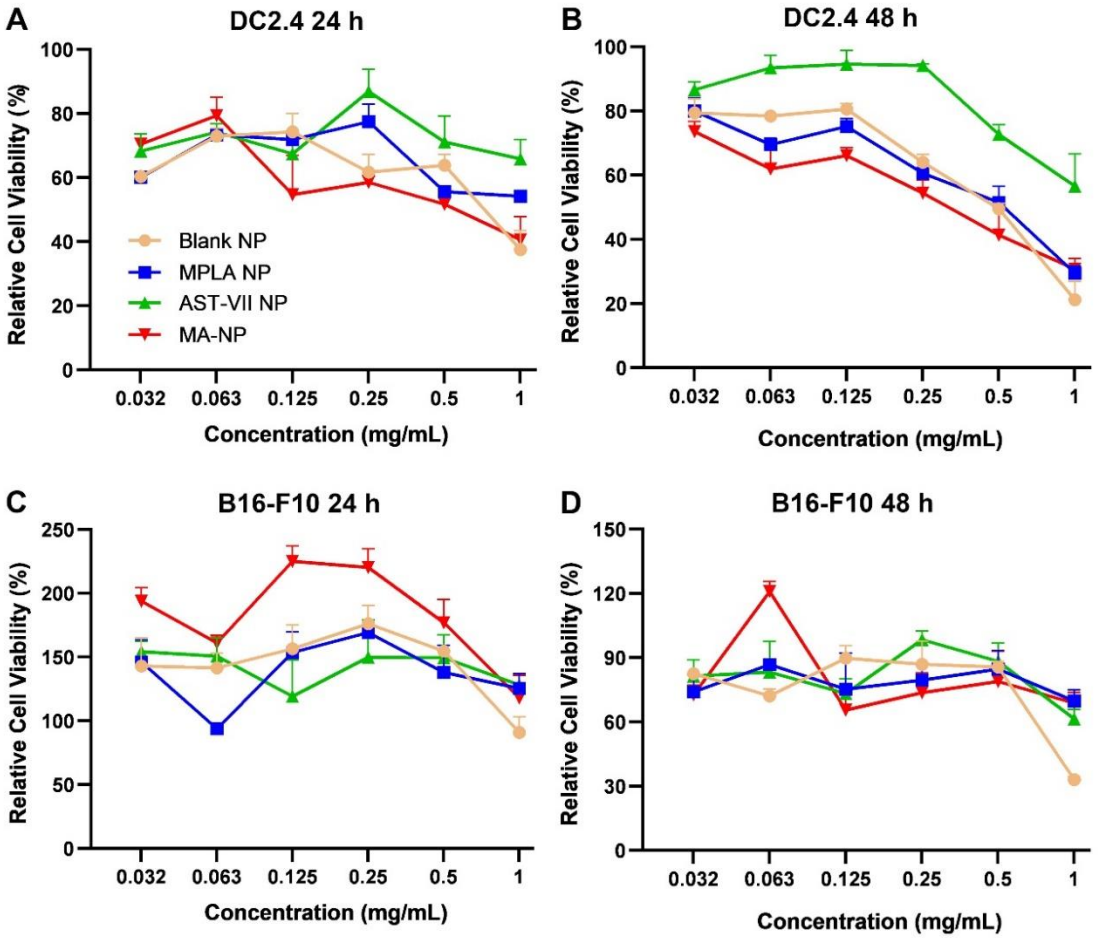

Figure 3.30. The relative cell viabilities (%) of DC2.4 cells in (A) 24 h, (B) 48 h, and B16-F10 cells in (C) 24 h, (D) 48 h incubation periods. The cells were treated with blank NP, MPLA NP, AST-VII NP, and MA-NP at the concentration of 0.032-1 mg/mL for 24 and 48 h. The cell viability was evaluated using an MTT assay. Data are shown as the mean ± SEM of two independent experiments.

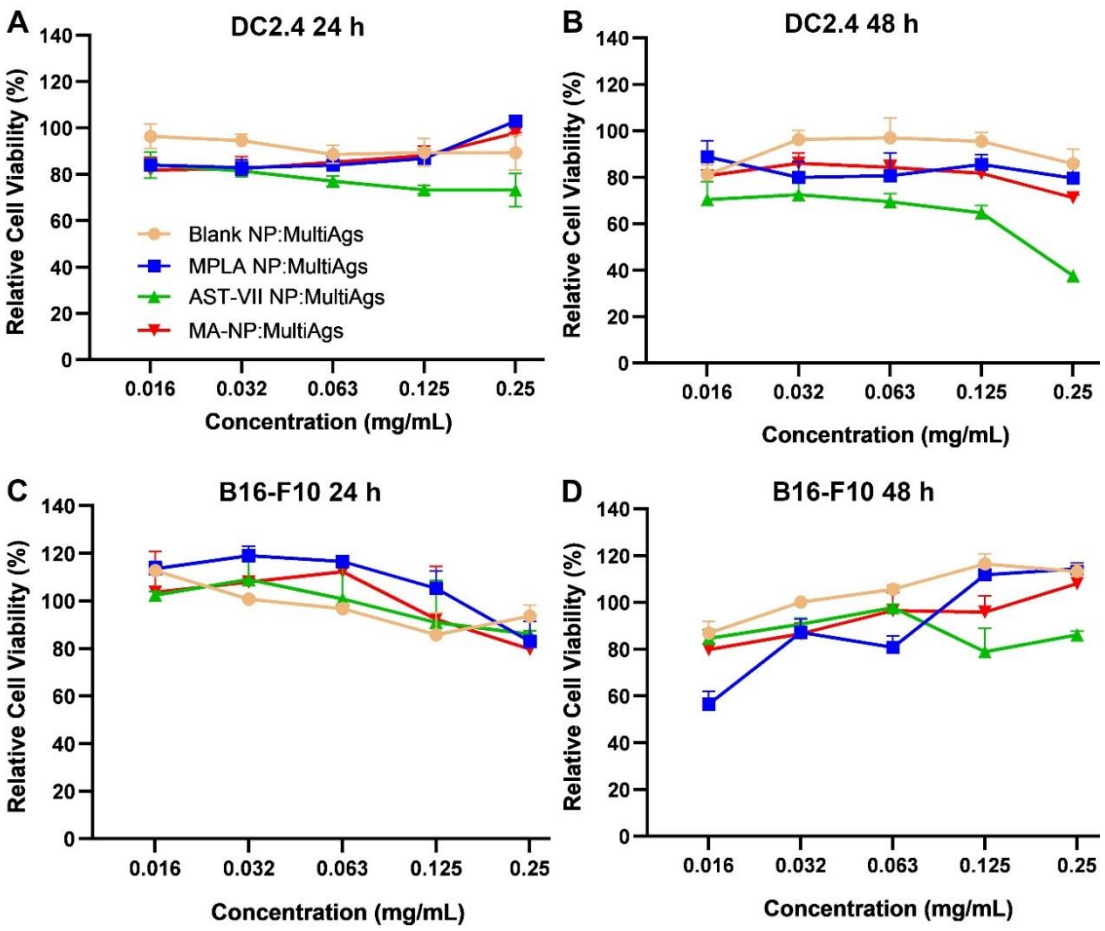

Figure 3.31. The relative cell viabilities (%) of DC2.4 cells in (A) 24 h, (B) 48 h, and B16-F10 cells in (C) 24 h, (D) 48 h incubation periods. The cells were treated with multiAgs-loaded NPs at the concentration of 0.016-0.25 mg/mL for 24 and 48 h. The cell viability was evaluated using an MTT assay. Data are shown as the mean ± SEM of two independent experiments.

3.2.2. Cellular Uptake and Subcellular Localization of MA-NP in Dendritic Cells

Engineered NPs should be efficiently taken by the target cell to show its functions. NPs have different uptake kinetics and mechanisms due to their various size and physicochemical properties. While NPs have improved the cellular uptake of compounds over their soluble form by interacting with biomolecules on the cell surface, this effect

has also contributed to the adsorption of proteins onto NPs, forming protein corona, causing some aggregates and affecting the uptake process. Therefore, it is important to investigate the cellular uptake of engineered NPs in target cells *in vitro*.[97]

In light of this information, dansyl chloride (DNS-Cl), a widely used green fluorescent probe in immunofluorescence assays,[98] was loaded into MA-NP to visualize its cellular uptake and subcellular localization. The excess amount of free DNS-Cl in MA-NP solution was removed by dialysis. The integration of DNS-Cl in MA-NP (DNS-MA-NP) was first investigated using UV-Vis spectroscopy (Peltier, Shimadzu-UV 2450). UV-Vis spectra of DNS-Cl and DNS-MA-NP resulted in three overlapping maximum absorbance peaks at 230, 278, and 327 nm, indicating the successful integration of DNS-Cl in MA-NP (Figure 3.32).

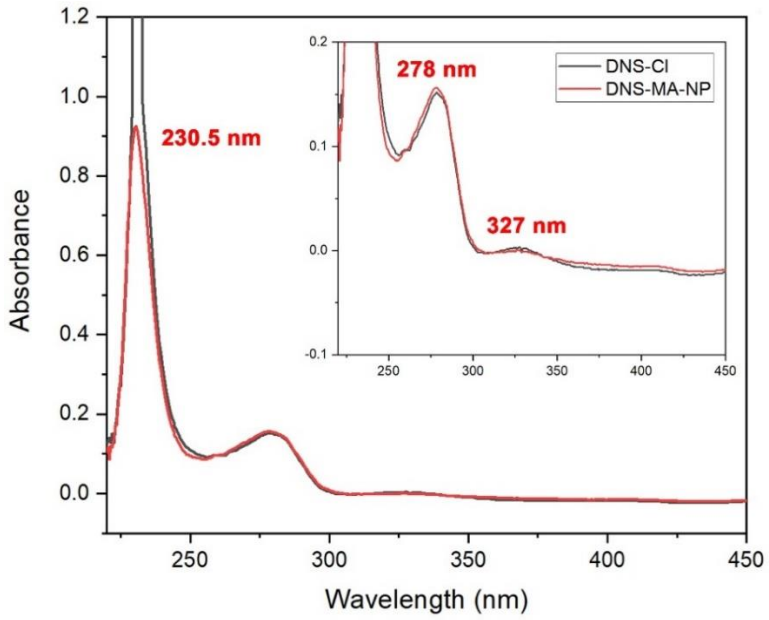

Figure 3.32. UV-Vis spectra of free DNS-Cl and DNS-MA-NP in DMF.

After successfully integrating DNS-Cl into MA-NP, DC2.4 cells were incubated with DNS-MA-NP (0.1 mg/mL) and visualized time-dependent by fluorescence microscopy (ZEISS – Observer Z1). DNS-MA-NP uptake was started as early as 30 min and continued for 2 h. However, the uptake rate slowed during 24 h incubation period (Figure 3.33).

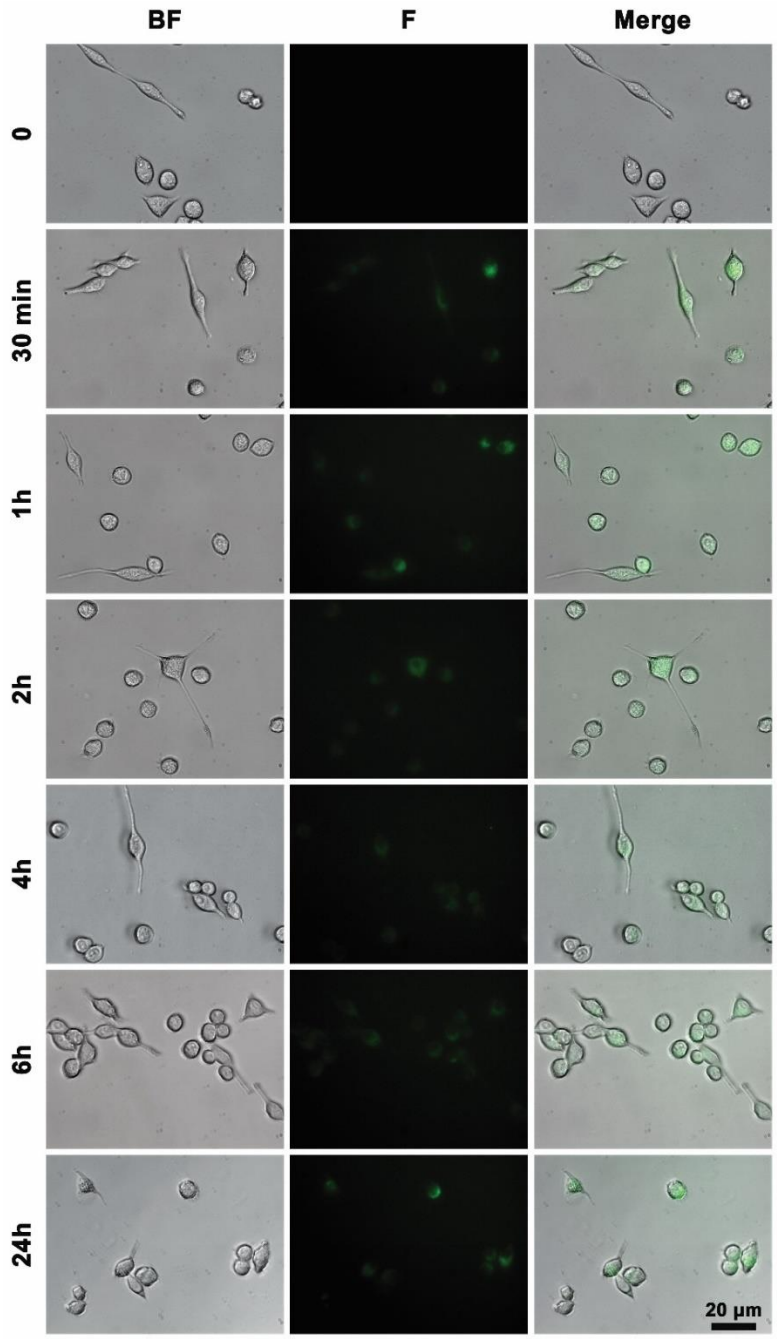

Figure 3.33. Time-dependent cellular uptake of dansyl chloride integrated MA-NP (DNS-MA-NP). DNS-MA-NP (0.1 mg/mL) was applied to DC2.4 cells and incubated for 24 h. DC2.4 cells were visualized at indicated time points by fluorescence microscopy. **BF:** Brightfield, **F:** Fluorescence.

Besides visualizing the cellular uptake of DNS-MA-NP by fluorescence microscopy, DNS-MA-NP uptake was also indirectly quantified by Varioskan measuring

the fluorescence intensity of the cell media. Consistent with fluorescence images, DNS-MA-NP was taken at 6.8% by dendritic cells in 30 min and reached its maximum in 2 h (12.6%). After 2 h, there was no alteration in cellular uptake till 24 h, reaching its maxima (Figure 3.34), showing the saturation of dendritic cells with DNS-MA-NP. Another possible explanation for this phenomenon could be the adsorption of proteins in the cell media onto DNS-MA-NP, and further formation of aggregates could prevent the cellular uptake of NPs.

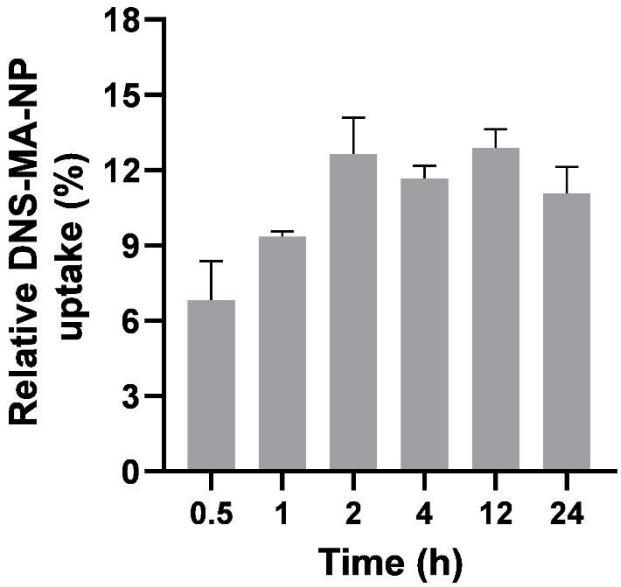

Figure 3.34. Time-dependent relative uptake (%) of DNS-MA-NP by DC2.4 cells. DC2.4 cells were incubated with DNS-MA-NP (0.1 mg/mL) at different time points. The fluorescence intensity in cell supernatant was measured by Varioskan Flash (Thermo), and interpreted relatively in terms of the fluorescence intensity at 0 h. Data are shown as the mean ± SEM of two independent experiments.

To investigate subcellular localization of DNS-MA-NP, DC2.4 cells were incubated with DNS-MA-NP (0.1 mg/mL) for 6 h, and then stained with Lysotracker Red and DAPI to visualize endolysosomal pathway and nuclei, respectively. As clearly seen in Figure 3.35, DNA-MA-NP (green fluorescence) accumulated primarily in the cytosol

with minimal overlap with the Lysotracker signal. As there was no overlap with the DAPI signal, it could be stated that DNS-MA-NP did not enter the nuclei. Overall, these data indicated that DNS-MA-NP was successfully taken by dendritic cells and co-localized with endolysosomal compartments by 6 h.

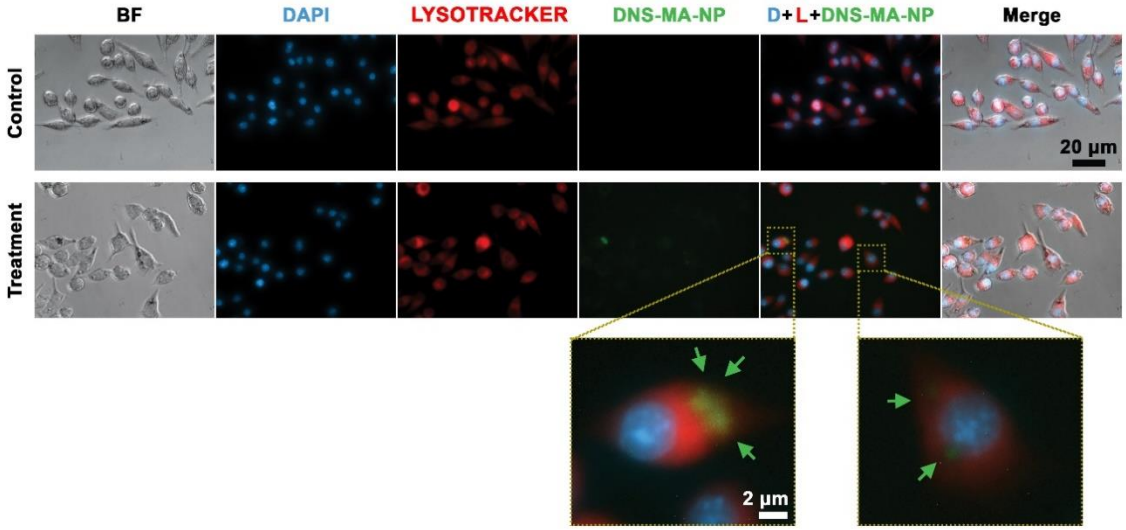

Figure 3.35. The subcellular localization of DNS-MA-NP in DC2.4 cells incubated for 6 h. DC2.4 cells were incubated with DNS-MA-NP (0.1 mg/mL) for 6 h, stained with Lysotracker and DAPI, and then visualized by fluorescence microscopy. **BF:** Brightfield, **D:** DAPI, **L:** Lysotracker

3.2.3. Investigating *in vitro* Immunomodulatory Activities of Adjuvant Systems

Dendritic cells are antigen-presenting cells that play a role in both innate and adaptive immunity. When immature DCs located in the periphery encounter a foreign antigen (viruses, cancer cells, etc.), these antigens are internalized and processed by DCs. During this process, immature DCs become mature by increasing the synthesis of major histocompatibility complex (MHC) II molecules and co-stimulatory molecules such as CD40, CD86, and CD80 and secrete pro-inflammatory cytokines.[99,100] Upon maturation,

DCs drain to adjacent lymph nodes to present antigens to naive T cells and differentiate them into specific T cell subsets to elucidate their anti- or pro-inflammatory functions.[101,102]

3.2.3.1. Assessment of Pro-inflammatory Cytokine Production

In this thesis, dendritic cell maturation and activation were first investigated by the secretion of pro-inflammatory cytokines such as IL-1β, IL-6, and IL-12. IL-1 signaling plays a central role during the activation of the innate immune system, driving upregulation of co-stimulatory molecules to release pro-inflammatory cytokines such as IL-6.[99] IL-6, in combination with transforming growth factor (TGF)-β, is indispensable for Th17 differentiation from naive $CD4^+$ T cells, but IL-6 also inhibits TGF-β-induced Treg differentiation. In addition, IL-6 induces the differentiation of $CD8^+$T cells into cytotoxic T cells.[103] On the other hand, one of the essential pro-inflammatory cytokines, IL-12, is critical for the induction of Th1-mediated immune response and priming naive CD8 T cells, indicating effective anti-tumor immune response in cancer vaccines.[49]

DC2.4 cells were treated with developed adjuvant systems (0.063 – 0.25 mg/mL), and the cell supernatant was collected to measure cytokines by ELISA. Blank NP and AST-VII NP did not increase IL-1β production as expected from the previous studies.[65] Incorporation of MPLA into the adjuvant systems led to statistically significant production of IL-1β (Figure 3.36), indicating the need for a TLR4 agonist. In the case of IL-6, only MA-NP demonstrated statistically significant augmentation in IL-6 production (Figure 3.37). IL-1β and IL-6 data obtained from *Astragalus*-based NPs were consistent with those obtained from QS-21 studies. Marty-Roix et al. demonstrated that QS-21 did not produce either IL-1β or IL-6 in dendritic cells; however, co-stimulation of dendritic cells with QS-21 and MPLA resulted in the production of both IL-1β and IL-6.[53]

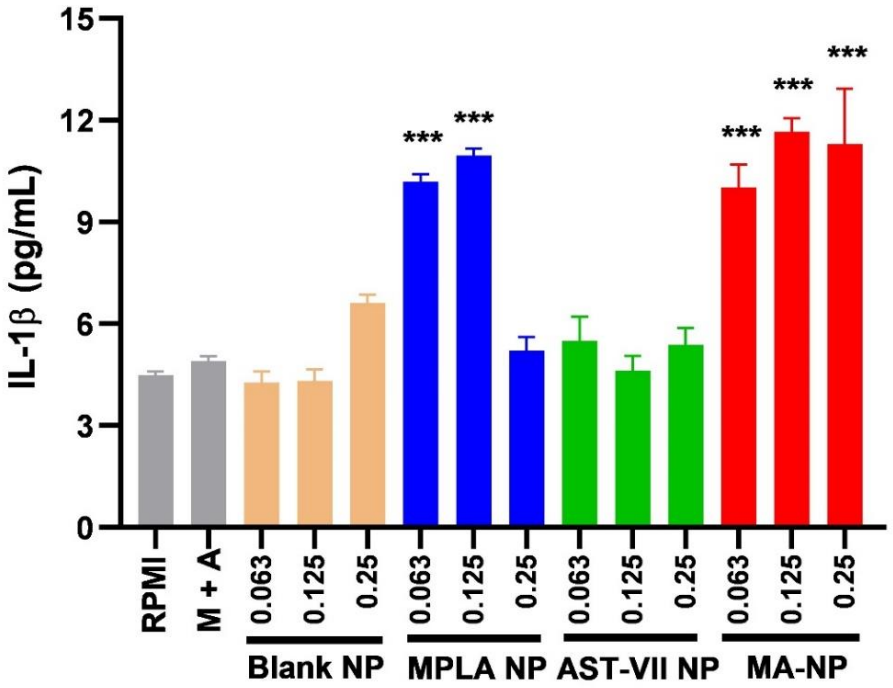

Figure 3.36. IL-1β production in DC2.4 cells treating with adjuvant systems. Dendritic cells were treated with nanoparticulate adjuvant systems (0.063–0.025 mg/mL) and soluble adjuvants (M+A, MPLA: 0.4 μg/mL and AST-VII: 6.75 μg/mL) for 6 h. The cell supernatant was collected to measure IL-1β by using ELISA. The data was presented as mean ± SEM of two independent experiments. The statistically significant differences between treatment groups and RPMI were shown by One-way ANOVA, Dunnett's multiple comparison test. ***$p<0.001$.

In the case of Th1-mediated cytokine, IL-12, Blank NP increased IL-12 production dose-dependently. MPLA NP (0.125 mg/mL) and MA-NP (0.063 mg/mL) provided statistically significant IL-12 augmentation, while AST-VII NP did not show any alteration in IL-12 levels (Figure 3.38). In a previous study, BMDCs were treated with AST-VII alone, but AST-VII did not increase IL-12 levels in the cell supernatant. As blank NP has the ability to boost IL-12 production, integration of AST-VII into blank NPs did not contribute to the production of IL-12 in dendritic cells.

Besides NP forms, DCs were also treated with active compounds in NPs (MPLA and AST-VII) with the same concentration in NP forms; however, the soluble form did

not enhance IL-1β, IL-6 and IL-12 productions, indicating the efficiency of NPs (MA-NP) over its soluble form.

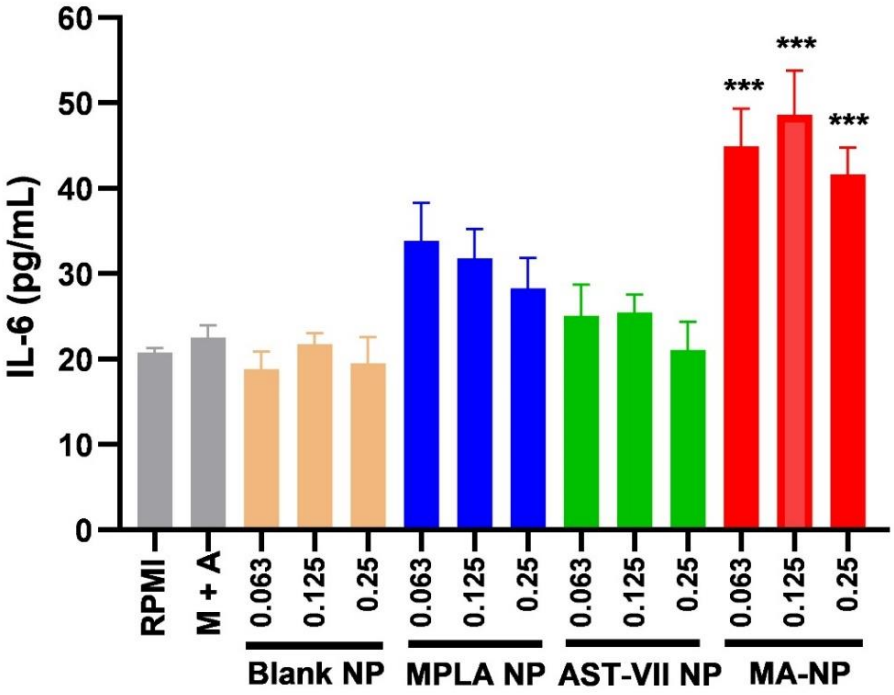

Figure 3.37. IL-6 production in DC2.4 cells treating with adjuvant systems. Dendritic cells were treated with nanoparticulate adjuvant systems (0.063–0.025 mg/mL) and soluble adjuvants (M+A, MPLA: 0.4 μg/mL and AST-VII: 6.75 μg/mL) for 48 h. The cell supernatant was collected to measure IL-6 by using ELISA. The data was presented as mean ± SEM of two independent experiments. The statistically significant differences between treatment groups and RPMI were shown by One-way ANOVA, Dunnett's multiple comparison test. ***$p<0.001$.

Overall, blank NP was effective in IL-12 production, consistent with literature.[104] MPLA NP has shown promise in IL-1β and IL-12 production. Combining all active components in one system, MA-NP, induced the production of IL-1β, IL-6, and IL-12. Therefore, further studies were continued with MA-NP.

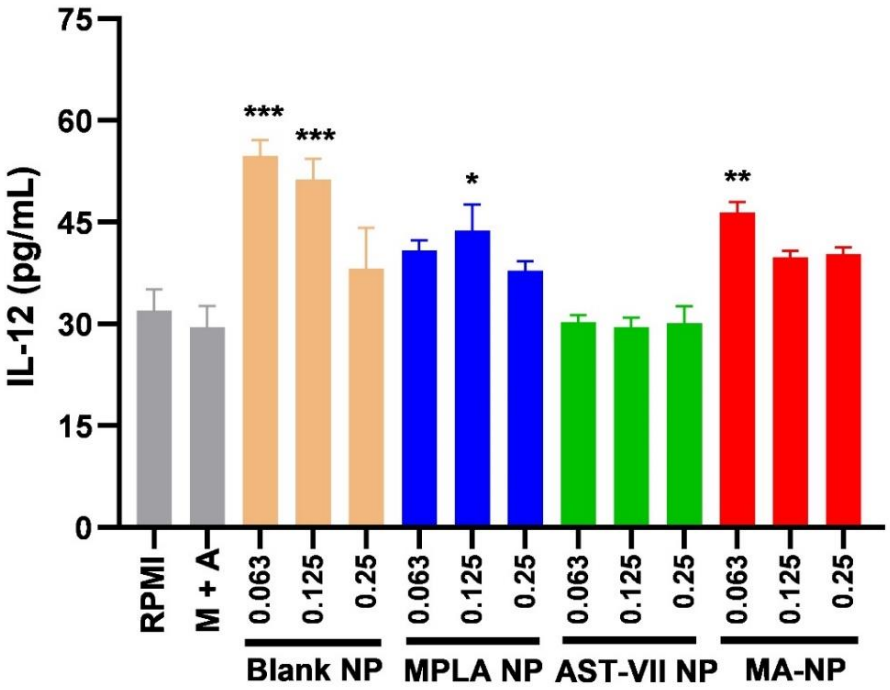

Figure 3.38. IL-12 production in DC2.4 cells treating with adjuvant systems. Dendritic cells were treated with nanoparticulate adjuvant systems (0.063–0.025 mg/mL) and soluble adjuvants (M+A, MPLA: 0.4 μg/mL and AST-VII: 6.75 μg/mL) for 48 h. The cell supernatant was collected to measure IL-12 by using ELISA. The data was presented as mean ± SEM of two independent experiments. The statistically significant differences between treatment groups and RPMI were shown by One-way ANOVA, Dunnett's multiple comparison test. *p<0.05, **p<0.01, ***p<0.001

3.2.3.2. Investigating Dendritic Cell Maturation

Functional maturation of dendritic cells is essential for successfully priming naive T cells and further induction of antigen-specific adaptive immune response.[101] In light of this information, adjuvant systems should primarily be taken up by DCs to demonstrate their immunomodulatory activities further. Therefore, the maturation and activation of DCs following treatment with an adjuvant system are investigated in terms of CD40, CD86, and CD80 expressions by flow cytometry. BMDCs were treated with

nanoparticulate adjuvant systems (MA-NP and blank NP, 0.1 mg/mL) and soluble adjuvants (MPLA+AST-VII and MPLA+QS-21, MPLA: 0.4 μg/mL, AST-VII: 6.75 μg/mL and QS-21: 2 μg/mL) for 24h. The cells were stained with anti-mouse PE-Cy7-CD11c, APC-Cy7-IA/IE, FITC-CD40, APC-CD86 and PE-CD80 antibodies and analyzed by flow cytometry (Cytek Aurora).

MA-NP adjuvant system increased the expression of all co-stimulatory molecules CD40, CD86, and CD80 on the surface of $MHCII^+CD11c^+$ BMDCs (Figure 3.39A-C). Blank NP is also capable of upregulating CD86 and CD80. Several studies have shown that APS itself could promote DC maturation and increase the expression of CD86 and CD80.[105–107] Hwang et al. showed that intranasal administration of *Astragalus membranaceus* polysaccharide into mice induced the CD86, CD80, and CD40 expressions and the production of IL-6, IL-12, and TNF-α cytokine in mediastinal lymph node redisent-DCs.[108] Obtaining different cytokine profiles following APS treatment may result from the varying polysaccharide content extracted from different *Astragalus* species. Moreover, soluble adjuvant (MPLA+AST-VII) also enhanced the expression of CD86 and CD80, similar to LPS+AST-VII-induced DCs.[65] On the other hand, MPLA+QS-21 did not increase the co-stimulatory molecules on BMDCs even if the concentrations for QS-21 were used as Marty-Roix et al. indicated.[53] Another *Quillaja* saponin containing nanoparticulated adjuvant system, ISCOMATRIX, enhanced the upregulation of CD86 and CD80 and provided the production of IL-5, IL-6 and macrophage inflammatory protein-a (MIP-a) on DCs *in vivo*.[109]

Overall, these results indicated that MA-NP, blank NP and MPLA+AST-VII provided dendritic cell maturation and activation by expressing co-stimulatory molecules CD86 and CD80, and producing pro-inflammatory cytokines. Saponin adjuvants alone did not induce dendritic cell maturation, but in combination with TLR agonists or integration into APS nanocarriers enhanced their maturation and activation.

Additionally, the upregulation of CD40 on DCs is important due to the interaction of CD40-CD40L between DCs and $CD8^+$ T cells, providing indirect support for $CD8^+$ T cell expansion as these precursor populations are relatively rare in cancer vaccinations.[110] Therefore, CD40 upregulation besides CD86/CD80 on DCs following MA-NP treatment encourages further investigation of cytotoxic T cell response activation against tumor antigens.

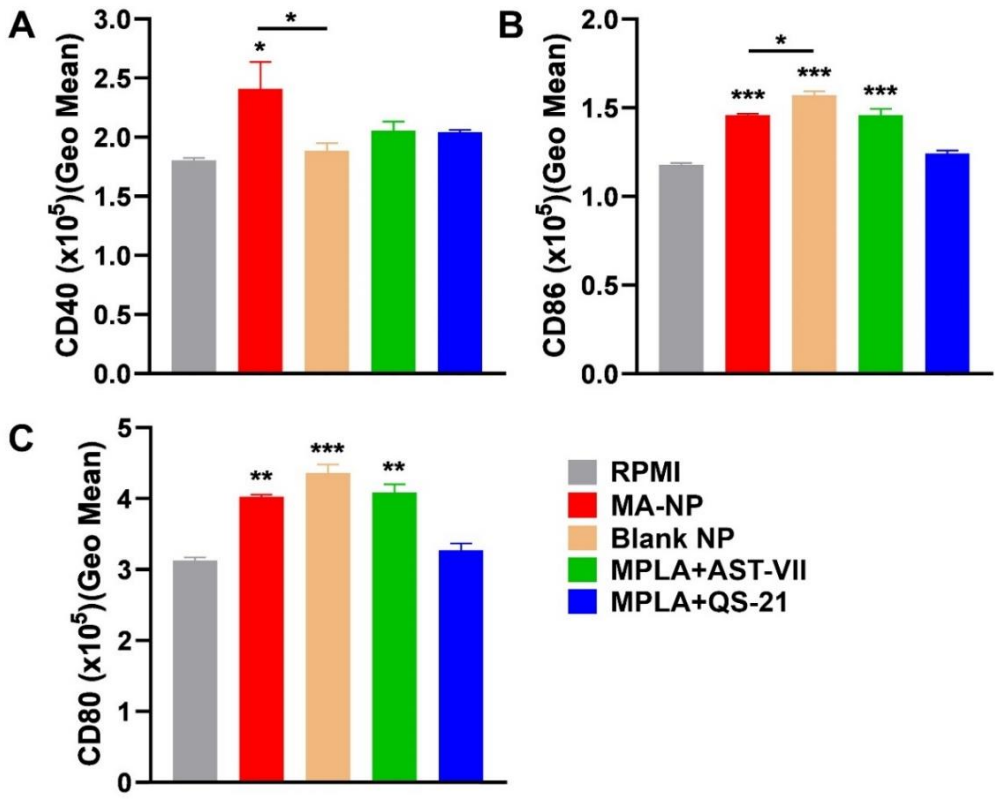

Figure 3.39. The effects of MA-NP and soluble adjuvants on dendritic cell maturation and activation. BMDCs were treated with MA-NP, blank NP (0.1 mg/mL), and soluble adjuvants (MPLA: 0.4 μg/mL, AST-VII: 6.75 μg/mL, QS-21: 2 μg/mL) for 24h. The cells were stained with fluorochrome-conjugated antibodies and analyzed by flow cytometry. Bar graphs show the expression of (A) CD40, (B) CD86, and (C) CD80 on the surface of $MHCII^{+}CD11c^{+}$ cells. Data are pooled from two independent experiments with similar results (mean ± SEM). The statistically significant differences were shown by One-way ANOVA and Tukey's multiple comparisons test. *$p < 0.05$, **$p < 0.01$, ***$p < 0.001$.

3.3. Evaluating *in vivo* Immunogenicity of NPs

MA-NP adjuvant system demonstrated desirable biological responses *in vitro*, providing dendritic cell maturation and activation by upregulating the co-stimulatory molecules and secreting pro-inflammatory cytokines with no cellular toxicity. Thus, *in*

vivo immunogenicity of MA-NP was investigated in female C57BL/6 mice. The mice were vaccinated twice with soluble and NP forms of peptide vaccine, and two weeks after the last immunization, the blood and spleen samples were collected for further analysis.

Identifying the primary cell population following vaccinations is essential to develop effective cancer immunotherapies. Thus, the immunophenotyping studies were conducted in spleen samples. In immune cell populations, while $CD4^+$ Th1 cells, $CD8^+$ T cells, natural killer (NK) cells, and M1 macrophages have a crucial role in fighting against tumors, M2 macrophages and Tregs support tumor progression. On the other hand, dendritic cells (DCs), neutrophils, and NKT cells have been shown to exert both tumor-suppressive and -promoting activities.[111] NKT cells, in particular, have the ability to rapidly produce large quantities of cytokines and directly cause cell death in tumor,[112] making them favorable cells in cancer immunotherapeutics.

The spleen is one of the favorable lymphoid organs for investigating the efficacy of immunotherapeutics. Immunophenotyping studies carried out in spleen collected from MA-NP injected mice revealed that MA-NP significantly increased the frequencies of $CD4^+$ T cells, $CD8^+$ T cells, NKT cells, and NK cells populations compared to PBS injected mice while decreasing the frequencies of macrophages and dendritic cells (Figure 3.40). In general, the frequencies for immune cell populations were consistent with the literature, and even the splenic immune cell population is altered in a sex- and age-dependent manner. The mouse spleen contains B cells (50%), monocytes (7%), neutrophils (1.8%), NK cells (3%), $CD4^+$ T cells (12%) and $CD8^+$ T cells (9%).[113]

No significant differences were observed in Tregs population between MA-NP and PBS. As Tregs suppress the expansion of anti-tumor effector cells, including NK cells and $CD4^+$ T cells,[114] an increase in the frequency of $CD4^+$, $CD8^+$ T cells, and NK cells after MA-NP immunization could be explained by the decrease in the Tregs population.

Injection of ISCOMATRIX adjuvant into mice increased the number of neutrophils, monocytes, NK, and NKT cells in lymph nodes.[115] As ISCOMATRIX is also used to evaluate saponin-based adjuvant systems, these results show that the MA-NP adjuvant system could be effective in priming strong T-cell-mediated anti-tumor immune responses.

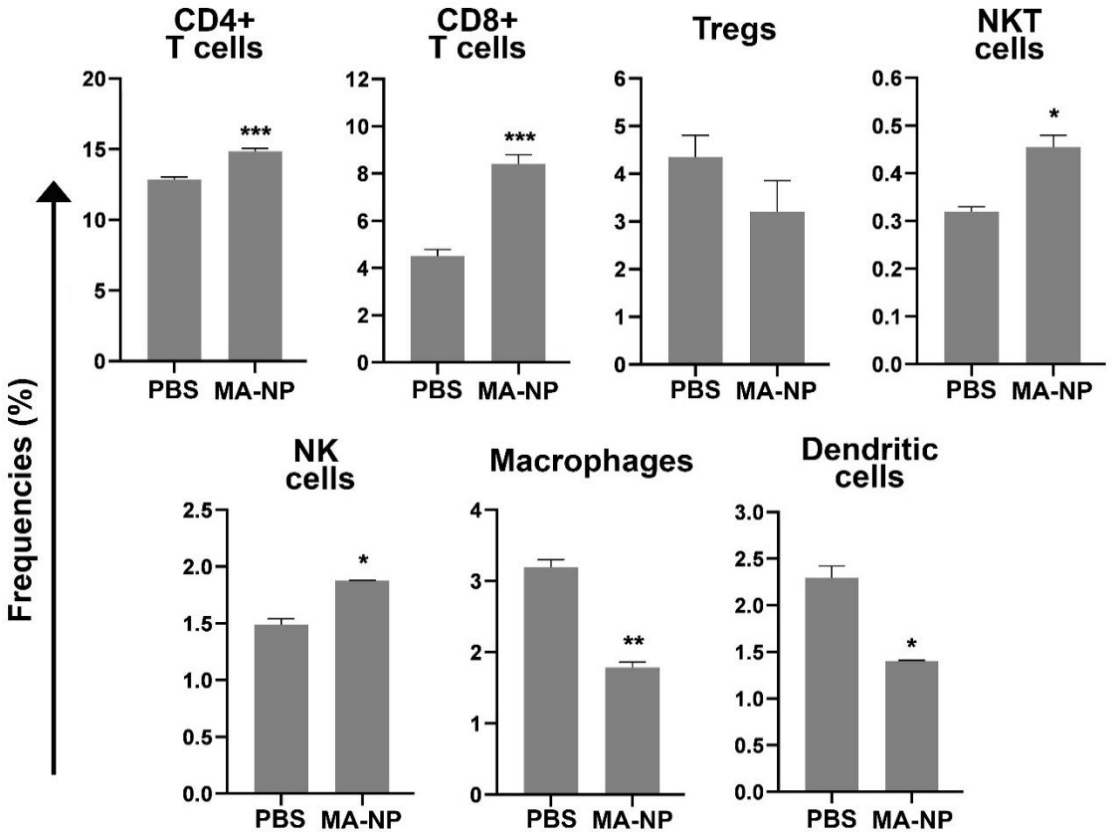

Figure 3.40. The immune cell populations in the spleen following vaccination with MA-NP. MA-NP was subcutaneously injected into C57BL/6 mice (n=7) twice at a one-week interval. After two weeks, the spleen was collected to analyze the immune cell profile by flow cytometry. Bar graphs show the frequencies (%) of $CD4^+$ T cells, $CD8^+$ T cells, NKT cells, NK cells, macrophages, dendritic cells (in % of live cells), and Tregs (in % of $CD4^+$ T cells) in the spleen. Data are pooled from two independent experiments with similar results (mean ± SEM). The statistically significant differences were shown by Student's t-test. *$p < 0.05$, **$p < 0.01$, ***$p < 0.001$.

3.3.1. Immunophenotyping Studies in Spleen Following Vaccination with MultiAgs Integrated Adjuvant Systems

MA-NP without peptide demonstrated promising results by increasing the tumor-fighting cell populations in the spleen. Therefore, it was decided to evaluate the *in vivo*

immunogenicity of multiAgs (Trp-2 + PADRE) integrated adjuvant systems. To show the effect of the delivery system, multiAgs were integrated into blank NP with the same methodology applied to MA-NP. On the other hand, to reveal the importance of NP system, MA-NP was compared with its soluble form (MPLA + AST-VII) and the golden standard for saponin-based adjuvants (MPLA + QS-21). C57BL/6 mice (n = 7-8) were immunized subcutaneously with vaccination groups twice, with a one-week interval between each administration. Two weeks after the last immunization, the spleens were collected using flow cytometry to analyze immune cell populations.

To analyze T cell populations, the cells were gated in accordance with the general leukocyte marker (CD45) and then subdivided into $CD4^+$ T cells ($TCR\beta^+CD4^+$), $CD8^+$ T cells ($TCR\beta^+CD8^+$) and Tregs ($TCR\beta^+CD4^+CD25^+Foxp3^+$) (Figure 3.41A). MultiAgs did not make a difference in $CD4^+$ T cell population compared to PBS-treated mice. However, when multiAgs adsorbed on MA-NP and blank NP, $CD4^+$ T cell population significantly increased compared to multiAgs (Figure 3.41B). On the other hand, multiAgs led to an increase in $CD8^+$ T cell population compared to PBS. Only MA-NP adjuvanted multiAgs demonstrated statistically significant augmentation on $CD8^+$ T cell population over multiAgs (Figure 3.41C). Both in $CD4^+$ and $CD8^+$ T cell populations, soluble adjuvants did not alter the cell frequencies compared to multiAgs, indicating MA-NP was superior to its soluble form (MPLA+AST-VII) or commercially alternative form (MPLA+QS-21).

Tregs have control over several immune cell populations, such as T cells, B cells, NK cells, dendritic cells, and macrophages, promoting tumor progression by suppressing anti-tumor immunity. Thus, manipulating Tregs or immunosuppressive factors produced by these cells is one of the promising anti-cancer strategies.[114] As clearly seen in Figure 3.41D, while multiAgs adsorbed on MA-NP and blank NP decreased Tregs populations, soluble saponin adjuvants increased the frequency of Tregs compared to multiAgs. APS is effective in the reduction of $CD4^+CD25^+$ Treg activity through binding to TLR4 on Tregs.[116,117] As nanoparticulated adjuvants were prepared using APS, a significant reduction in Treg population induced by NP adjuvants compared to soluble forms could result from the regulatory activities of APS.

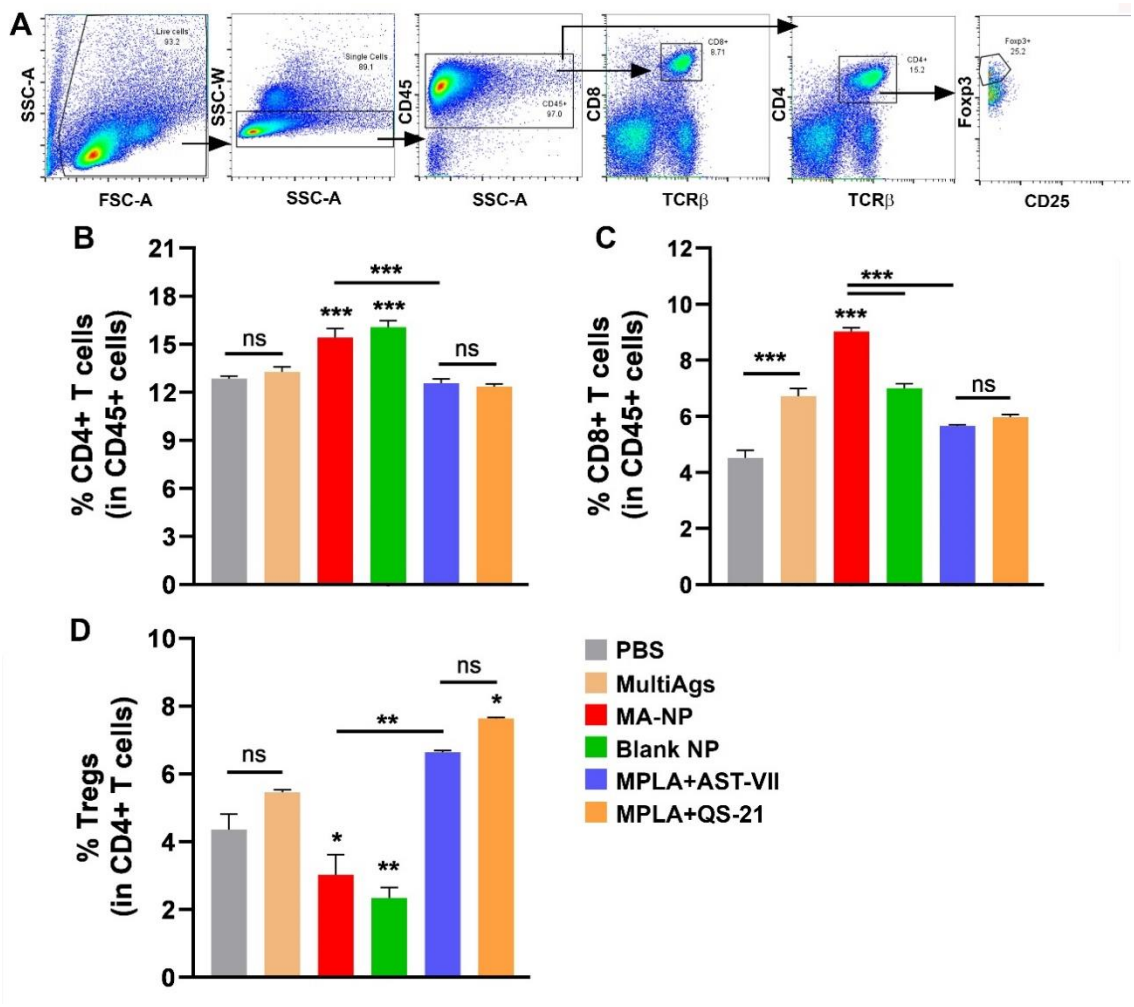

Figure 3.41. MultiAgs loaded MA-NP increased CD4 and CD8 T cell populations and decreased Tregs. (A) Gating strategies to identify $CD4^+$ T, $CD8^+$ T cells, and Tregs in the spleen. (B-D) Bar graphs show the frequencies (%) of $CD4^+$ T cells, $CD8^+$ T cells (in $CD45^+$ cells), and Tregs (in $CD4^+$ T cells). Data are pooled from two independent experiments (mean ± SEM). The statistical analyses were performed between multiAgs and vaccination groups using One-way ANOVA and Tukey's multiple comparison test. ns: non-significant, $*p < 0.05$, $**p < 0.01$, $***p < 0.001$.

NK cells are one of the critical cells in the innate immune system, showing cytotoxic and cytokine-producing effector functions against several types of tumor and microbial infectious.[120] To investigate NK cell population, cells were gated for general leukocyte marker (CD45) and then sub-gated into NK cells ($NK1.1^+$) and NKT cells

(NK1.1^{+}TCRβ^{+}) (Figure 3.42A). The frequencies of NK and NKT cells only increased with vaccination by multiAgs loaded MA-NP (Figure 3.42B-C). As clearly observed in T cell populations, the integration of MPLA/AST-VII into NP adjuvant system evidently enhanced the populations of tumor-fighting NK and NKT cells compared to its soluble form (MPLA+AST-VII). A chemically similar adjuvant system to MA-NP, AS01, which is the licensed MPLA/saponin-containing adjuvant system, was investigated for its adjuvant activities with RTS,S vaccine in mice. The results showed that administration of AS01 elicited polyfunctional CD4^{+} T cell response, activated NK cells, and induced CD8^{+} T cell responses in lymph nodes.[118] MA-NP adjuvanted multiAgs vaccine demonstrated similar T cell and NK cell responses compared to AS01, indicating its strong potency as a new saponin-based adjuvant system.

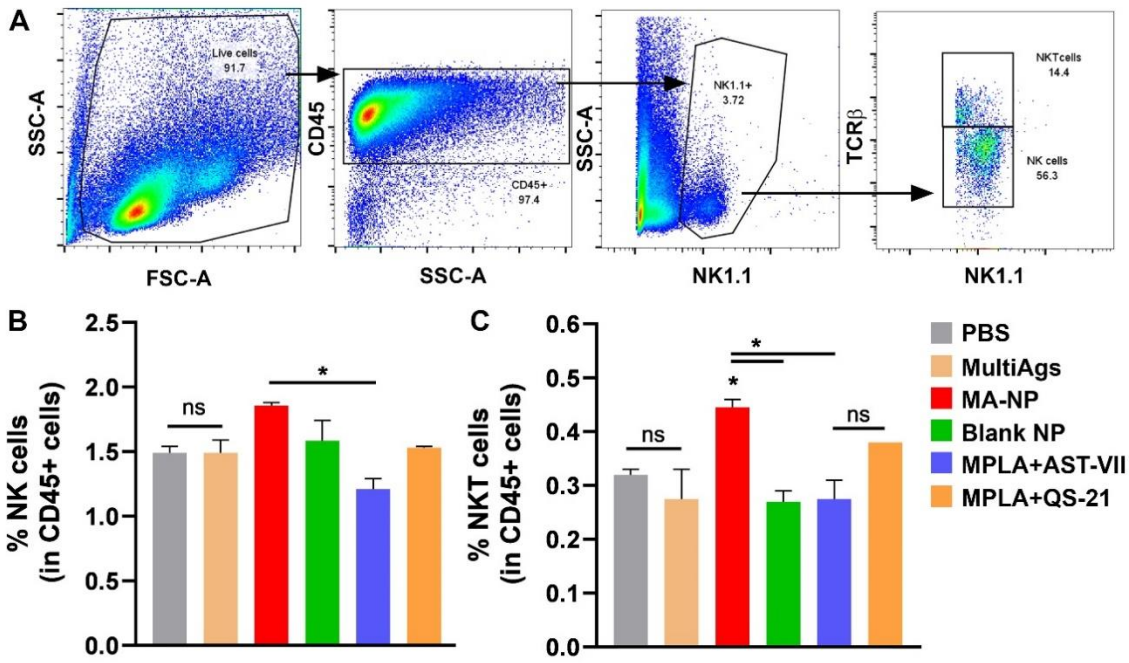

Figure 3.42. MultiAgs loaded MA-NP enhanced NKT cell population. (A) Gating strategies to identify NK cells and NKT cells in the spleen. (B-C) Bar graphs show the frequencies (%) of NK and NKT cells (in CD45^{+} cells) in the spleen. Data are pooled from two independent experiments (mean ± SEM). The statistical analyses were performed between multiAgs and vaccination groups using One-way ANOVA and Tukey's multiple comparison test. ns: non-significant, *$p < 0.05$.

Dendritic cells and macrophages are other innate immune cells found in the spleen. These cells were gated in general with a leukocyte marker (CD45) and then subgated into macrophages ($CD11b^{+}F4/80^{+}$) and dendritic cells ($CD11b^{+}F4/80^{-}CD11c^{+}$) (Figure 3.43A). Interestingly, none of the adjuvanted multiAgs vaccines could increase macrophages and dendritic cell populations while significantly reducing macrophage populations compared to multiAgs (Figure 3.43B-C).

In summary, MA-NP adjuvant systems augmented tumor-fighting immune cells while decreasing tumor-suppressive immune cells in the spleen. Therefore, MA-NP adjuvant systems demonstrated a potential for use in cancer immunotherapy.

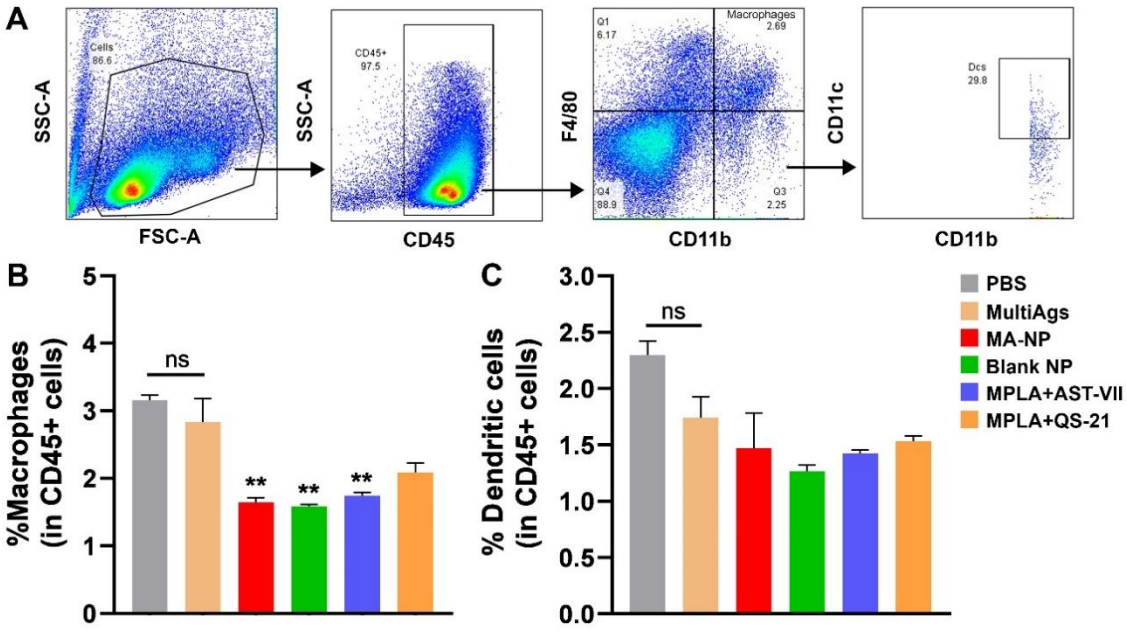

Figure 3.43. MultiAgs loaded MA-NP decreased macrophage and dendritic cell populations in the spleen. (A) Gating strategies to identify macrophages and dendritic cells in the spleen. (B-C) Bar graphs show the frequencies (%) of macrophages and dendritic cells (in $CD45^{+}$ cells). Data are pooled from two independent experiments (mean ± SEM). The statistical analyses were performed between multiAgs and vaccination groups using One-way ANOVA and Tukey's multiple comparison test. ns: non-significant, **p < 0.01.

3.3.2. Assessment of Cytokine Production Following Vaccination with MultiAgs Integrated Adjuvant Systems

Antigen-specific memory T cell responses are subdivided phenotypically and functionally as effector and central memory T cells by producing different cytokines.[119] To evaluate functional T cell responses, Th1-mediated (IFN-γ and IL-2) and Th2-mediated cytokines (IL-10 and IL-4) were measured in splenocytes obtained from mice (un)vaccinated with multiAgs and adjuvant systems. For this purpose, the splenocytes were restimulated with multiAgs (10 μg/mL) for 24 h (IL-4) or 72 h (IFN-γ, IL-2 and IL-10). After that, the cell supernatant was analyzed by ELISA to elucidate cytokine responses.

Upon antigenic restimulation, soluble saponin adjuvants significantly increased IFN-γ levels compared to multiAgs (Figure 3.44A). In particular, MPLA+QS-21 adjuvanted multiAgs vaccine was more potent than MPLA+AST-VII adjuvanted multiAgs. In the case of IL-2, multiAgs augmented IL-2 levels compared to PBS. On the other hand, soluble saponin adjuvants were able to enhance IL-2 productions in contrast to multiAgs (Figure 3.44B). NP adjuvant systems did not alter the production of IFN-γ and IL-2. Th2-mediated cytokines were not detected in the cell supernatant by ELISA. As IFN-γ is predominantly produced by effector T cells while IL-2 is produced by central memory T cells,[119] these results showed that soluble saponin adjuvants were effective on memory T cell responses compared to NP form.

The administration of AS01 adjuvant system into mice showed that MPLA and QS-21 contributed to the synergistic production of IFN-γ in the spleen seven days after the last immunization.[120] In our study, soluble saponin adjuvant, MPLA+QS-21 demonstrated IFN-γ and IL-2 production in the spleen, even 14 days after the last immunization. Furthermore, there are reports showing that APS also improved IFN-γ and IL-2 productions in mice sera.[121] To better evaluate the cytokine response induced by NP adjuvant systems, cytokine kinetic studies could be conducted, as Th1-mediated cytokines were not significantly elevated following injection of NP adjuvant systems 14 days after final immunization.

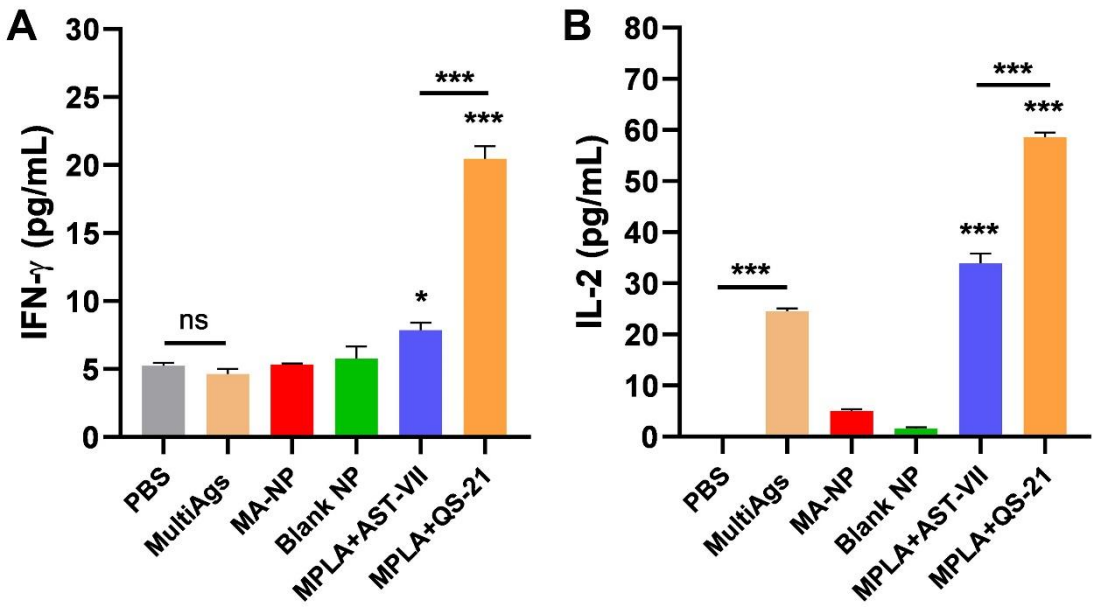

Figure 3.44. Soluble saponin adjuvants increased the production of Th1-mediated cytokines in the spleen. The splenocytes obtained from (un)vaccinated C57BL/6 mice were restimulated with multiAgs (10 μg/mL) for 72 h. The cell supernatant was collected to analyze IFN-γ and IL-2 by ELISA. The statistical analysis was performed between multiAgs and vaccination groups using One-way ANOVA and Tukey's multiple comparison test. ns: non-significant, *$p < 0.05$, ***$p < 0.001$.

3.3.3. Investigating Humoral Immune Response Following Vaccination with MultiAgs Integrated Adjuvant Systems

Monoclonal antibodies (mAbs) can specifically bind to a target antigen and induce cytotoxicity by showing pro-apoptotic effects in cancer cells. This effect is promoted by innate immune response through antibody-dependent cellular cytotoxicity (ADCC), complement-dependent cytotoxicity (CDC), and antibody-dependent cellular phagocytosis (ADCP). Thus, determining antibody responses to specific tumor antigens as a measure of the anti-tumor activity is essential, and there have been enormous mAbs studies currently carried out in clinical trials.[122,123] In light of this information, the production of Trp-2 and PADRE-specific antibodies following vaccination with multiAgs

integrated adjuvant systems has been investigated in mice sera by ELISA. In all IgG subsets, multiAgs did not make any difference compared to PBS. For Trp-2 specific IgG response, MA-NP and MPLA+QS-21 adjuvanted multiAgs increased IgG titers (Figure 3.45A).

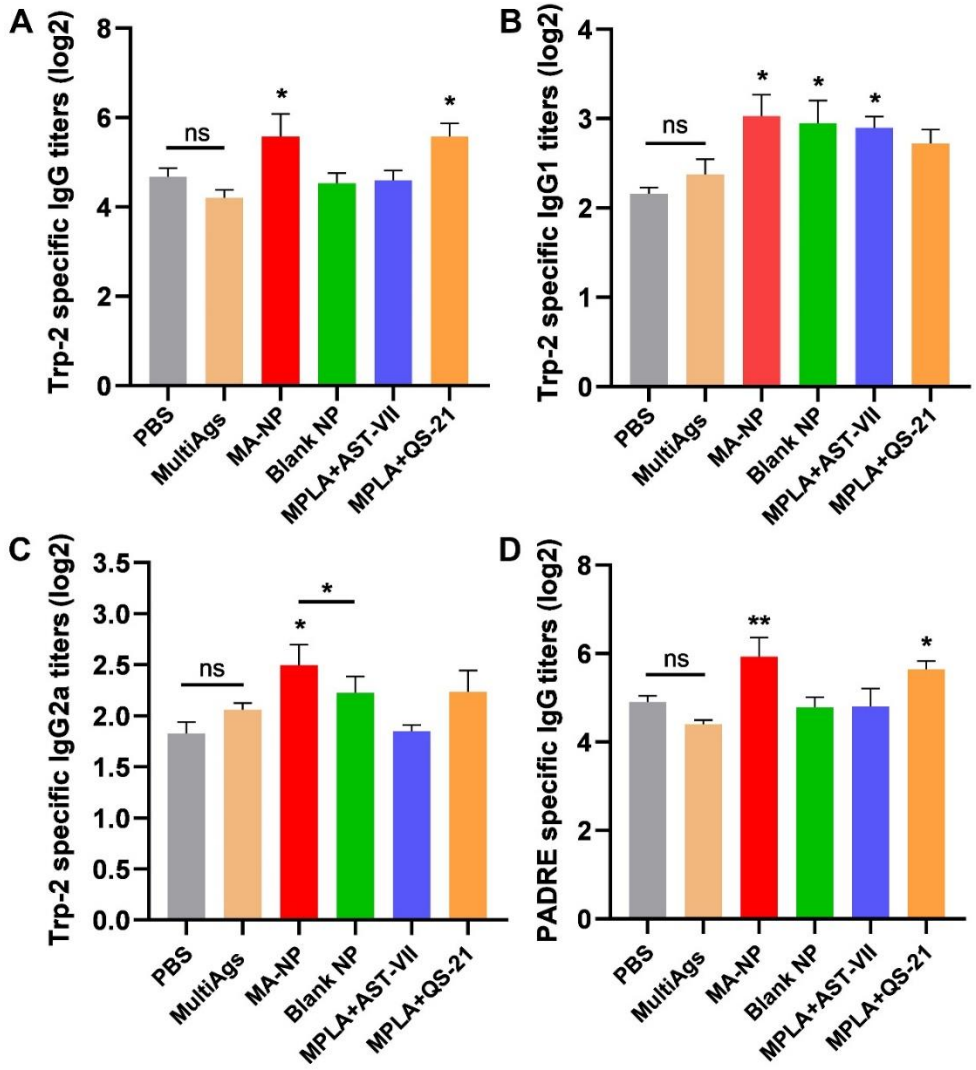

Figure 3.45. MA-NP adjuvanted multiAgs enhanced humoral immune response. The blood samples were obtained from (un)vaccinated C57BL/6 mice on day 21. Trp-2 specific (A) IgG, (B) IgG1, (C) IgG2a, and (D) PADRE-specific IgG titers in mice sera were measured by ELISA. The statistical analyses were performed between multiAgs and vaccination groups using One-way ANOVA and Tukey's multiple comparison test. ns: non-significant, *$p < 0.05$, **$p < 0.01$.

Trp-2 specific IgG1 titers were detected in MA-NP, blank NP, and MPLA+AST-VII adjuvanted multiAgs, demonstrating Th2-mediated immune response as IgG1 is an indicator of this response (Figure 3.45B).[124] On the other hand, IgG2a production, which represents Th1-mediated response,[124] was only enhanced by MA-NP adjuvanted multiAgs (Figure 3.45C). In addition to Trp-2 specific IgG responses, MA-NP and MPLA+QS-21 adjuvanted multiAgs augmented PADRE-specific IgG response compared to multiAgs (Figure 3.45D). These results indicated that the MA-NP adjuvanted vaccine enhances Th1/Th2 balanced humoral immune response.

QS-21 saponin adjuvant and the nanoparticulate adjuvant system containing *Quillaja* saponins (ISCOMATRIX, AS01, etc.) promote high antigen-specific antibody response in pre-clinical and clinical studies.[4,115,120,125] A comparable antigen-specific antibody response in MA-NP vaccinated mice was observed in those treated with MPLA+QS-21, highlighting the potential of MA-NP as a candidate for vaccines that require a robust humoral immune response.

In summary, multiAgs integrated MA-NP demonstrated promising results, particularly in increasing the tumor-fighting immune cells and decreasing tumor-promoting immune cell populations. Additionally, this adjuvant system enhanced the production of multiAgs-specific Th1/Th2 balanced antibody responses. On the other hand, soluble saponin adjuvants provided Th1-mediated cytokine productions upon antigen restimulation, signifying memory T cell responses. Therefore, it was decided to investigate the efficacy of MA-NP and soluble saponin adjuvants in murine melanoma models.

3.4. Investigating Anti-tumor Efficacy of Antigen Loaded NPs in Murine Melanoma Models

The murine B16 melanoma model is a metastatic clone of B16 cell line derived from spontaneous melanoma of C57BL/6 mice and a widely used subcutaneous model for *in vivo* evaluation of cancer immunotherapies. B16-F10 cells are highly aggressive, poorly immunogenic, and hard to treat with conventional cancer vaccines.[74,126] Thus, the initial step in elucidating the efficacy of cancer immunotherapies involves establishing a

B16-OVA melanoma model, which expresses ovalbumin (OVA). This model is utilized to facilitate robust immune responses to tumor antigens. Therefore, in this thesis, the anti-tumor efficacy of MA-NP adjuvant system formulated with tumor antigens was investigated, initially using B16-OVA model and, subsequently B16-F10 model.

3.4.1. Prophylactic B16-OVA Model

MA-NP nanoparticulate and soluble adjuvants (MPLA+AST-VII and MPLA+QS-21) were formulated with SIINFEKL peptide. The vaccine formulations were subcutaneously administrated into C57BL/6 mice twice at one-week intervals. One week after the last immunization, the mice were challenged with B16-OVA cells. Tumor growth and body weight were measured every other day. Following vaccinations, there was no body weight loss observed in mice (Figure 3.46).

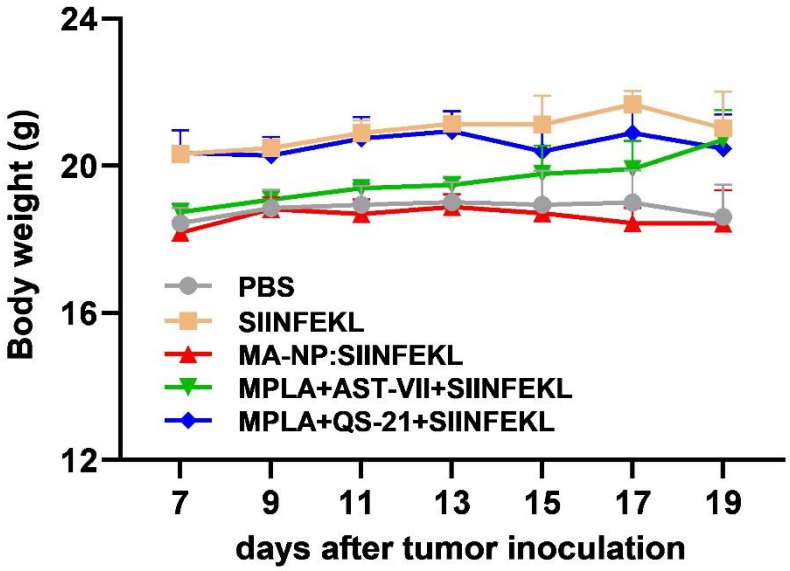

Figure 3.46. The body weight measurement of pre-vaccinated mice after B16-OVA tumor cell inoculation.

The tumor volume in SIINFEKL-injected mice remarkably increased compared to PBS injected group, showing the low immunogenicity of the peptide itself. MA-NP adjuvanted vaccine statistically slowed the tumor growth compared to PBS and SIINFEKL injected groups (Figure 3.47). Furthermore, MA-NP adjuvanted vaccine demonstrated superior anti-tumor response in terms of tumor progression over soluble saponin adjuvants (MPLA+AST-VII and MPLA+QS-21) ($p<0.01$), indicating the effectiveness of nanoparticulate form over soluble form. As shown in individual B16-OVA tumor growth curves (Figure 3.48), the tumor progression exhibited a sharp peak, especially in MA-NP vaccinated group 13 days after tumor inoculation. Luo et al. developed a nanoadjuvant with Saponin D, formulated with OVA antigen, and evaluated its anti-tumor efficacy in E.G7-OVA murine thymic lymphoma model. Similar to the data obtained from MA-NP:SIINFEKL, the tumor growth was significantly inhibited in saponin nanoadjuvant:OVA compared to OVA alone.[127]

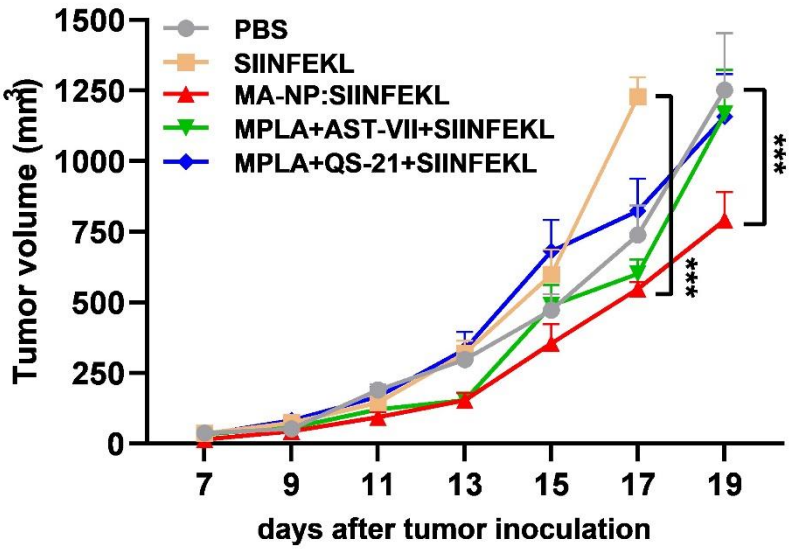

Figure 3.47. MA-NP reduced the tumor growth in B16-OVA prophylactic model. Pre-vaccinated mice were challenged with subcutaneous flank injection of B16-OVA cells, and tumor growth was measured over time. The data shown mean ± SEM from two independent experiments (n=5). The statistically significant differences between MA-NP and PBS or SIINFEKL were shown by One-way ANOVA, Dunnett's multiple comparisons, and Student-t tests. ***$p\leq0.001$.

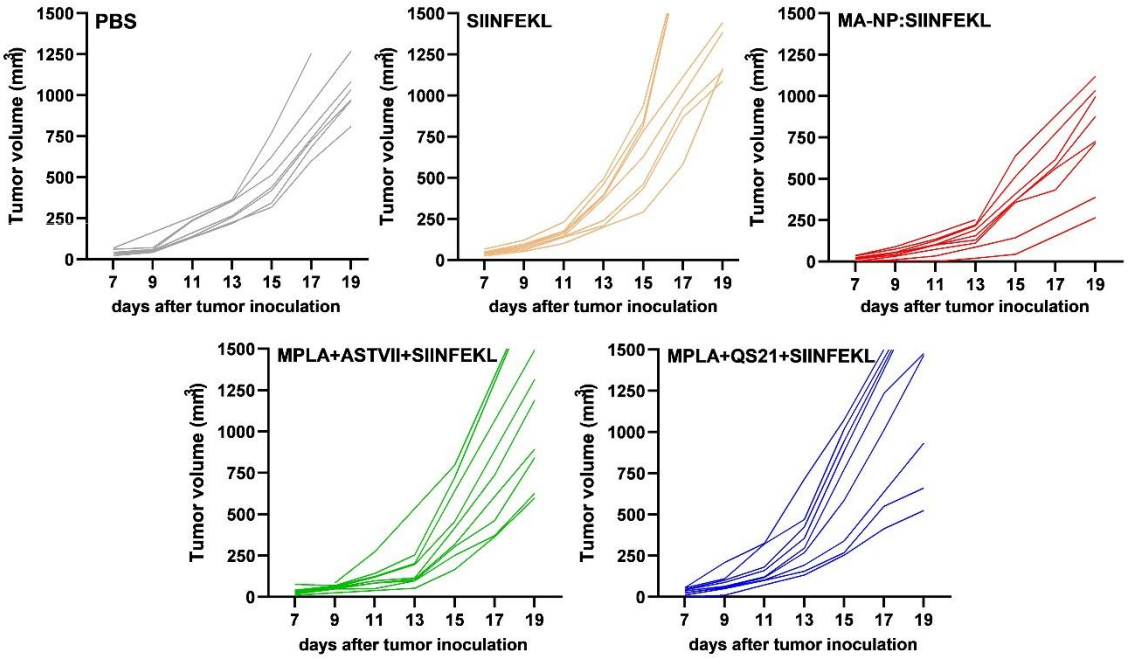

Figure 3.48. Individual tumor growth curves corresponding to each vaccination group in the prophylactic B16-OVA tumor model.

To clarify IFN-γ/IL-10 response following vaccinations, the blood samples were taken from pre-vaccinated mice 24 h after vaccinations. The blood sera were analyzed for IFN-γ, IL-10 and CXCL-10. Comparable IFN-γ levels between vaccination groups and PBS were detected in blood sera, whereas MPLA+QS-21+SIINFEKL vaccination significantly increased the level of anti-inflammatory cytokine IL-10 compared to PBS, MA-NP and MPLA+AST-VII+SIINFEKL (Figure 3.49A). As IL-10 has a prominent role in the down-regulating pathways for anti-tumor immune response,[128] comparable levels between MA-NP and PBS provided a promising result for its anti-tumor activity.

CXCL-10 chemokine and its receptor CXCR3 are important for the infiltration of effector T cells to tumor tissue.[129] Therefore, CXCL-10 level in mice sera was measured, and a substantial CXCL-10 induction following vaccination with MPLA+QS-21+SIINFEKL was achieved (Figure 3.49B), indicating the potential role of this soluble adjuvant in T cell infiltration into the tumor. This result is also consistent with literature demonstrating that the nanoparticulate form of MPLA+QS-21, AS01, induced CXCL-10 chemokine at the injection site and draining lymph nodes. Taken together, these results showed that MA-NP did not alter systemic IFN-γ/IL-10/CXCL-10 levels in mice sera.

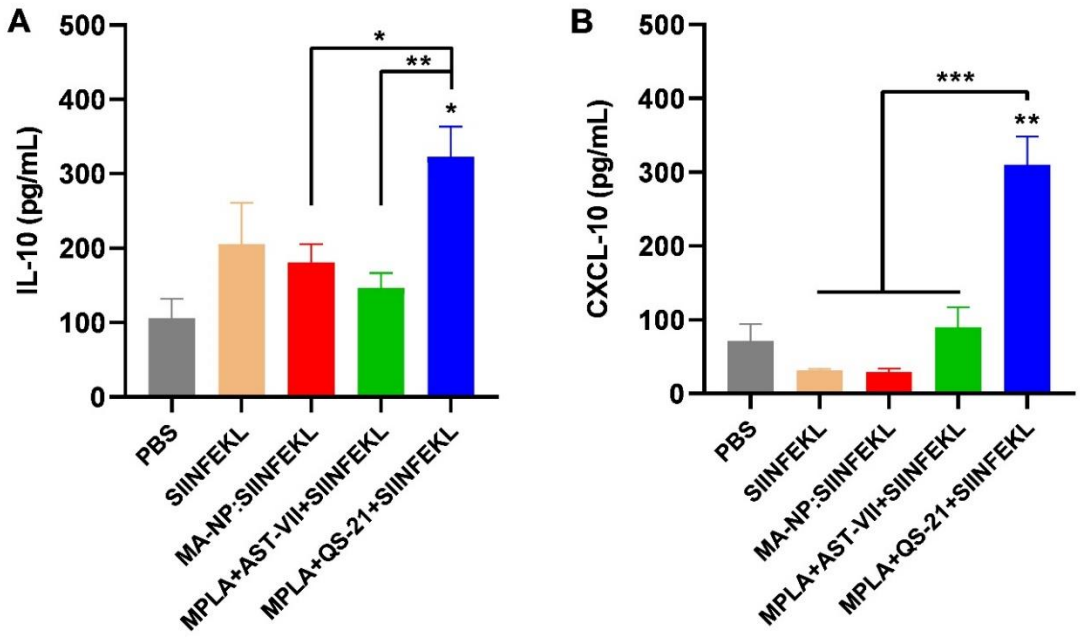

Figure 3.49. The levels of (A) IL-10 and (B) CXCL-10 in mice sera. The mice were subcutaneously injected with vaccination groups. 24 h after vaccinations, the blood samples were collected, and the mice sera were analyzed for IL-10 and CXCL-10 by ELISA. The data shown mean ± SEM from a representative experiment (n = 5). The statistically significant differences between MPLA+QS-21+SIINFEKL and PBS or treatment groups were shown by One-way ANOVA, Tukey's multiple comparison test. *$p \leq 0.05$, **$p \leq 0.01$, ***$p \leq 0.001$.

To elucidate the immune cell populations involved in the effective anti-tumor response, immune cell populations in PBMCs and tumor tissue were analyzed both phenotypically and functionally. Tumor antigen-specific cytotoxic T cells (CTLs) are fundamental effector cells in TME, providing recognition and elimination of tumor cells; thus, augmenting the number of functional CTLs is a key objective in developing cancer immunotherapeutics. Considering this knowledge, SIINFEKL-specific effector CTL response was investigated in PBMCs following tetramer staining. Only MA-NP adjuvanted SIINFEKL vaccine demonstrated a statistically significant increase in the frequency of $SIINFEKL^{+}CD8^{+}$ T cell population compared to SIINFEKL vaccine on day 7 (Figure 3.50A).

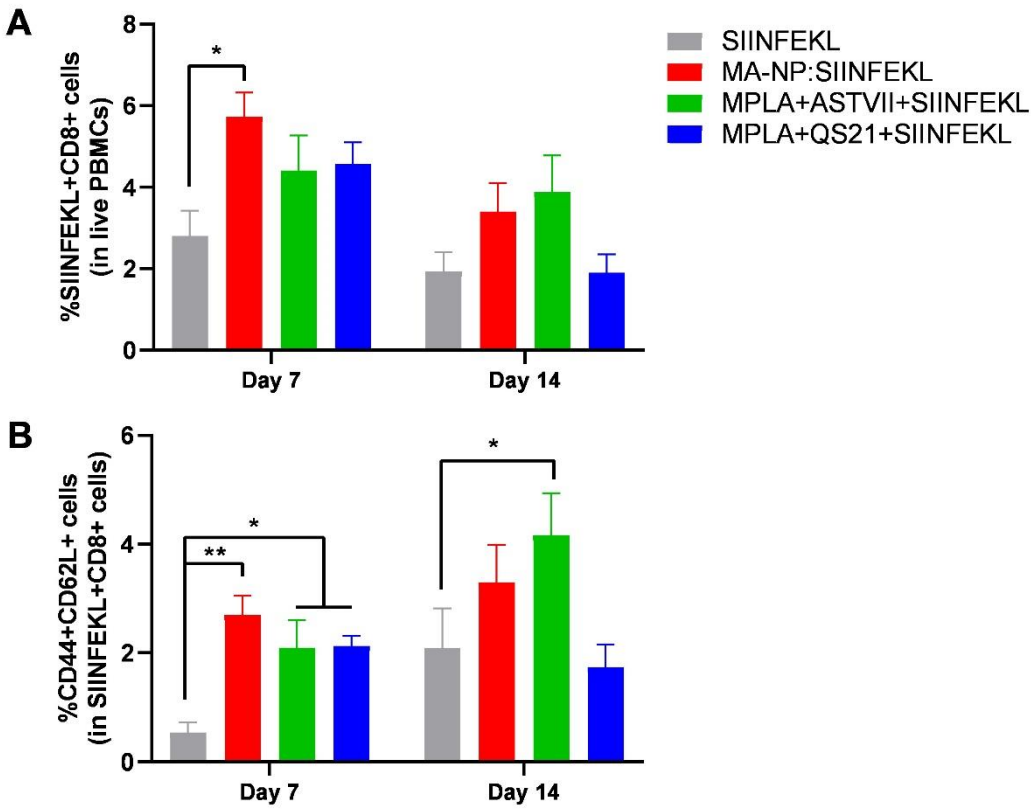

Figure 3.50. MA-NP enhanced SIINFEKL-specific CD8 T cells with central memory response. The mice were vaccinated twice with nanoparticulate and soluble saponin adjuvants. The blood samples were collected one-week after each vaccination. The frequencies of (A) $SIINFEKL^{+}CD8^{+}$ and (B) $CD44^{+}CD62L^{+}$ T cells in PBMCs were analyzed by flow cytometry. The data shown mean ± SEM from two independent experiments (n = 5). The statistically significant differences between vaccination groups and SIINFEKL were shown by One-way ANOVA, Tukey's multiple comparison test. *$p \leq 0.05$, **$p \leq 0.01$.

Moreover, there was a decreasing pattern in the frequencies of $SIINFEKL^{+}CD8^{+}$ T cells following boosting injections on day 14. Raaijmakers et al. revealed that the mice treated with cryoablation and immunized with saponin-based adjuvant, ISCOMS, and CpG showed an increase in OVA antigen-specific T cells compared to saponin adjuvant alone.[130] These data, consistent with the literature, indicate that TLR agonist-inserted nanoparticulate saponin-based adjuvants demonstrated strong antigen-specific CTL

responses compared to their soluble forms.

Selective generation of central memory T cells (Tcm), having a role in viral and tumor models to provide protective and therapeutic immunity, is one of the important cell populations in the field of cancer immunotherapy.[131] Within this context, the frequency of $CD44^+CD62L^+$ cell population in $SIINFEKL^+CD8^+$ T cells, a phenotype for central memory T cells, was investigated in PBMCs. On day 7, MA-NP and soluble saponin adjuvants enhanced $CD44^+CD62L^+$ cells compared to SIINFEKL alone (Figure 3.50B). Although MA-NP demonstrated superior Tcm response over soluble saponin adjuvants on day 7, MPLA+AST-VII increased Tcm populations compared to MA-NP on day 14. These data suggest that MA-NP adjuvant provided SIINFEKL-specific CTLs primarily exhibiting central memory CD8 T cell response.

Next, the effect of immunomodulation on the anti-tumor response elicited by the treatment of MA-NP and soluble saponin adjuvants was investigated within the tumor microenvironment (TME). MA-NP vaccination led to significantly higher intratumoral infiltration of total $CD3^+$ T and $CD4^+$ T cells than SIINFEKL (Figure 3.51A-B). As hot tumors are characterized by a high infiltration of lymphocytes, MA-NP vaccination turned the local TME into a more inflamed TME.[132] On the other hand, there were no significant changes in the population of $CD25^+CD4^+$ T, $CD8^+$ T, and $CD25^+CD8^+$ T cells following the treatment of vaccination groups (Figure 3.51C-F). However, an increase in the $CD4^+$ T cell population by MA-NP could result in the induction of effector function of $CD8^+$ T cells like cytotoxic activity on tumor cells and secretion of tumoricidal cytokines. Silva et al. showed that ISCOMATRIX-OVA vaccine provided significant protection in B16-OVA tumor model with long-term memory $CD8^+$ T cell response. In contrast to MA-NP:SIINFEKL vaccine, a $CD4^+$ T cell response is not required to achieve protection following ISCOMATRIX-OVA vaccination.[133]

Recent studies showed that immunization with synthetic long peptides induced a sustained $CD8^+$ T cell response due to $CD4^+$ T cell help, whereas immunization with antigenic epitope for $CD8^+$ T cells provided fleeting $CD8^+$ T cell response.[134] Here, adjuvant type and formulation also contributed to $CD4^+$ T cell and $CD8^+$ T cell responses besides peptide length and type.

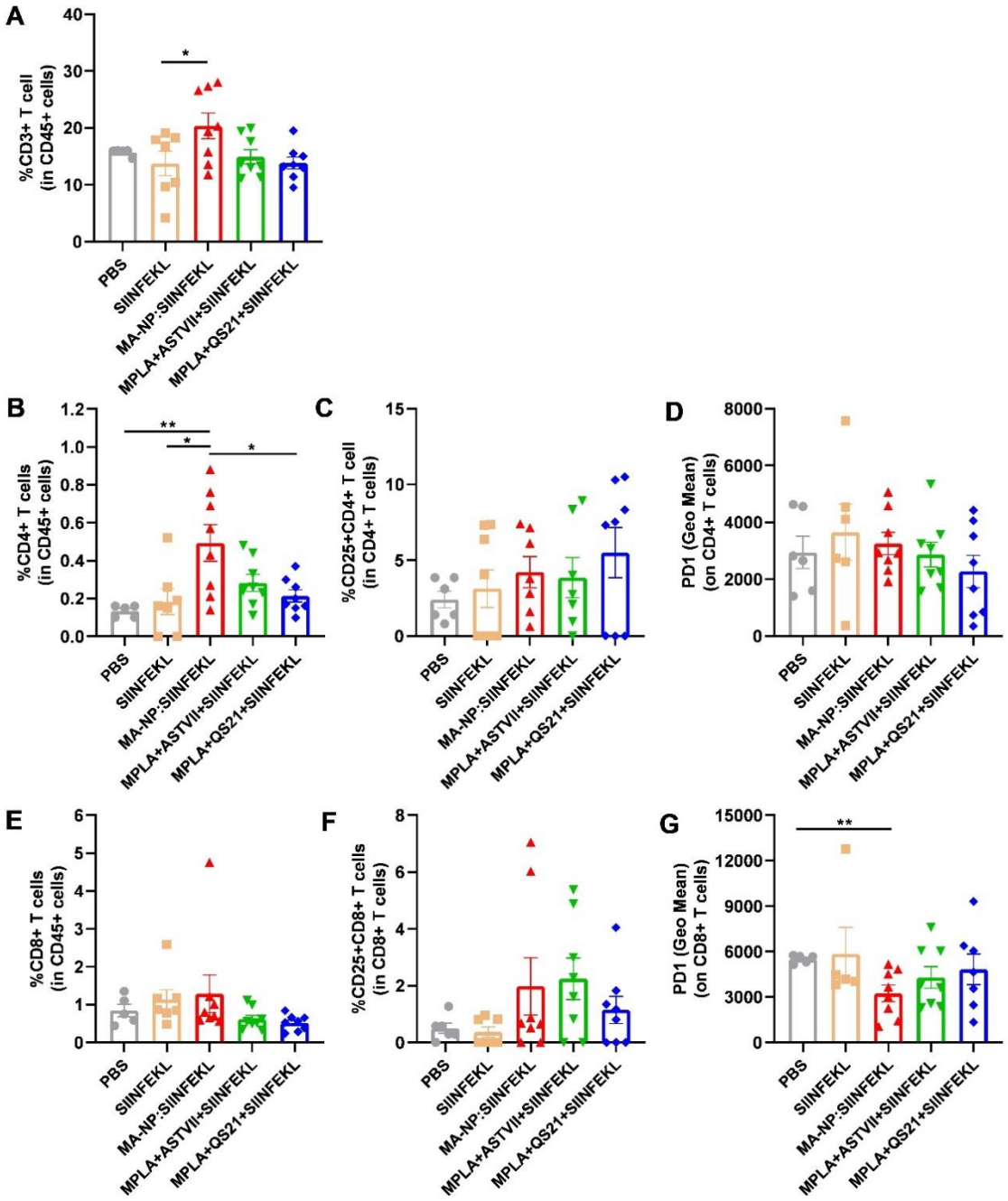

Figure 3.51. MA-NP increased the population of total $CD3^+$ and $CD4^+$ T cells in TME. The mice were immunized twice with vaccination groups and challenged with B16-OVA tumor cells. Intratumoral immune cell phenotypes were analyzed by flow cytometry. (A-F) Particular immune cell populations and (D, G) PD1 expression on T cells were shown. The data shown mean ± SEM from two independent experiments (n = 4). The statistically significant differences between vaccination groups were shown by One-way ANOVA, Student-t test, and Tukey's multiple comparison test. *p≤0.05, **p≤0.01.

Programmed cell death-1 (PD-1) is one of the major immune checkpoint pathways. The interactions between PD-1 on T cells and PD ligand-1 (PD-L1) on tumor cells or APCs silence T cell activation and T cell-mediated tumor cell killing.[135] Therefore, TME could lead to upregulation of PD-1 on tumor antigen reactive T cells, eventually contributing to impaired anti-tumor immune response.[136] For that reason, PD-1 expression on $CD4^+$ and $CD8^+$ T cells was also investigated in TME.

The comparable PD-1 expression on $CD4^+$ T cells was observed between vaccination groups and PBS (Figure 3.51D). On the other hand, MA-NP treatment substantially decreased PD-1 expression on $CD8^+$ T cells compared to PBS (Figure 3.50G), indicating the active status of CTLs. Taken together, MA-NP adjuvanted vaccine provided $CD4^+$ T and $CD8^+$ T cell-mediated anti-tumor response.

Meanwhile, macrophage and dendritic cell populations in TME were also investigated. The vaccination groups demonstrated comparable macrophage populations in TME with PBS (Figure 3.52A). There was an increase in CD86 expression on macrophages, especially in response to soluble saponin adjuvants (Figure 3.52B). In the case of DCs, these cells could cross-present tumor antigens to naive T cells, making them crucial in the generation of antigen-specific T cell-mediated anti-tumor response in the control of tumor growth and tumor cell elimination. However, an immunosuppressive TME can impair the effector functions of DCs.[137] In light of this information, only MA-NP significantly induced the frequency and expression of CD86 on dendritic cells in TME (Figure 3.52C-D), indicating the presence of functional DCs in TME.

den Brok et al. demonstrated that saponin-based adjuvants provided cross-presentation of antigen, the induction of tumor-specific CTL responses and long-lasting tumor protection.[54,138] Inspired by this work, it could be concluded that MA-NP may be effective in the cross-presentation of tumor antigen by intratumoral DCs and further enhances CTL response, reducing tumor growth.

Overall, these results suggest that vaccination with MA-NP amplifies antigen-specific cytotoxic T cell and central memory responses and potently activates intratumoral total $CD3^+$, $CD4^+$ T cells, and DCs, thus leading to regression of established tumors in prophylactic B16-OVA melanoma model. With these encouraging results, it was decided to investigate the anti-tumor efficacy of MA-NP with a melanoma-associated antigen in a highly aggressive prophylactic B16-F10 melanoma model.

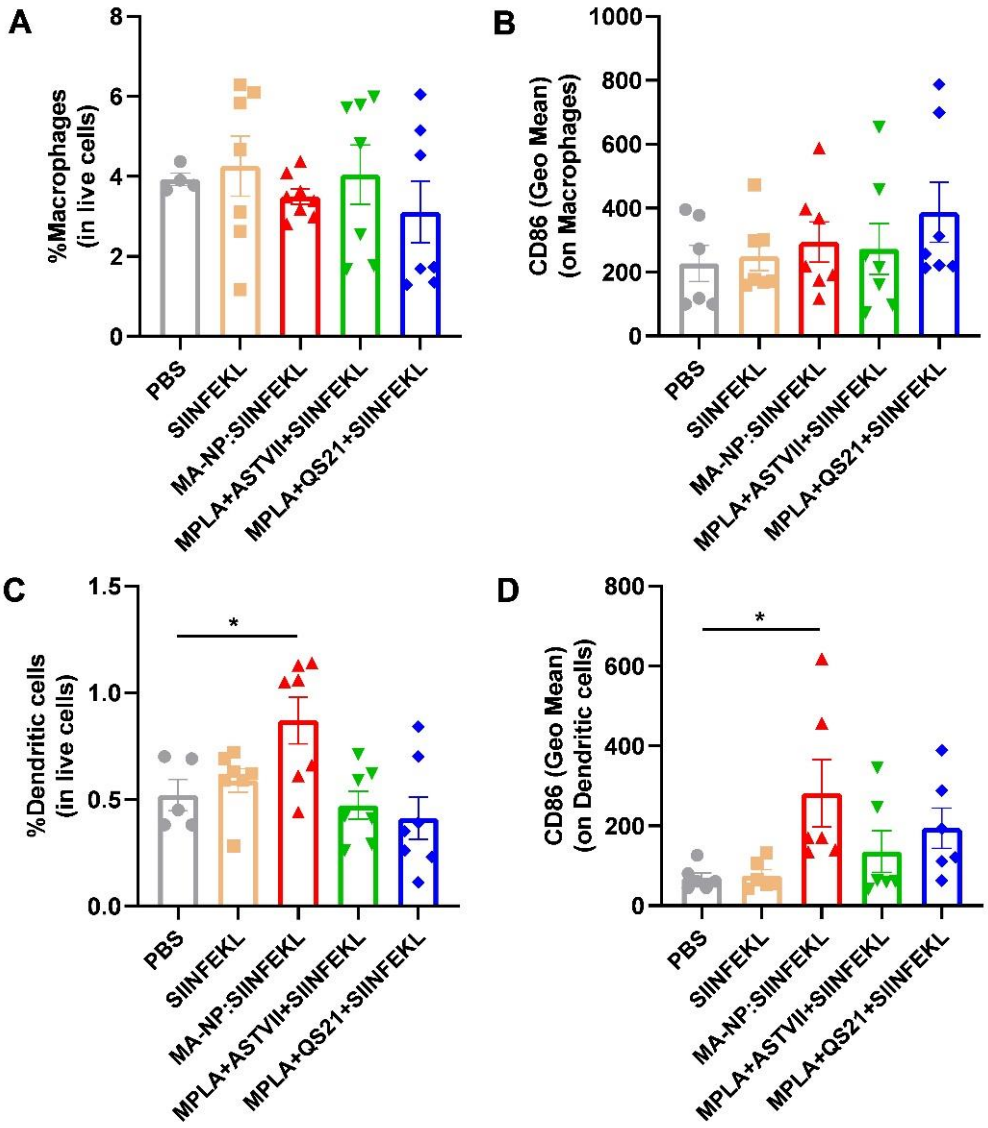

Figure 3.52. MA-NP increased functional DC populations in TME. (A) Macrophage population (%) in live cells, (B) CD86 expression on macrophages, (C) DCs population (%) in live cells, (D) CD86 expression on DCs. The data shown mean ± SEM from two independent experiments (n = 4). The statistically significant differences between vaccination groups were shown by One-way ANOVA, Student-t test, and Tukey's multiple comparison test. *p≤0.05.

3.4.2. Prophylactic B16-F10 Model

To elicit broad-spectrum T cell responses, the peptides corresponding to CD8 T cell and CD4 T cell epitopes were selected for B16-F10 melanoma models. Tyrosinase-related protein-2 (Trp-2) is an MHC-I-restricted epitope recognized by both human and murine CTLs. As Trp-2 peptide is a melanoma-associated antigen, this peptide is widely used in the development of new cancer immunotherapeutics against melanoma in pre-clinical and clinical trials.[139–142] On the other hand, Pan HLA-DR epitope (PADRE) is a universal MHC-II restricted epitope used for $CD4^+$ T cell-mediated $CD8^+$ T cell activation.[143]

MA-NP nanoparticulate and soluble saponin adjuvants (MPLA+AST-VII and MPLA+QS21) were formulated with Trp-2 and PADRE (multiAgs) peptides. The vaccine formulations were subcutaneously administrated into C57BL/6 mice twice at one-week intervals. The mice were challenged with B16-F10 tumor cells one week after the last immunization. Tumor growth and body weight were measured every other day. No body weight loss was observed in mice following immunizations with multiAgs formulated vaccination groups (Figure 3.53).

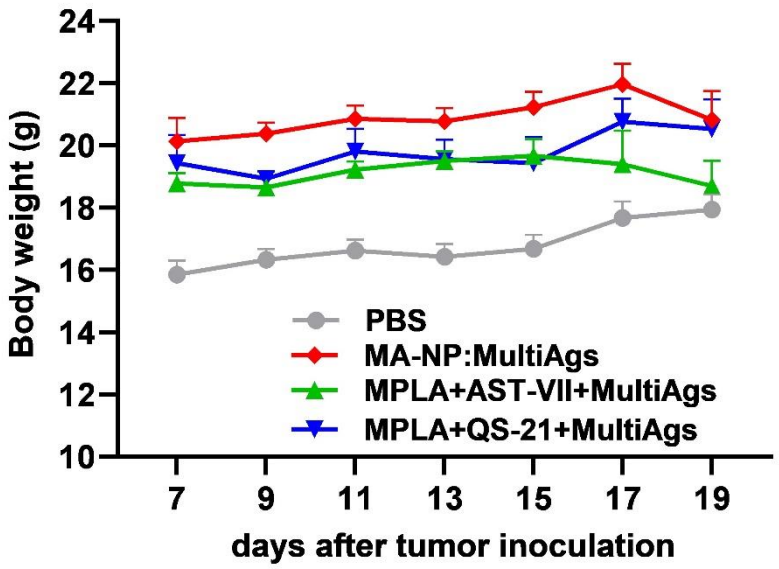

Figure 3.53. The body weight measurement of pre-vaccinated mice after B16-F10 tumor cell inoculation.

As shown in Figure 3.54, MA-NP and soluble saponin adjuvants significantly decreased tumor growth compared to PBS-injected mice. When individual tumor growth curves were analyzed, MA-NP demonstrated superior anti-tumor activity over soluble saponin adjuvants (Figure 3.55), similar to the results obtained from B16-OVA tumor model.

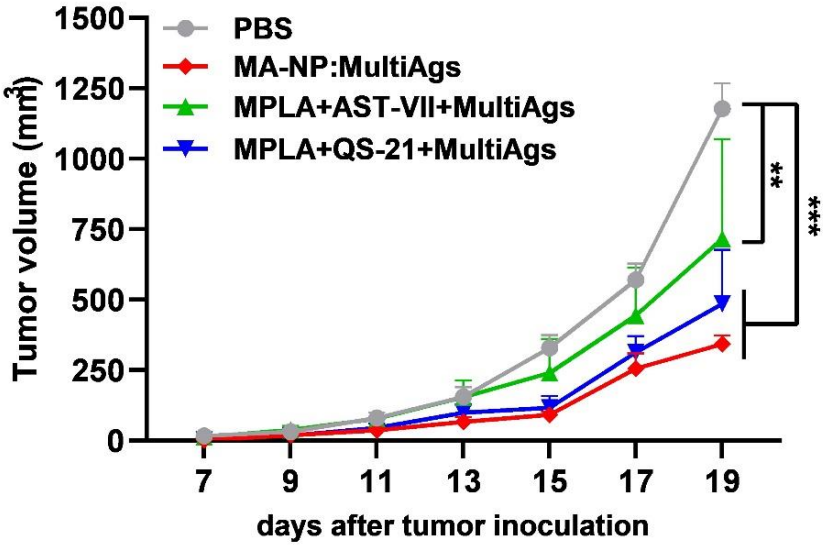

Figure 3.54. MA-NP was able to delay tumor growth in B16-F10 prophylactic model. Pre-vaccinated mice were challenged with subcutaneous flank injection of B16-F10 cells, and tumor growth was measured over time. The data shown mean ± SEM from two independent experiments (n=5). The statistically significant differences between vaccination groups and PBS were shown by One-way ANOVA, Dunnett's multiple comparisons, and Student-t test. **p≤0.01, ***p≤0.001.

Even et al. developed lipids implants containing Trp-2 peptide and Quil-A saponin adjuvant for cancer therapy. *In vivo* studies showed that Trp-2 and Quil-A implants were similarly able to delay tumor growth with Trp-2 injected mice group.[144] In another study, Highton et al. prepared chitosan hydrogel consisting Trp-2 peptide and Quil-A, and revealed that vaccination with this formulation protects mice against subcutaneous B16 challenge.[145] The studies carried out with an AS01 adjuvant system containing

MPLA/QS-21 adjuvants in a liposomal carrier system demonstrated that the mice were immunized with AS01 and MAGE-A3 peptide poorly protected mice following challenge with TC-1 tumor cells.[146] Therefore, AS01 adjuvant system is not preferable in cancer immunotherapy studies. On the other hand, consistent with literature, integration of MPLA/AST-VII into APS nanocarriers provided slower tumor growth than its soluble form and soluble QS-21 adjuvant, demonstrating a potency to be utilized in cancer immunotherapy studies.

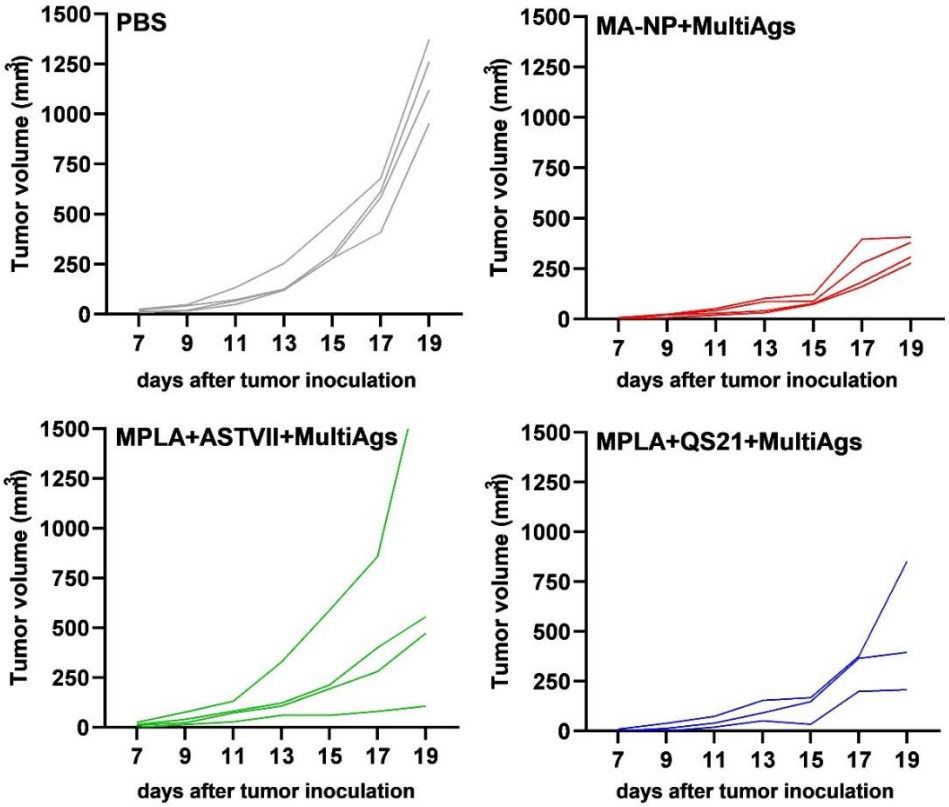

Figure 3.55. Individual tumor growth curves corresponding to each vaccination group in the prophylactic B16-F10 tumor model.

To assess the functionality of $CD8^+$ T cells, the blood samples were collected in mice one week after the last immunization. PBMCs were re-stimulated with Trp-2 and PADRE peptides, and IFN-γ^+CD8^+ T cell population was analyzed by flow cytometry. Only MA-NP:MultiAgs significantly augmented IFN-γ^+CD8^+ T cell population in

PBMCs compared to PBS (Figure 3.56). These results demonstrated that MA-NP:MultiAgs vaccination provided a functional cytotoxic T cell response. Similar to MA-NP, CpG/ISCOM vaccinated mice also showed higher IFN-γ^+CD8$^+$ T cell response compared to its soluble forms.[130]

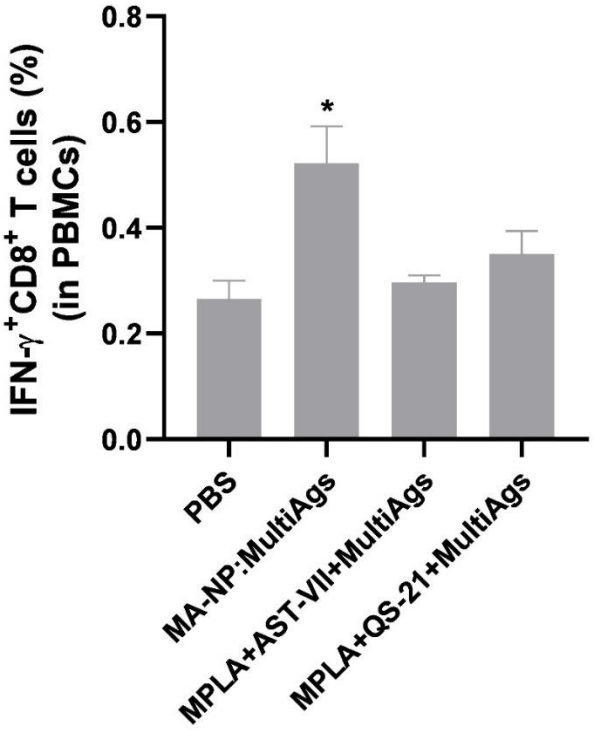

Figure 3.56. MA-NP enhanced the population of functional cytotoxic T cells. The blood samples were collected one-week after the last vaccination. PBMCs were re-stimulated with Trp-2 and PADRE peptide for 6 h and the frequencies of IFN-γ^+CD8$^+$ T cells were analyzed using flow cytometry. The data shown mean ± SEM from two-independent experiments (n = 5). The statistically significant differences between vaccination groups and PBS were shown by One-way ANOVA, Tukey's multiple comparison test. *$p \leq 0.05$.

Next, the immune cell populations in TME following vaccination with multiAgs formulated MA-NP and soluble saponin adjuvants were analyzed by flow cytometry. MPLA+AST-VII significantly increased total (CD3$^+$ T cell) and CD8$^+$ tumor-infiltrating lymphocytes, while MA-NP substantially augmented CD8$^+$ T cell populations in TME.

Moreover, MA-NP and MPLA led to a slight increase in $CD4^+$ T cells comparable with soluble adjuvants (Figure 3.57A-C).

Similar to data obtained from B16-OVA tumor model, neither MA-NP nor soluble saponin adjuvants provide an increase in $CD25^+CD4^+$ T and $CD25^+CD8^+$ T cell populations. CXCR3 is a chemokine receptor, highly expressed on Th1-type $CD4^+$T cells and $CD8^+$ T cells, providing effector cell trafficking to tumors.[147] MA-NP and soluble saponin adjuvants enhanced the upregulation of CXCR3 on $CD4^+$ T cells. Moreover, MPLA+QS-21 showed superior CXCR3 expression on $CD4^+$ T cells compared to MA-NP and MPLA+AST-VII, consistent with robust CXCL-10 production in mice following injection with MPLA+QS-21 (Figure 3.57D-H). Additionally, MA-NP vaccination led to a substantial increase in PD-1 expression on $CD8^+$ T cells in TME (Figure 3.57I), thus correlating the exhausted phenotype and impaired effector function of tumor antigen-specific $CD8^+$ T cells, eventually causing progression on tumor growth. Hwang et al. revealed that APS enhanced the growth-inhibitory activity of anti-PD-L1 mAbs against metastatic melanoma in mice.[148] PD-L1 is typically expressed on the surface of tumor cells and plays a crucial role in allowing tumors to evade CTLs. Therefore, therapies targeting PD-1/PD-L1 are vital for rescuing exhausted T cells.[149] However, APS containing MA-NP may not be effective in reducing PD-L1 expression in melanoma due to the high expression of PD-1 on $CD8^+$ T cells.

Macrophage and dendritic cell populations in TME following vaccination were also investigated. MA-NP and MPLA+AST-VII increased the functional macrophage populations, whereas only MA-NP enhanced the infiltration of DCs in TME. MA-NP and soluble saponin adjuvants were significantly able to increase CD86 expression both on macrophages and DCs (Figure 3.58), showing their effector functions even in highly immunosuppressive TME.

Taken together, prophylactic vaccination with MA-NP induced functional IFN-γ+CD8+ T cells, augmenting intratumoral $CD8^+$ T cell, macrophage and DC populations and substantially slowed B16-F10 tumor growth compared to PBS and soluble saponin adjuvants. However, no tumor rejection was observed in either vaccination group. As high expression of PD-1 on tumor-infiltrating $CD8^+$ T cells was detected in the most potent vaccine formulation, MA-NP:MultiAgs, it could be feasible to combine MA-NP vaccinations with anti-PD1 antibody therapy in B16-F10 tumor models to block immunosuppressive PD-1/PD-L1 pathway.[150]

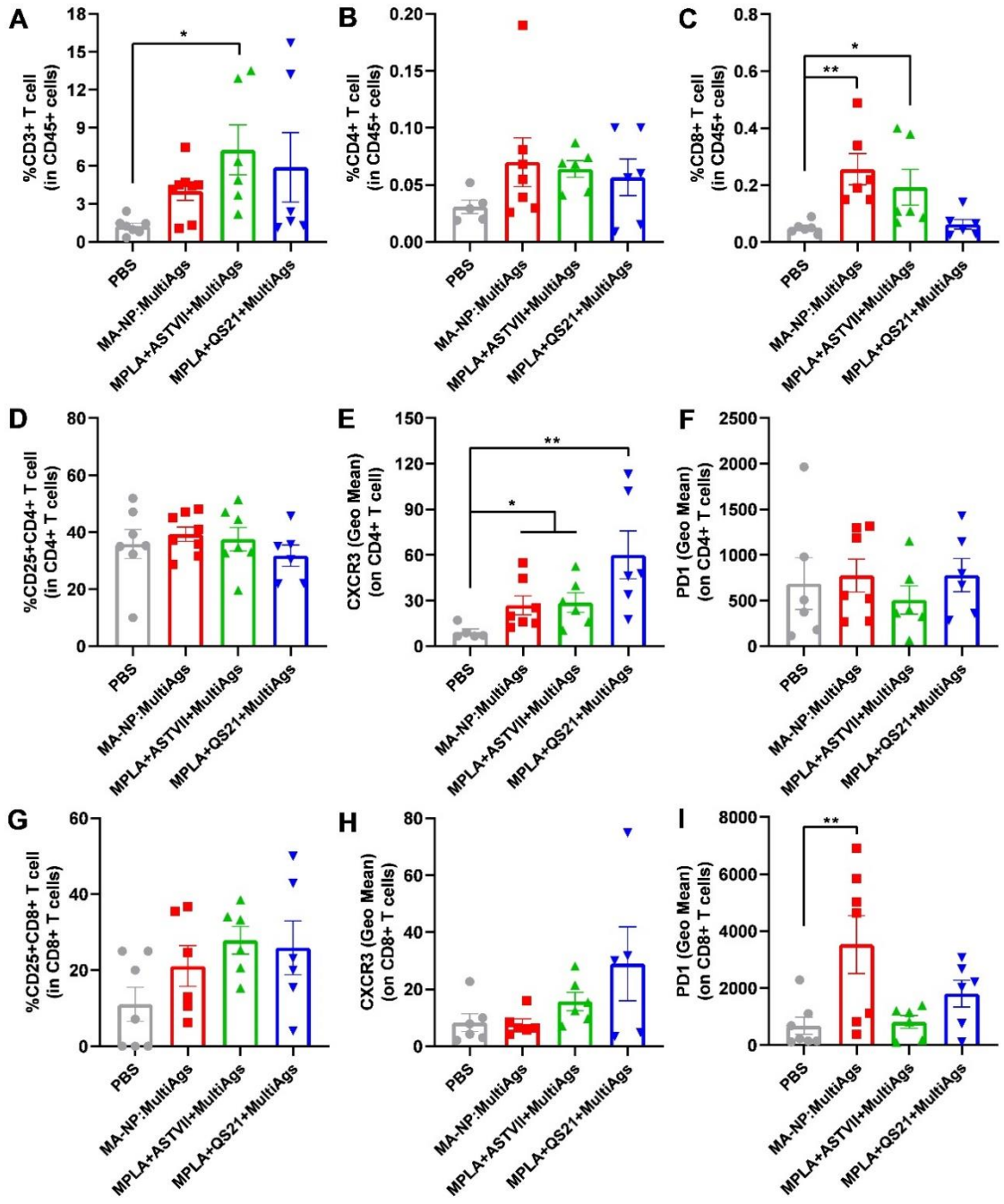

Figure 3.57. MA-NP increased the frequency of $CD8^+$ T cells and their PD-1 expressions in TME in the prophylactic B16-F10 model. Tumor tissues were collected on day 33, and immune cell phenotypes were analyzed by flow cytometry. The populations of $CD45^+$ cells, CXCR3, and PD-1 expression on T cells were shown. The data shown mean ± SEM from two independent experiments (n = 4). The statistically significant differences between vaccination groups were shown by One-way ANOVA, Student-t test, and Dunnett's multiple comparison test. *p≤0.05, **p≤0.01.

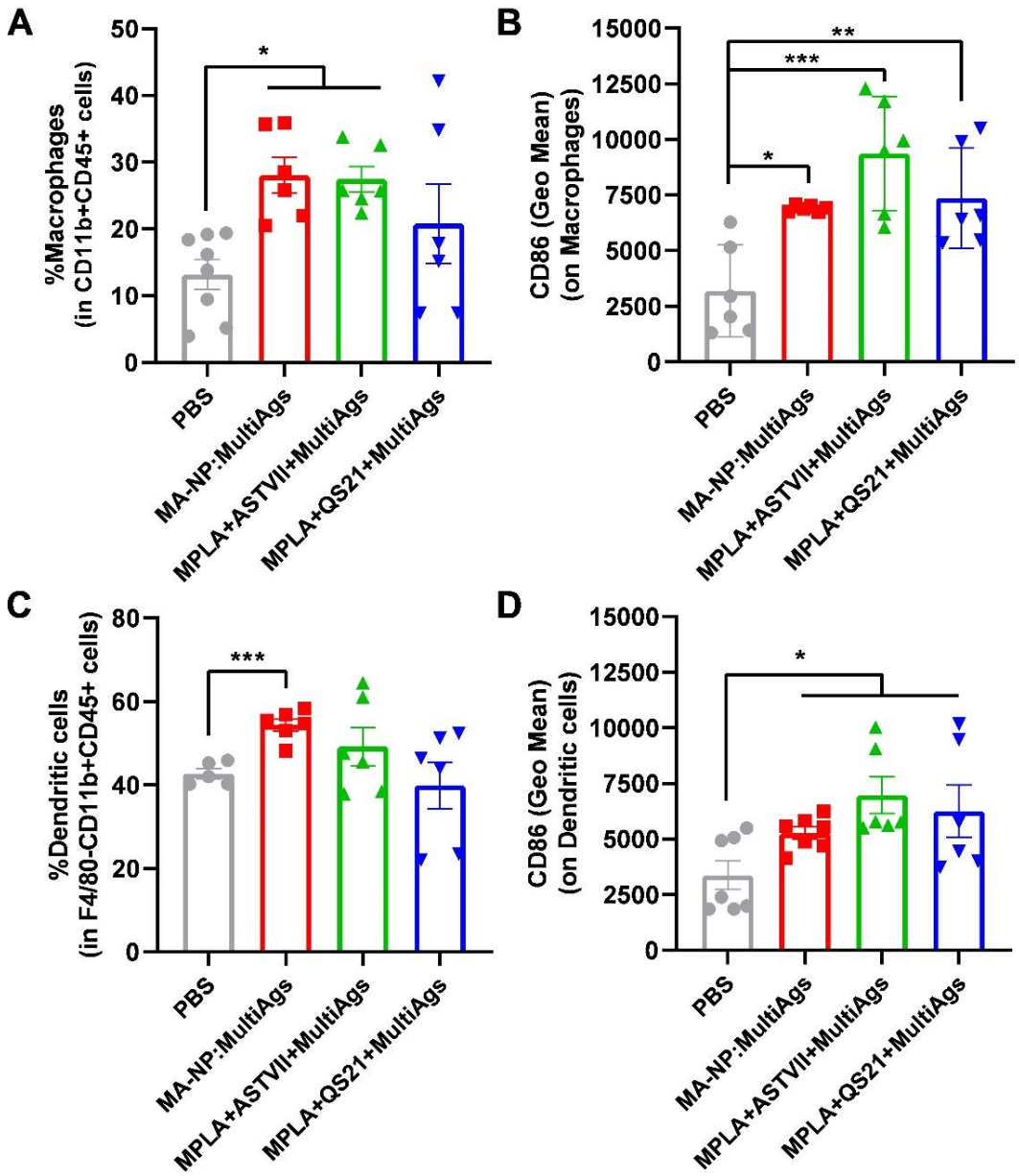

Figure 3.58. MA-NP increased functional macrophage and dendritic cell populations in TME. The frequency (%) of macrophages and DCs and the expression of CD86 on their surfaces were given. The data shown mean ± SEM from two independent experiments (n = 4). The statistically significant differences between vaccination groups were shown by One-way ANOVA, Student-t test, and Dunnett's multiple comparison test. *p≤0.05, **p≤0.01, ***p≤0.001.

3.4.3. Therapeutic B16-F10 Model

MA-NP adjuvanted peptide vaccines demonstrated superior anti-tumor activity compared to its soluble form (MPLA+AST-VII+MultiAgs) in prophylactic B16-OVA and B16-F10 tumor models. Therefore, therapeutic efficacy studies were conducted using MA-NP and MPLA+QS-21 as a positive control. For the therapeutic B16-F10 model, C57BL/6 mice were injected with B16-F10 cells. On days 3 and 10, the mice were s.c. vaccinated with MA-NP:MultiAgs and MPLA+QS-21+MultiAgs. To reveal the effect of combinatory therapy with anti-PD1, the mice were also injected with anti-PD1 two times after each vaccination. Tumor growth and body weight were measured every other day. As shown in Figure 3.59, no body weight loss was observed following vaccinations.

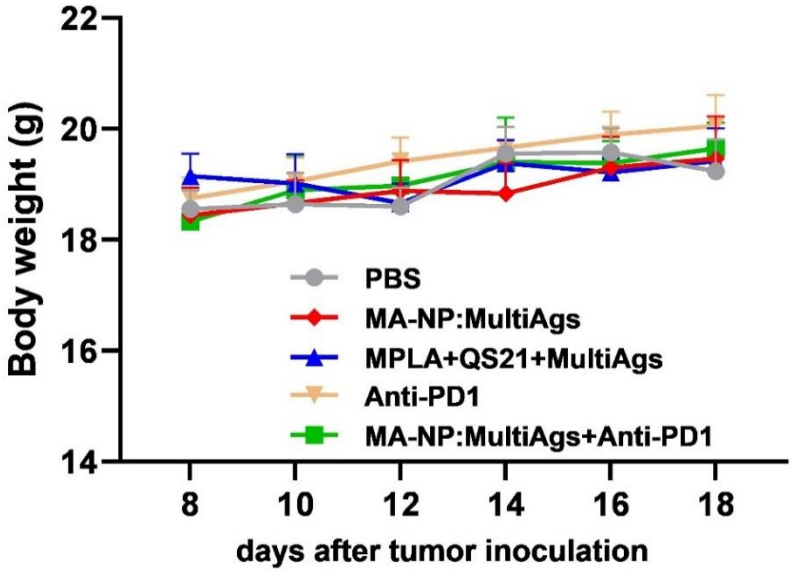

Figure 3.59. The body weight measurement of mice treated vaccination groups after B16-F10 tumor cell inoculation.

MA-NP:MultiAgs as a monotherapy significantly slowed down tumor growth compared to PBS (Figure 3.60). MPLA+QS-21+MultiAgs was not effective in the reduction of tumor growth. However, no tumor rejection was observed in MA-NP vaccinations in the therapeutic B16-F10 model, similar to the prophylactic B16-F10

model. As high PD-1 expression on intratumoral $CD8^+$ T cells was detected in the prophylactic B16-F10 model, combinatory immunotherapy with MA-NP:MultiAgs and anti-PD1 treatment was investigated. The anti-tumor effect of dual immunotherapy was also compared with anti-PD1 monotherapy, which is not an effective treatment alone against B16-F10 tumors.[151] The combination immunotherapy with MA-NP:MultiAgs and anti-PD1 treatment led to complete tumor elimination, as clearly seen in individual tumor growth curves and representative photographs of mice (Figure 3.60-62). Moreover, MA-NP monotherapy was also more effective than anti-PD1 monotherapy (Figure 3.60-62). These results showed that dual immunotherapy with MA-NP:MultiAgs and anti-PD1 has great potential as a new approach in cancer immunotherapy.

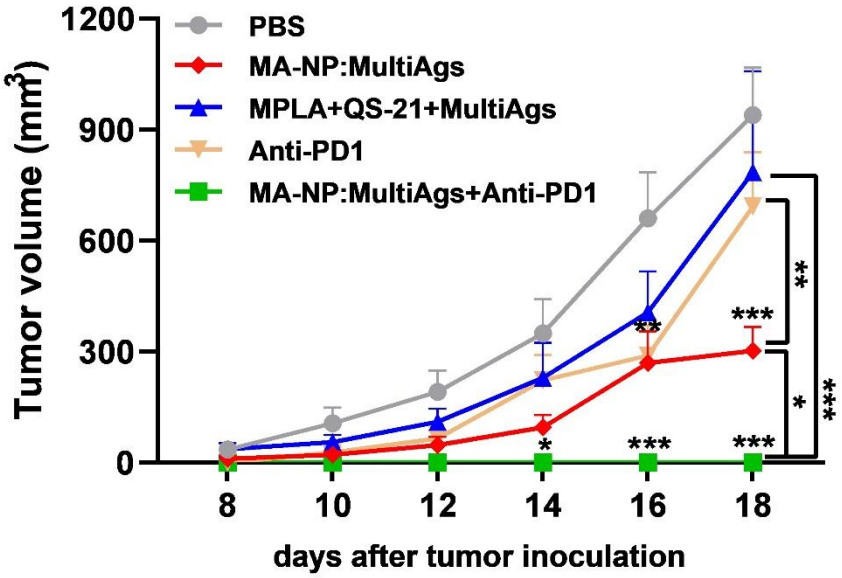

Figure 3.60. MA-NP was able to delay tumor growth, and its combination therapy with α-PD1 eradicated tumor tissue in B16-F10 therapeutic model. The mice were injected with s.c. in the flank of B16-F10 cells, and vaccination groups were s.c. administrated on days 3 and 10. Anti-PD1 was injected i.p. two times after each vaccination. Tumor growth was measured over time. The data shown mean ± SEM from two independent experiments (n=5). The statistically significant differences between vaccination groups and PBS were shown by One-way ANOVA, Dunnett's multiple comparison test and Student-t test. *p≤0.01, **p≤0.01, ***p≤0.001.

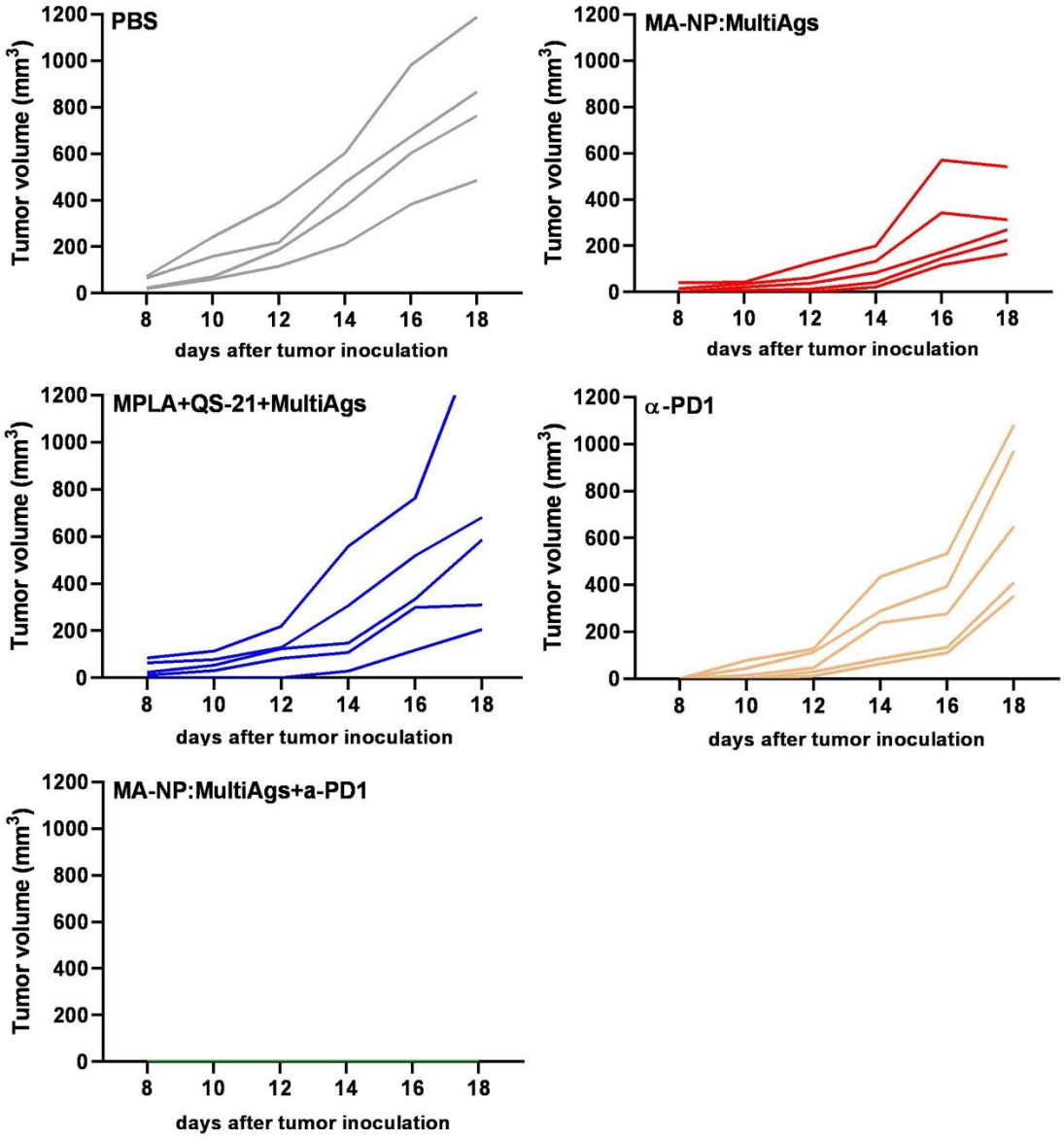

Figure 3.61. Individual tumor growth curves corresponding to each vaccination group in therapeutic B16-F10 tumor model.

Next, the immune cell population in TME was investigated by flow cytometry. MA-NP significantly increased intratumoral total immune cell and $CD8^+$ T cell populations and enhanced the upregulation of CD25 on $CD4^+$ T cells consistent with the prophylactic B16-F10 model (Figure 3.63). No PD1 expression was observed on either $CD8^+$ T cells or $CD4^+$ T cells following MA-NP treatment.

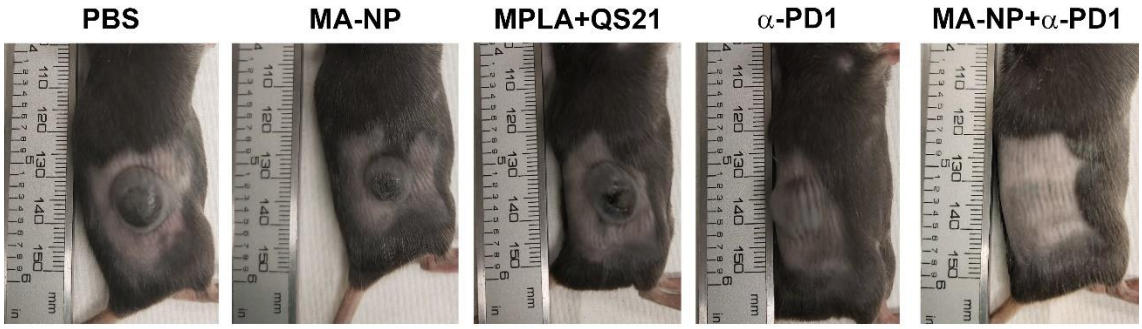

Figure 3.62. Representative photographs of tumors on day 21.

On the other hand, anti-PD1 treatment augmented intratumoral $CD4^+$ and $CD8^+$ T cells populations and CD25 expression on $CD8^+$ T cells (Figure 3.63B-F). As MA-NP was more effective in reducing tumor growth compared to anti-PD1 treatment, innate immune cell populations in TME were also investigated.

Tumor-associated macrophages (TAMs) constitute essential components of TME. While M1 macrophages play a crucial role in fighting against tumors, M2 macrophages, according to their subgroups, are involved in tumor progression and metastasis.[152] There was no alteration in $CD11b^+F4/80^+$ macrophage populations between each vaccination group (Figure 3.64A). When the phenotypes of macrophages were investigated towards M1- or M2-like, it was clearly shown that MA-NP increased the populations of M1-like macrophages and promoted M2- to M1- repolarization of intratumoral macrophages (Figure 3.64B-D). Another critical innate immune cell in TME is dendritic cells. DCs are instrumental in the generation of tumor-antigen specific T cell-mediated anti-tumor immune response and control of tumor growth due to their ability to cross-present tumor-antigens to naïve T cells.[137] Only MA-NP substantially increased the intratumoral dendritic cell population compared to PBS (Figure 3.64E). The superior anti-tumor effect induced by MA-NP could be promoted with intratumoral M1-like macrophages and dendritic cells compared to anti-PD1 treatment. These results indicated that MA-NP adjuvanted melanoma nanovaccine was also a potent cancer vaccine for therapeutic approaches.

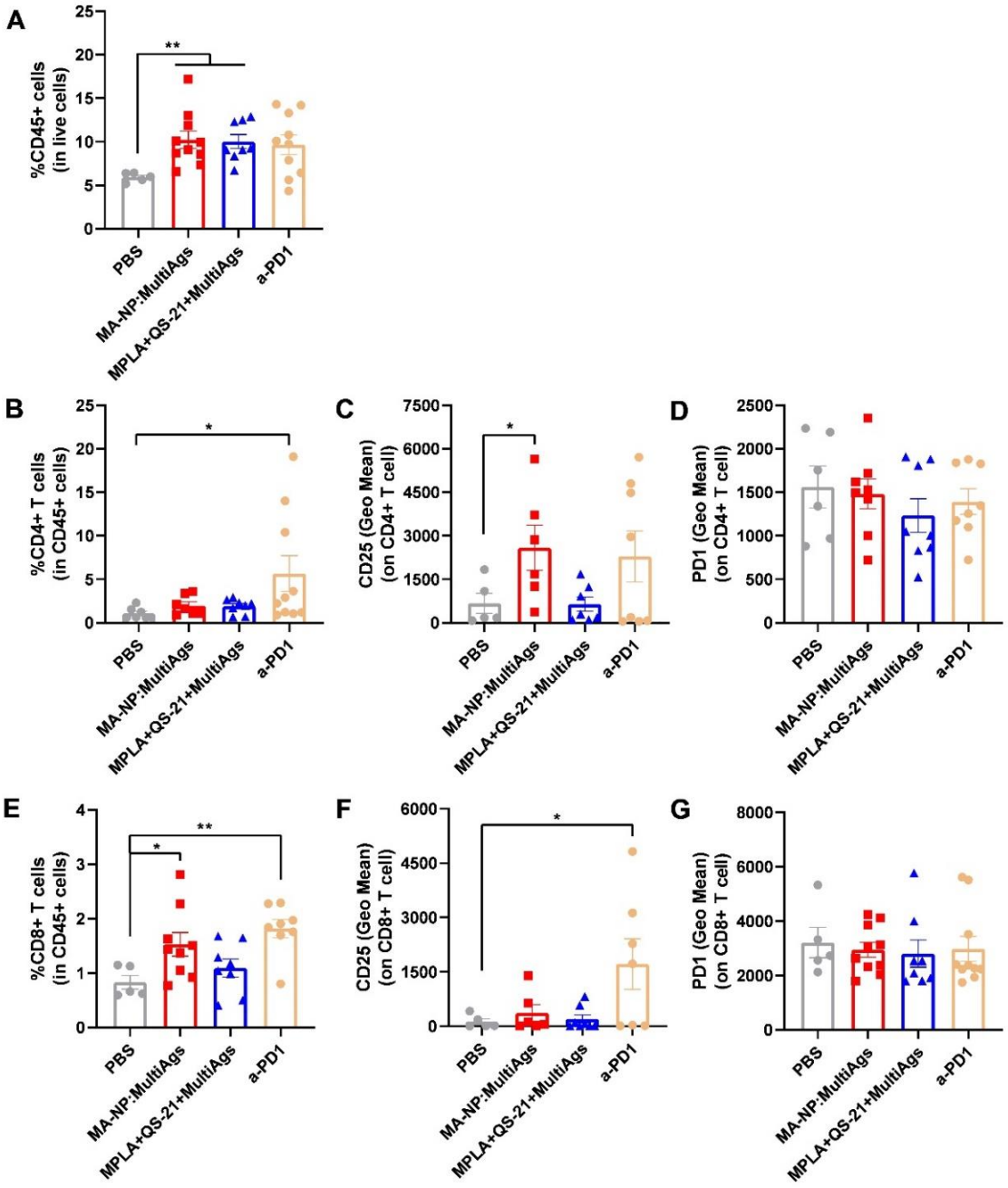

Figure 3.63. MA-NP increased intratumoral $CD8^+$ T cell population in therapeutic B16-F10 model. Tumor tissues were collected on day 21, and immune cell phenotypes were analyzed by flow cytometry. The population of $CD45^+$ cells, $CD4^+$ and $CD8^+$ T cells, and the expressions of CD25 and PD1 on T cells were shown. The data shown mean ± SEM from two independent experiments (n = 4-5). The statistically significant differences between vaccination groups were shown by One-way ANOVA, Student-t test, and Dunnett's multiple comparison test. *p≤0.05, **p≤0.01.

To investigate long-term memory response by vaccination groups, the effector and memory phenotype of T cells in the spleen on day 21 was analyzed by flow cytometry. Combinatory therapy with MA-NP:MultiAgs and anti-PD1 increased the total immune cell population in the spleen (Figure 3.65A). MA-NP:MultiAgs and MPLA+QS-21+MultiAgs significantly increased $CD4^+$ T cell and effector memory ($CD44^+CD62L^-$) $CD4^+$ T cell populations compared to PBS (Figure 3.65B-D). On the other hand, a comparable CD8+ T cell population was obtained between vaccination groups. However, only MA-NP substantially increased central ($CD44^+CD62L^+$) and effector memory ($CD44^+CD62L^-$) $CD8^+$ T cells in contrast to PBS (Figure 3.65 E-G). Central memory T cells are prominent cell groups in cancer immunotherapies due to their superior activities over effector T cells in terms of cytokine production, cytotoxic activities, and eradication of tumor cells.[153] In light of this information, MA-NP vaccination mediated effector and central memory T cell response may contribute to delay in tumor growth.

Overall, MA-NP adjuvanted nanovaccine revealed that it could be used as an alternative adjuvant system with various peptides in cancer immunotherapy studies by increasing intratumoral $CD8^+$ T cell, M1-like macrophages and DCs populations, inducing functional antigen-specific cytotoxic T cell responses with long term memory, reducing tumor growth all in prophylactic and therapeutic melanoma models and eradicating tumor cells in therapeutic B16-F10 melanoma model when combined with anti-PD1.

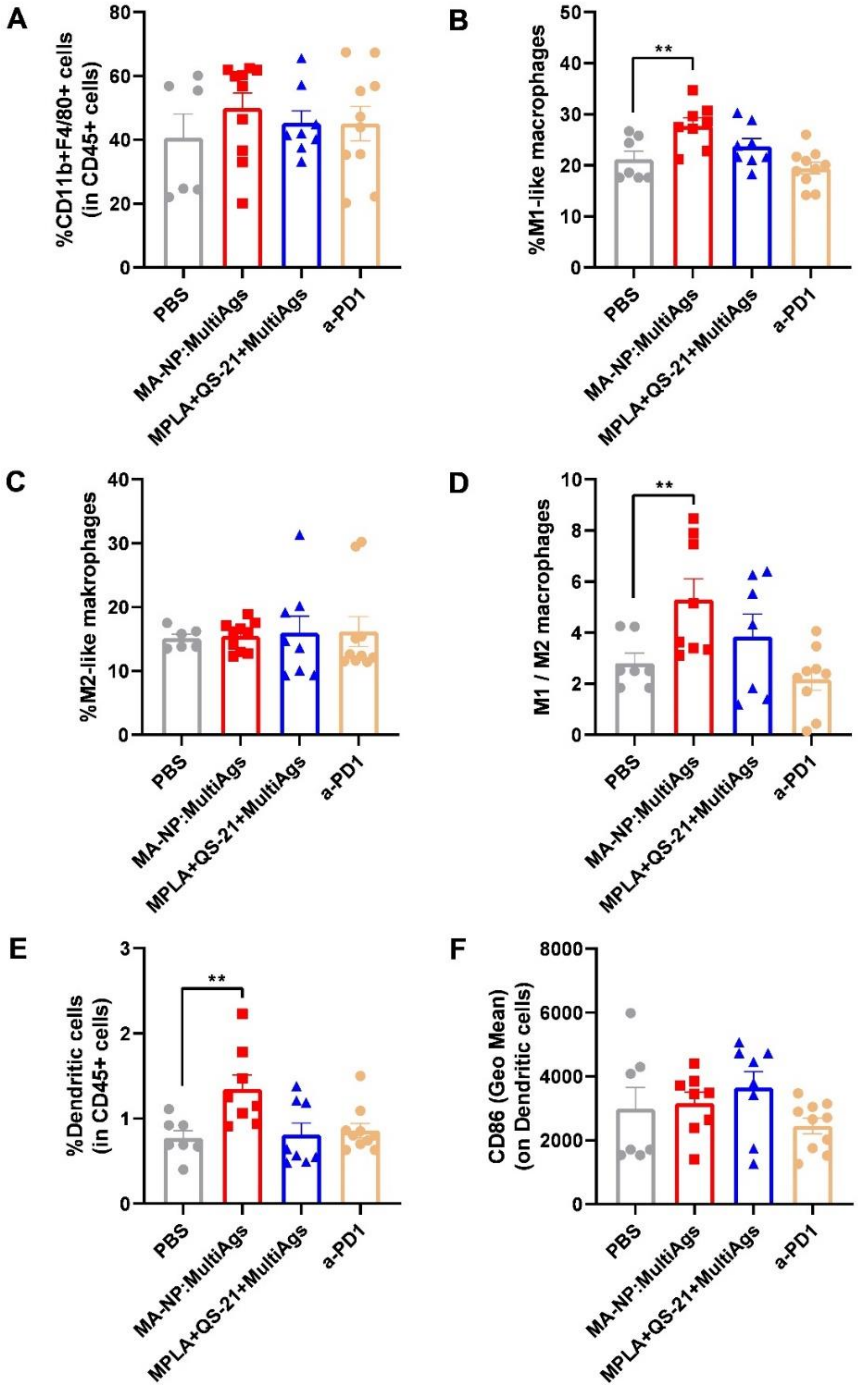

Figure 3.64. MA-NP increased M1-like macrophages and dendritic cell populations in TME. The population of $CD11b^{+}F4/80^{+}$ cells, M1-like and M2-like macrophages, DCs, and the expression of CD86 on their surfaces were given. The data shown mean ± SEM from two-independent experiments (n = 4-5). The statistically significant differences between vaccination groups were shown by One-way ANOVA, Student-t test and Dunnett's multiple comparison test. **$p \leq 0.01$.

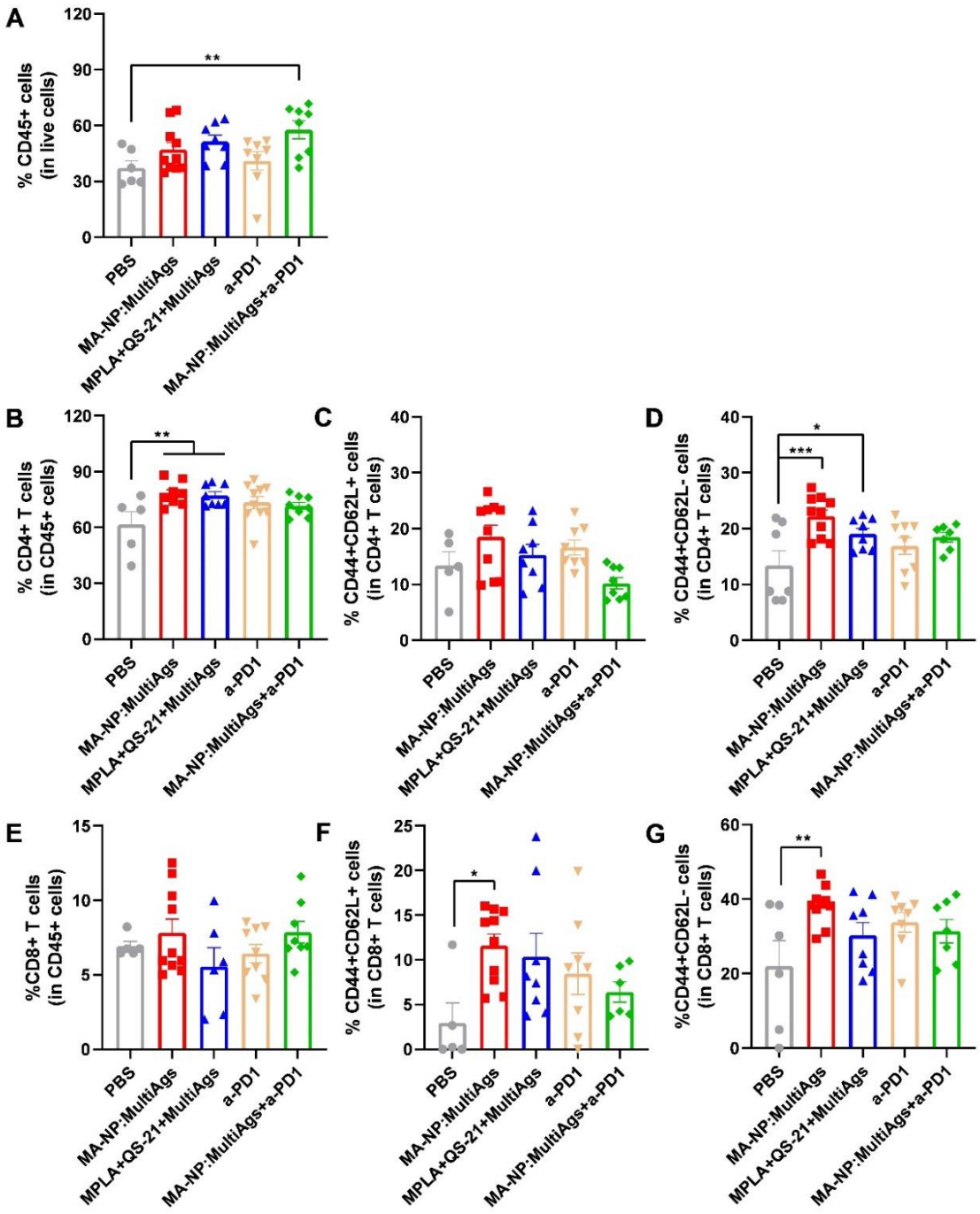

Figure 3.65. MA-NP increased the populations of splenic $CD4^+$ T cells, effector and central memory T cells in spleen. The populations of $CD45^+$ cells, $CD4^+$ and $CD8^+$ T cells, $CD44^+CD62L^-$ and $CD44^+CD62L^+$ cells were analyzed by flow cytometry.. The data shown mean ± SEM from two independent experiments (n = 4-5). The statistical significant differences between vaccination groups were shown by One-way ANOVA, Student-t test and Dunnett's multiple comparison test. *p≤0.05, **p≤0.01, ***p≤0.001.

CHAPTER IV

CONCLUSION

Cancer immunotherapies are treatments aiming to manipulate a patient's immune system to recognize and destroy tumor cells. Although there are several milestones suggesting promise in this field, cancer is still a major challenge in medicine. Traditional cancer therapies are not effective due to safety issues and the complexity of signals regulating the proper functioning of the immune system.[154] A potential solution to overcome these problems and engineer the delivery of immunotherapeutics to target cells is to develop nanomedicine-based approaches. The formulations of immunostimulatory agents/adjuvants in a carrier material provide uptake by target cells, alter systemic exposure, provide a safe profile, and increase the therapeutic efficacy of immunotherapeutics.[68]

In cancer vaccine development, peptides are preferable as antigens due to their safer profile, tumor-specific response, ease of manufacturing and characterization. However, their low immunogenicity limits the effective antigen-specific immune response, requiring the presence of adjuvant.[155] Adjuvants can stimulate humoral and cellular immune response, prevent antigen degradation, provide controlled antigen release, and deliver its cargo specifically to target cells. Saponins are plant- or marine-derived natural products and extensively studied as vaccine adjuvants due to their immunomodulatory properties. Adjuvant systems prepared by combining QS-21 saponin with TLR4 agonist in the liposomal system (AS01) have led to the first licensed Shingrix® and Mosquirix® vaccines with saponin adjuvants.[48]

In the context of this thesis, new saponin/TLR4 agonist-integrated adjuvant systems were designed and developed for cancer immunotherapy. The preliminary studies carried out by our group demonstrated that nanocarriers produced with *Astragalus* polysaccharide have <100 nm-sized nanoparticulate structures and these NPs were effective in the stimulation of the immune system. Astragaloside-VII (AST-VII), a triterpenoid saponin like QS-21, has been shown to have cellular and humoral immune responses as a potent adjuvant candidate. Moreover, AST-VII synergistically worked

with TLR4 agonist and induced dendritic cell maturation and further T cell activation. Therefore, following pH jump methodology, new adjuvant systems are prepared by integrating AST-VII and MPLA into APS-based nanocarriers (MA-NP). In the first chapter of the thesis, to obtain a more straightforward method, this preparation process has been optimized for operation parameter conditions and material concentrations by using the statistical design of the experiment tool. Physicochemical characterizations of NPs revealed that a 20-50 nm-sized, negatively charged, spherical MA-NP adjuvant system was successfully prepared. The particles in the 10-50 nm range are optimal for lymphatic targeting.[156] TLR agonist conjugated 30 nm in sized polymeric particles accumulated in tumor-draining lymph nodes in melanoma and subsequently induced DCs activation and T cell priming.[157,158] Therefore, the physicochemical properties of MA-NP possess the potential to be used in cancer vaccines.

Furthermore, the entrapment efficiency of AST-VII and peptide antigens was maximized to 67% and 75%, respectively. Moreover, MA-NP provided a sustained release of antigen over time, which is important to obtain long-term immunity.[95] Liposomes and poly(lactide-co-glycolide) polymers have been widely studied for particulate vaccine carriers, but they have several limitations, including low levels of antigen entrapment and the need for organic solvents for their preparations.[156] On the other hand, MA-NP allows highly efficient entrapment of immunostimulatory agents and antigens with ease and a solvent-free manufacturing process.

ISCOM and AS01 are nanoparticulate saponin-based adjuvant systems that use *Quillaja* saponins for particle formation. However, *Quillaja* saponins have several drawbacks, including toxicity, low isolation yield from plant material, insufficient purity, and inconsistent composition.[159] In contrast, AST-VII in MA-NP adjuvant system can be isolated with high yield, is stable and soluble in water and shows mild hemolytic activity,[65] making AST-VII a good alternative to other saponin-based adjuvants.

In the second chapter of this thesis, *in vitro* cytotoxic and immunomodulatory properties of engineered NPs were investigated in dendritic cells and melanoma. The biocompatible MA-NP adjuvant system was uptake by dendritic cells and co-localized with endolysosomal compartments by 6 h. Encapsulation/entrapment of antigen into NPs promotes their capture by antigen presenting cells and prevents their rapid clearance in the body like soluble forms.[156,160] These findings have motivated us to use antigen-adsorbed MA-NP to co-deliver both antigen and immunostimulatory agents to the same APC, resulting in the effective priming of T cells. Functional maturation of DCs is crucial

to polarize and activate T cells to achieve the desired immune response. Following the uptake of antigen and adjuvants, DCs undergo a maturation process by presenting antigen onto MHCII molecules, upregulating co-stimulatory molecules and secreting cytokines. MA-NP induced the upregulation of CD86, CD80 and CD40 on the surface of DCs and the production of IL-1β, IL-6 and IL-12. AST-VII/MPLA integration in MA-NP provided a synergistic effect for DC maturation and activation. In recent studies, TLR4 agonist has been combined with ISCOM or with QS-21 in a liposomal formulation (AS01), and the data show that saponin exhibited substantial synergy with MPLA and enhanced innate immune activation similar to MA-NP.[48,53,118,133]

Following the physicochemical and *in vitro* biological characterization of MA-NP, as a third part of this thesis, *in vivo* immunogenicity of engineered MA-NP alone or formulation with melanoma-associated MHCI-restricted and universal MHCII-restricted peptides was investigated. MA-NP alone or formulated multiAgs demonstrated an increase in tumor-fighting immune cells ($CD8^+$, $CD4^+$ T cells, NKT and NK cells), while decreasing the percentage of tumor-promoting immune cell population (Tregs) in the spleen. Early studies carried out with QS-21 demonstrated high Ag-specific antibody and $CD8^+$ T cell responses by providing a cross-presentation of Ag in DCs.[54,161] On the other hand, preclinical and clinical studies of AS01-formulated candidate vaccines revealed that AS01 promoted Ag-specific antibody and $CD4^+$ T cell responses. Moreover, the mice vaccinated with OVA/AS01 showed that OVA antigen-specific $CD8^+$ and $CD4^+$ T cell response.[118] MA-NP also promoted Ag-specific Th1/Th2 balanced antibody response. Compared to the licensed saponin adjuvant system, MA-NP has shown encouraging *in vivo* results, suggesting it could be an effective adjuvant for cancer vaccines.

As a final part of this thesis, the anti-tumor efficacy of MA-NP and soluble saponin adjuvants were evaluated in murine melanoma models. Prophylactic vaccination of MA-NP augmented intratumoral $CD8^+$ T cell, $CD4^+$ T cells, macrophage, and DC populations that significantly inhibit tumor growth. Intratumoral infiltration of lymphocytes by MA-NP provided more inflamed TME, presenting an important condition for treating malignant tumors. Moreover, MA-NP induced antigen-specific functional $CD8^+$ T cell populations compared to soluble saponin adjuvants, resulting in a reduction of tumor growth. TLR agonist integrated nanoparticulate saponin adjuvant systems (ISCOMs) also demonstrated superior antigen-specific $CD8^+$ T cell responses and significantly controlled tumor growth compared to their soluble form,[133] signifying the importance of nanomedicines in cancer immunotherapy.

Intratumoral DCs play a critical role in the initiation and maintenance of anti-tumor immunity because of their ability to present tumor antigens and stimulate T cell responses. Various tumor models demonstrated that infiltration of stimulatory DCs correlated with response to immunotherapy in solid tumors. However, immunosuppressive TME may lead to the differentiation of DCs into dysfunctional state, causing impaired anti-tumor immune response and promoting tumor progression.[162,163] The superior anti-tumor response following immunization with MA-NP compared to other vaccination groups could be a substantial increase in functional intratumoral DCs, leading to maintain cytotoxic T cell response and regression of tumor growth.

Tumor-associated macrophages are a promising target in cancer immunotherapy. Numerous agents have been developed to polarize macrophages to tumor-fighting pro-inflammatory M1 phenotype.[164] Our findings show that MA-NP adjuvanted vaccine increases intratumoral M1-like macrophage population and promotes M2 to M1 repolarization, contributing MA-NP induced anti-tumor immune response.

MA-NP administrated as a monotherapy failed to eradicate tumors despite a strong anti-tumor T cell response, leading a substantial increase in the expression of PD-1 on intratumoral $CD8^+$ T cells. To alter the impaired effector function of $CD8^+$ T cells, MA-NP vaccination combined with anti-PD1 resulted in the complete eradication of established B16-F10 tumors in mice. Although there have been extensive studies describing using nanomedicine for prophylactic and therapeutic cancer immunotherapy, this is, to the best of our knowledge, the first demonstration of anti-tumor efficacy of MPLA/AST-VII integrated adjuvant system tailored with tumor-specific antigens and combinatory therapy with anti-PD1.

Consequently, the ease and solvent-free manufacturing process, safer profile, strong prophylactic and therapeutic efficacy in tumor models demonstrated that MA-NP offers an alternative adjuvant system for cancer vaccines. Benchmarking and validation studies in multiple tumor models are warranted to further evaluate the potency of MA-NP as an effective adjuvant platform in cancer immunotherapy.

REFERENCES

1. Zhang, Y.; Zhang, Z. The History and Advances in Cancer Immunotherapy: Understanding the Characteristics of Tumor-Infiltrating Immune Cells and Their Therapeutic Implications. *Cell. Mol. Immunol.* **2020**, *17*, 807–821. DOI: 10.1038/s41423-020-0488-6

2. Stratton, M. R.; Campbell, P. J.; Futreal, P. A. The Cancer Genome. *Nature* **2009**, *458*, 719–724. DOI: 10.1038/nature07943

3. Global cancer burden growing, amidst mounting need for services https://www.who.int/news/item/01-02-2024-global-cancer-burden-growing-ami-mounting-need-for-services (accessed 2024-03-10).

4. Fan, T.; Zhang, M.; Yang, J.; Zhu, Z.; Cao, W.; Dong, C. Therapeutic Cancer Vaccines: Advancements, Challenges, and Prospects. *Signal Transduct. Target. Ther.* **2023**, *8*, 450. DOI: 10.1038/s41392-023-01674-3

5. Chidambaram, M.; Manavalan, R.; Kathiresan, K. Nanotherapeutics to Overcome Conventional Cancer Chemotherapy Limitations. *J. Pharm. Pharm. Sci.* **2011**, *14* (1), 67–77. DOI: 10.18433/j30c7d

6. Decker, W. K.; Safdar, A. Bioimmunoadjuvants for the Treatment of Neoplastic and Infectious Disease: Coley's Legacy Revisited. *Cytokine Growth Factor Rev.* **2009**, *20*, 271–281. DOI: 10.1016/j.cytogfr.2009.07.004

7. Decker, W.; da Silva, R.; Sanabria, M.; Angelo, L.; Guimarães, F.; Burt, B.; Kheradmand, F.; Paust, S. Cancer Immunotherapy: Historical Perspective of a Clinical Revolution and Emerging Preclinical Animal Models. *Front. Immunol.* **2017**, *8*, 829. DOI: 10.3389/fimmu.2017.00829

8. Waldman, A. D.; Fritz, J. M.; Lenardo, M. J. A Guide to Cancer Immunotherapy: From T Cell Basic Science to Clinical Practice. *Nat. Rev. Immunol.* **2020**, *20*, 651–668. DOI: 10.1038/s41577-020-0306-5

9. Burg, S. H. van der; Arens, R.; Ossendorp, F.; Hall, T. van; Melief, C. J. M. Vaccines for Established Cancer: Overcoming the Challenges Posed by Immune Evasion. *Nat. Rev. Cancer* **2016**, *16*, 219–233. DOI: 10.1038/nrc.2016.16

10. Dunn, G. P.; Old, L. J.; Schreiber, R. D. The Immunobiology of Cancer Immunosurveillance and Immunoediting. *Immunity* **2004**, *21* (2), 137–148. DOI: 10.1016/j.immuni.2004.07.017

11. Gubin, M.; Zhang, X.; Schuster, H.; Caron, E.; Ward, J.; Noguchi, T.; Ivanova, Y.; Hundal, J.; Arthur, C.; Krebber, W.; Mulder, G.; Toebes, M.; Vesely, M.; Lam, S.; Korman, A.; Allison, J.; Freeman, G.; Sharpe, A.; Pearce, E.; Schumacher, T.; Aebersold, R.; Rammensee, H.; Melief, C.; Mardis, E.; Gillanders, W.; Artyomov, M.; Schreiber, R. Checkpoint Blockade Cancer Immunotherapy Targets Tumour-Specific Mutant Antigens. *Nature* **2014**, *515*, 577–581. DOI: 10.1038/nature13988

12. Sharma, P.; Allison, J. P. The Future of Immune Checkpoint Therapy. *Science* **2015**, *348*, 56–61. DOI: 10.1126/science.aaa8172

13. Hodi, F. S.; O'Day, S. J.; McDermott, D. F.; Weber, R. W.; Sosman, J. A.; Haanen, J. B.; Gonzalez, R.; Robert, C.; Schadendorf, D.; Hassel, J. C.; Akerley, W.; Eertwegh, A. J. M. van den; Lutzky, J.; Lorigan, P.; Vaubel, J. M.; Linette, G. P.; Hogg, D.; Ottensmeier, C. H.; Lebbé, C.; Peschel, C.; Quirt, I.; Clark, J. I.; Wolchok, J. D.; Weber, J. S.; Tian, J.; Yellin, M. J.; Nichol, G. M.; Hoos, A.; Urba, W. J. Improved Survival with Ipilimumab in Patients with Metastatic Melanoma. *N. Engl. J. Med.* **2010**, *363*, 711–723. DOI: 10.1056/NEJMoa1003466

14. Wherry, E. J.; Kurachi, M. Molecular and Cellular Insights into T Cell Exhaustion. *Nat. Rev. Immunol.* **2015**, *15*, 486–499. DOI: 10.1038/nri3862

15. Gong, J.; Chehrazi-Raffle, A.; Reddi, S.; Salgia, R. Development of PD-1 and PD-L1 Inhibitors as a Form of Cancer Immunotherapy: A Comprehensive Review of Registration Trials and Future Considerations. *J. Immunother. cancer* **2018**, *6*, 8. DOI: 10.1186/s40425-018-0316-z

16. Weber, J. S.; D'Angelo, S.P.; Minor, D.; Hodi, F.S.; Gutzmer, R.; Neyns, B.; Hoeller, C.; Khushalani, N.I.; Miller, W.H. Jr; Lao, C.D.; Linette, G.P.; Thomas, L.; Lorigan, P.; Grossmann, K.F.; Hassel, J.C.; Maio, M.; Sznol, M.; Ascierto, P.A.; Mohr, P.; Chmielowski, B.; Bryce, A.; Svane, I.M.; Grob, J.J.; Krackhardt, A.M.; Horak, C.; Lambert, A.; Yang, A.S.; Larkin, J. Nivolumab versus Chemotherapy in Patients with Advanced Melanoma Who Progressed after Anti-CTLA-4 Treatment (CheckMate 037): A Randomised, Controlled, Open-Label, Phase 3 Trial. *Lancet Oncol.* **2015**, *16*, 375–384. DOI: 10.1016/S1470-2045(15)70076-8

17. Rosenberg, J. E.; Hoffman-Censits, J.; Powles, T.; van der Heijden, M.S.; Balar, A.V.; Necchi, A.; Dawson, N.; O'Donnell, P.H.; Balmanoukian, A.; Loriot, Y.;

Srinivas, S.; Retz, M.M.; Grivas, P.; Joseph, R.W.; Galsky, M.D.; Fleming, M.T.; Petrylak, D.P.; Perez-Gracia, J.L.; Burris, H.A.; Castellano, D.; Canil, C.; Bellmunt, J.; Bajorin, D.; Nickles, D.; Bourgon, R.; Frampton, G.M.; Cui, N.; Mariathasan, S.; Abidoye, O.; Fine, G.D.; Dreicer, R. Atezolizumab in Patients with Locally Advanced and Metastatic Urothelial Carcinoma Who Have Progressed Following Treatment with Platinum-Based Chemotherapy: A Single-Arm, Multicentre, Phase 2 Trial. *Lancet* **2016**, *387*, 1909–1920. DOI: 10.1016/S0140-6736(16)00561-4

18. Du, X.; Tang, F.; Liu, M.; Su, J.; Zhang, Y.; Wu, W.; Devenport, M.; Lazarski, C.A.; Zhang, P.; Wang, X.; Ye, P.; Wang, C.; Hwang, E.; Zhu, T.; Xu, T.; Zheng, P.; Liu, Y. A Reappraisal of CTLA-4 Checkpoint Blockade in Cancer Immunotherapy. *Cell Res.* **2018**, *28*, 416–432. DOI: 10.1038/s41422-018-0011-0

19. Liu, J.; Blake, S. J.; Smyth, M. J.; Teng, M. W. Improved Mouse Models to Assess Tumour Immunity and IrAEs after Combination Cancer Immunotherapies. *Clin. Transl. Immunol.* **2014**, *3*, e22. DOI: 10.1038/cti.2014.18

20. Kumar, V.; Chaudhary, N.; Garg, M.; Floudas, C.S.; Soni, P.; Chandra, A.B.Current Diagnosis and Management of Immune Related Adverse Events (IrAEs) Induced by Immune Checkpoint Inhibitor Therapy. *Front. Pharmacol.* **2017**, *8* (49). DOI: 10.3389/fphar.2017.00049

21. Rosenberg, S. A.; Yannelli, J.R.; Yang, J.C.; Topalian, S.L.; Schwartzentruber, D.J.; Weber, J.S.; Parkinson, D.R.; Seipp, C.A.; Einhorn, J.H.; White, D.E. Treatment of Patients with Metastatic Melanoma with Autologous Tumor-Infiltrating Lymphocytes and Interleukin 2. *J. Natl. Cancer Inst.* **1994**, *86*, 1159–1166. DOI: 10.1093/jnci/86.15.1159

22. Garrido, F.; Aptsiauri, N.; Doorduijn, E. M.; Garcia Lora, A. M.; van Hall, T. The Urgent Need to Recover MHC Class I in Cancers for Effective Immunotherapy. *Curr. Opin. Immunol.* **2016**, *39*, 44–51. DOI: 10.1016/j.coi.2015.12.007

23. Brudno, J. N.; Kochenderfer, J. N. Toxicities of Chimeric Antigen Receptor T Cells: Recognition and Management. *Blood* **2016**, *127*, 3321–3330. DOI: 10.1182/blood-2016-04-703751

24. Andtbacka, R. H.; Kaufman, H. L.; Collichio, F.; Amatruda, T.; Senzer, N.; Chesney, J.; Delman, K. A.; Spitler, L. E.; Puzanov, I.; Agarwala, S. S.; Milhem, M.; Cranmer, L.; Curti, B.; Lewis, K.; Ross, M.; Guthrie, T.; Linette, G. P.; Daniels, G. A.; Harrington, K.; Middleton, M. R.; Miller, W.H. Jr; Zager, J. S.; Ye, Y.; Yao, B.; Li, A.; Doleman, S.; VanderWalde, A.; Gansert, J.; Coffin, R. S.Talimogene Laherparepvec Improves Durable Response Rate in Patients with

Advanced Melanoma. *J. Clin. Oncol.* **2015**, *33*, 2780–2788. DOI: 10.1200/jco.2014.58.3377

25. Shalhout, S. Z.; Miller, D. M.; Emerick, K. S.; Kaufman, H. L. Therapy with Oncolytic Viruses: Progress and Challenges. *Nat. Rev. Clin. Oncol.* **2023**, *20*, 160–177. DOI: 10.1038/s41571-022-00719-w

26. Zheng, M.; Huang, J.; Tong, A.; Yang, H. Oncolytic Viruses for Cancer Therapy: Barriers and Recent Advances. *Mol. Ther. Oncol.* **2019**, *15*, 234–247. DOI: 10.1016/j.omto.2019.10.007

27. Hoover, H.; Surdyke, M.; Dangel, R.; Peters, L.; Hanna, M. Prospectively Randomized Trial of Adjuvant Active-Specific Immunotherapy for Human Colorectal-Cancer. *Cancer* **1985**, *55* (6), 1236–1243. DOI: 10.1002/1097-0142(19850315)55:6<1236::aid-cncr2820550616>3.0.co;2-#

28. Vanderbruggen, P.; Traversari, C.; Chomez, P.; Lurquin, C.; Deplaen, E.; Van den Eynde, B.; Knuth, A.; Boon, T. AGene Encoding an Antigen Recognized by Cytolytic Lymphocytes-T on a Human-Melanoma. *Science* **1991**, *254* (5038), 1643–1647. DOI: 10.1126/science.1840703

29 Sondak, Vernon, K.; Sosman, J. A. Results of Clinical Trials with an Allogeneic Melanoma Tumor Cell Lysate Vaccine: Melacine®. *Semin. Cancer Biol.* **2003**, *13* (6), 409–415. DOI: 10.1016/j.semcancer.2003.09.004

30. Abd-Aziz, N.; Poh, C. L. Development of Peptide-Based Vaccines for Cancer. *J. Oncol.* **2022**, 9749363. DOI: 10.1155/2022/9749363

31. Kantoff, P. W.; Higano, C.S.; Shore, N.D.; Berger, E.R.; Small, E.J.; Penson, D. F.; Redfern, C. H.; Ferrari, A. C.; Dreicer, R.; Sims, R. B.; Xu, Y.; Frohlich, M. W.; Schellhammer ,P. F.; IMPACT Study Investigators. Sipuleucel-T Immunotherapy for Castration-Resistant Prostate Cancer. *N. Engl. J. Med.* **2010**, *363*, 411–422. DOI: 10.1056/NEJMoa1001294

32. Sahin, U.; Derhovanessian, E.; Miller, M.; Kloke, B. J.; Simon, P.; Löwer, M.; Bukur, V.; Tadmor, A. D.; Luxemburger, U.; Schrörs, B.; Omokoko, T.; Vormehr, M.; Albrecht, C.; Paruzynski, A.; Kuhn, A. N.; Buck, J.; Heesch, S.; Schreeb, K. H.; Müller, F.; Ortseifer, I.; Vogler, I.; Godehardt, E.; Attig, S.; Rae, R.; Breitkreuz, A.; Tolliver, C.; Suchan, M.; Martic, G.; Hohberger, A.; Sorn, P.; Diekmann, J.; Ciesla, J.; Waksmann, O.; Brück, A. K.; Witt, M.; Zillgen, M.; Rothermel, A.; Kasemann, B.; Langer, D.; Bolte, S.; Diken, M.; Kreiter, S.; Nemecek, R.; Gebhardt, C.; Grabbe, S.; Höller, C.; Utikal, J.; Huber, C.; Loquai,

C.; Türeci, Ö. Personalized RNA Mutanome Vaccines Mobilize Poly-Specific Therapeutic Immunity against Cancer. *Nature* **2017**, *547*, 222–226. DOI: 10.1038/nature23003

33. Zhang, X.; Yang, B.; Ni, Q.; Chen, X. Materials Engineering Strategies for Cancer Vaccine Adjuvant Development. *Chem. Soc. Rev.* **2023**, *52*, 2886. DOI: 10.1039/D2CS00647B

34. Chatzikleanthous, D.; O'Hagan, D. T.; Adamo, R. Lipid-Based Nanoparticles for Delivery of Vaccine Adjuvants and Antigens: Toward Multicomponent Vaccines. *Mol. Pharm.* **2021**, *18* (8), 2867–2888. DOI: 10.1021/acs.molpharmaceut.1c0044

35 Kuai, R.; Sun, X.; Yuan, W.; Ochyl, L. J.; Xu, Y.; Najafabadi, A. H.; Scheetz, L.; Yu, M.-Z.; Balwani, I.; Schwendeman, A.; Moon, J. J. Dual TLR Agonist Nanodiscs as a Strong Adjuvant System for Vaccines and Immunotherapy. *J. Control. Release* **2018**, *282*, 131–139. DOI: 10.1016/j.jconrel.2018.04.041

36. Wan, D.; Que, H.; Chen, L.; Lan, T.; Hong, W.; He, C.; Yang, J.; Wei, Y.; Wei, X. Lymph-Node-Targeted Cholesterolized TLR7 Agonist Liposomes Provoke a Safe and Durable Antitumor Response. *Nano Lett.* **2021**, *21* (19), 7960–7969. DOI: 10.1021/acs.nanolett.1c01968

37. Lynn, G. M.; Sedlik, C.; Baharom, F.; Zhu, Y.; Ramirez-Valdez, R. A.; Coble, V. L.; Tobin, K.; Nichols, S. R.; Itzkowitz, Y.; Zaidi, N.; Gammon, J. M.; Blobel, N. J.; Denizeau, J.; de la Rochere, P.; Francica, B. J.; Decker, B.; Maciejewski, M.; Cheung, J.; Yamane, H.; Smelkinson, M. G.; Francica, J. R.; Laga, R.; Bernstock, J. D.; Seymour, L. W.; Drake, C. G.; Jewell, C. M.; Lantz, O.; Piaggio, E.; Ishizuka, A. S.; Seder, R. A. Peptide–TLR-7/8a Conjugate Vaccines Chemically Programmed for Nanoparticle Self-Assembly Enhance CD8 T-Cell Immunity to Tumor Antigens. *Nat. Biotechnol.* **2020**, *38* (3), 320–332. DOI: 10.1038/s41587-019-0390-x

38. Shae, D.; Becker, K. W.; Christov, P.; Yun, D. S.; Lytton-Jean, A. K. R.; Sevimli, S.; Ascano, M.; Kelley, M.; Johnson, D. B.; Balko, J. M.; Wilson, J. T.Endosomolytic Polymersomes Increase the Activity of Cyclic Dinucleotide STING Agonists to Enhance Cancer Immunotherapy. *Nat. Nanotechnol.* **2019**, *14*, 269–278. DOI: 10.1038/s41565-018-0342-5

39. Lu, X.; Miao, L.; Gao, W.; Chen, Z.; McHugh, K.; Sun, Y.; Tochka, Z.; Tomasic, S.; Sadtler, K.; Hyacinthe, A.; Huang, Y.; Graf, T.; Hu, Q.; Sarmadi, M.; Langer, R.; Anderson, D.; Jaklenec, A.; Lu, X.; Miao, L.; Gao, W.; Chen, Z.; McHugh, K.; Sun, Y.; Tochka, Z.; Tomasic, S.; Sadtler, K.; Hyacinthe, A.; Huang, Y.; Graf, T.; Hu, Q.; Sarmadi, M.; Langer, R.; Anderson, D.; Jaklenec, A. Engineered

PLGA Microparticles for Long-Term, Pulsatile Release of STING Agonist for Cancer Immunotherapy. *Sci. Transl. Med.* **2020**, *12* (556), eaaz6606. DOI: 10.1126/scitranslmed.aaz6606

40. Sun, X.; Zhang, Y.; Li, J.; Park, K. S.; Han, K.; Zhou, X.; Xu, Y.; Nam, J.; Xu, J.; Shi, X.; Wei, L.; Lei, Y. L.; Moon, J. J. Amplifying STING Activation by Cyclic Dinucleotide–Manganese Particles for Local and Systemic Cancer Metalloimmunotherapy. *Nat. Nanotechnol.* **2021**, *16*, 1260–1270. DOI: 10.1038/s41565-021-00962-9

41. Dane, E. L.; Belessiotis-Richards, A.; Backlund, C.; Wang, J.; Hidaka, K.; Milling, L. E.; Bhagchandani, S.; Melo, M. B.; Wu, S.; Li, N.; Donahue, N.; Ni, K.; Ma, L.; Okaniwa, M.; Stevens, M. M.; Alexander-Katz, A.; Irvine, D. J STING Agonist Delivery by Tumour-Penetrating PEG-Lipid Nanodiscs Primes Robust Anticancer Immunity. *Nat. Mater.* **2022**, *21*, 710–720. DOI: 10.1038/s41563-022-01251-z

42. Zheng, B.; Xu, J.; Chen, G.; Zhang, S.; Xiao, Z.; Lu, W. Bacterium-Mimicking Vector with Enhanced Adjuvanticity for Cancer Immunotherapy and Minimized Toxicity. *Adv. Funct. Mater.* **2019**, *29*, 1901437. DOI: 10.1002/adfm.201901437

43. Shi T, Sun M, L. C. and M. F. Self-Assembled Nanoparticles: A New Platform for Revolutionizing Therapeutic Cancer Vaccines. *Front. Immunol.* **2023**, *14*, 1125253. DOI: 10.3389/fimmu.2023.1125253

44. Melanoma. https://www.mayoclinic.org/diseases-condition/melanoma/symptom-causes/syc-20374884 (accessed 2024-03-15).

45. Arnold, M.; Singh, D.; Laversanne, M.; Vignat, J.; Vaccarella, S.; Meheus, F.; Cust, A. E.; Vries, E. de; Whiteman, D. C.; Bray, F. Global Burden of Cutaneous Melanoma in 2020 and Projections to 2040. *JAMA Dermatology* **2022**, *158* (5), 495–503. DOI: 10.3390/cancers16020250

46. Dhanyamraju, P.; Patel, T. Melanoma Therapeutics: A Literature Review. *J. Biomed. Res.* **2022**, *36* (2), 77–97. DOI: 10.7555/JBR.36.20210163

47. Leonardi, G. C.; Massimo; Candido, S.; Falzone, L.; Spandidos, D. A.; Libra, M. Cutaneous Melanoma and the Immunotherapy Revolution. *Int. J. Oncol.* **2020**, *57* (3), 609–618. DOI: 10.3892/ijo.2020.5088

48. Silva, M.; Kato, Y.; Melo, M. B.; Phung, I.; Freeman, B. L.; Li, Z.; Roh, K.;

Wijnbergen, J. W. Van; Watkins, H.; Enemuo, C. A.; Hartwell, B. L.; Chang, J. Y. H.; Xiao, S.; Rodrigues, K. A.; Cirelli, K. M.; Li, N.; Haupt, S.; Aung, A.; Cossette, B.; Abraham, W.; Kataria1, S.; Bastidas, R.; Bhiman, J.; Linde, C.; Bloom, N. I.; Groschel, B.; Georgeson, E.; Phelps, N.; Thomas, A.; Bals, J.; Carnathan, D. G.; Lingwood, D.; Burton, D. R.; Alter, G.; Padera, T. P.; Belcher, A. M.; Schief, W. R.; Silvestri, G.; Ruprecht, R. M.; Crotty, S.; Irvine, D. J. A Particulate Saponin/TLR Agonist Vaccine Adjuvant Alters Lymph Flow and Modulates Adaptive Immunity. *Sci. Immunol.* **2021**, *6*, eabf1152. DOI: 10.1126/sciimmunol.abf1152

49. Park, K. S.; Nam, J.; Son, S.; Moon, J. J. Personalized Combination Nano-Immunotherapy for Robust Induction and Tumor Infiltration of CD8+ T Cells. *Biomaterials* **2021**, *274*, 120844. DOI: 10.1016/j.biomaterials.2021.120844

50. Kakwere, H.; Ingham, E. S.; Allen, R.; Mahakian, L. M.; Tam, S. M.; Zhang, H.; Silvestrini, M. T.; Lewis, J. S.; Ferrara, K. W. Unimicellar Hyperstars as Multi-Antigen Cancer Nanovaccines Displaying Clustered Epitopes of Immunostimulating Peptides. *Biomater. Sci.* **2018**, *6* (11), 2850–2858. DOI: 10.1039/c8bm00891d

51. Ben-Akiva, E.; Karlsson, J.; Hemmati, S.; Green, J. J. Biodegradable Lipophilic Polymeric MRNA Nanoparticles for Ligand-Free Targeting of Splenic Dendritic Cells for Cancer Vaccination. *PNAS* **2023**, *120* (26), e2301606120. DOI: 10.1073/pnas.2301606120

52. Cuzzubbo, S.; Mangsbo, S.; Nagarajan, D.; Habra, K.; Pockley, A. G.; McArdle, S. E. B. Cancer Vaccines: Adjuvant Potency, Importance of Age, Lifestyle, and Treatments. *Front. Immunol.* **2021**, *11*, 615240. DOI: 10.3389/fimmu.2020.61524

53. Marty-Roix, R.; Vladimer, G. I.; Pouliot, K.; Weng, D.; Buglione-Corbett, R.; West, K.; MacMicking, J. D.; Chee, J. D.; Wang, S.; Lu, S.; Lien, E. Identification of QS-21 as an Inflammasome-Activating Molecular Component of Saponin Adjuvants. *J. Biol. Chem.* **2016**, *291* (3), 1123–1136. DOI:10.1074/jbc.M115.683011

54. Den Brok, M. H.; Büll, C.; Wassink, M.; De Graaf, A. M.; Wagenaars, J. A.; Minderman, M.; Thakur, M.; Amigorena, S.; Rijke, E. O.; Schrier, C. C.; Adema, G. J. Saponin-Based Adjuvants Induce Cross-Presentation in Dendritic Cells by Intracellular Lipid Body Formation. *Nat. Commun.* **2016**, *7*,. 13324 DOI: 10.1038/ncomms13324

55. Pifferi, C.; Fuentes, R.; Fernández-Tejada, A. Natural and Synthetic Carbohydratebased Vaccine Adjuvants and Their Mechanisms of Action. *Nat.*

Rev. Chem. **2021**, *5*, 197–216. DOI: 10.1038/s41570-020-00244-3

56. Garcon, N.; Van Mechelen, M. Recent Clinical Experience with Vaccines Using MPL- and QS-21- Containing Adjuvant Systems. *Expert Rev. Vaccines* **2011**, *10* (4), 471–486. DOI: 10.1586/erv.11.29

57. Lin, M. J.; Svensson-Arvelund, J.; Lubitz, G. S.; Marabelle, A.; Melero, I.; Brown, B. D.; Brody, J. D. Cancer Vaccines: The next Immunotherapy Frontier. *Nat. Cancer* **2022**, *3*, 911–926. DOI: 10.1038/s43018-022-00418-6

58. Ragupathi, G.; Gardner, J. R.; Livingston, P. O.; Gin, D. Y. Natural and Synthetic Saponin Adjuvant QS-21 for Vaccines against Cancer. *Expert Rev Vaccines* **2011**, *10* (4), 463–470. DOI: 10.1586/erv.11.18

59. Yakuboğulları, N.; Bedir, E. Astragalus Sp. In *Medicinal Plants of Turkey*; Taylor & Francis, 2023; pp 17–25.

60. Yesilada, E.; Bedir, E.; Çalış, İ.; Takaishic, Y.; Ohmotod, Y. Effects of Triterpene Saponins from Astragalus Species on in Vitro Cytokine Release. *J. Ethnopharmacol.* **2005**, *96*, 71–77. DOI: 10.1016/j.jep.2004.08.036

61. Nalbantsoy, A.; Nesil, T.; Erden, S.; Calış, I.; Bedir, E. Adjuvant Effects of Astragalus Saponins Macrophyllosaponin B and Astragaloside VII. *J. Ethnopharmacol.* **2011**, *134* (3), 897–903. DOI: 10.1016/j.jep.2011.01.054

62. Nalbantsoy, A.; Nesil, T.; Yilmaz-Dilsiz, Ö.; Aksu, G.; Khan, S.; Bedir, E. Evaluation of the Immunomodulatory Properties in Mice and in Vitro Anti-Inflammatory Activity of Cycloartane Type Saponins from Astragalus Species. *J. Ethnopharmacol.* **2012**, *139* (2), 574–581. DOI: 10.1016/j.jep.2011.11.053

63. Yakuboğulları, N.; Genç, R.; Çöven, F.; Nalbantsoy, A.; Bedir, E. Development of Adjuvant Nanocarrier Systems for Seasonal Influenza A (H3N2) Vaccine Based on Astragaloside VII and Gum Tragacanth (APS). *Vaccine* **2019**, *37*, 3638–3645. DOI: 10.1016/j.vaccine.2019.05.038

64. Yakubogullari, N.; Coven, F. O.; Cebi, N.; Coven, F.; Coven, N.; Genc, R.; Bedir, E.; Nalbantsoy, A. Evaluation of Adjuvant Activity of Astragaloside VII and Its Combination with Different Immunostimulating Agents in Newcastle Disease Vaccine. *Biologicals* **2021**, *70*, 28-37. DOI: 10.1016/j.biologicals.2021.01.005

65. Yakubogullari, N.; Cagir, A.; Bedir, E.; Sag, D. Astragalus Saponins, Astragaloside VII and Newly Synthesized Derivatives, Induce Dendritic Cell Maturation and T Cell Activation. *Vaccines* **2023**, *11*, 495. DOI: 10.3390/vaccines 11030495

66. Kregiel, D.; Berlowska, J.; Witonska, I.; Antolak, H.; Proestos, C.; Zhang, M. B.; Babic, L.; Zhang, B. Saponin-Based, Biological-Active Surfactants from Plants. In *Application and Characterization of Surfactants*; Intechopen, 2017; pp 183–205.

67. Adams, M.; Damani, P.; Perl, N.; Won, A.; Hong, F.; Livingston, P.; Ragupathi, G.; Gin, D. Design and Synthesis of Potent Quillaja Saponin Vaccine Adjuvants. *J. Am. Chem. Soc.* **2010**, *132* (6), 1939–1945. DOI: 10.1021/ja9082842

68. Irvine, D. J.; Dane, E. L. Enhancing Cancer Immunotherapy with Nanomedicine. *Nat. Rev. Immunol.* **2020**, *20*, 321–334. DOI: 10.1038/s41577-019-0269-6

69. Backlund, C.; Jalili-Firoozinezhad, S.; Kim, B.; Irvine, D. J. Biomaterials-Mediated Engineering of the Immune System. *Annu. Rev. Immunol.* **2023**, *41*, 153–179. DOI: 10.1146/annurev-immunol-101721-040259

70. Genç, R.; Ortiz, M.; O'Sullivan, C. K. Curvature-Tuned Preparation of Nanoliposomes. *Langmuir* **2009**, *25* (21), 12604–12613. DOI: 10.1021/la9017 89h

71. Didierlaurent, A. M.; Collignon, C.; Bourguignon, P.; Wouters, S.; Fierens, K.; Fochesato, M.; Dendouga, N.; Langlet, C.; Malissen, B.; Lambrecht, B. N.; Garçon, N.; Van Mechelen, M.; Morel, S. Enhancement of Adaptive Immunity by the Human Vaccine Adjuvant AS01 Depends on Activated Dendritic Cells. *J. Immunol.* **2014**, *193* (4), 1920–1930. DOI: 10.4049/jimmunol.1400948

72. Zhang, T. T.; Kang, T. H.; Ma, B.; Xu, Y.; Hung, C.-F.; Wu, T. C. LAH4 Enhances CD8+ T Cell Immunity of Protein/Peptide-Based Vaccines. *Vaccine* **2012**, *30*, 784– 793. DOI: 10.1016/j.vaccine.2011.11.056

73. Kakwere, H.; Ingham, E. S.; Allen, R.; Mahakian, L. M.; Tam, S. M.; Zhang, H.; Silvestrini, M. T.; Lewis, J. S.; Ferrara, K. W. Toward Personalized Peptide-Based Cancer Nanovaccines: A Facile and Versatile Synthetic Approach. *Bioconjug. Chem.* **2017**, *28* (11), 2756–2771. DOI: 10.1021/acs.bioconjchem.7b00502

74. Kuai, R.; Ochyl, L. J.; Bahjat, K. S.; Schwendeman, A.; Moon, J. J. Designer

Vaccine Nanodiscs for Personalized Cancer Immunotherapy. *Nat. Mater.* **2017**, *16*, 489–496. DOI: 10.1038/nmat4822

75. Weilhammer, D. R.; Blanchette, C. D.; Fischer, N. O.; Alam, S.; Loots, G. G.; Corzett, M.; Thomas, C.; Lychak, C.; Dunkle, A. D.; Ruitenberg, J. J.; Ghanekar, S. A.; Sant, A. J.; Rasley, A. The Use of Nanolipoprotein Particles to Enhance the Immunostimulatory Properties of Innate Immune Agonists against Lethal Influenza Challenge. *Biomaterials* **2013**, *34* (38), 10305–10318. DOI: 10.1016/j.biomaterials.2013.09.038

76. Lutz, M. B.; Kukutsch, N.; Ogilvie, A. L.; Rößner, S.; Koch, F.; Romani, N.; Schuler, G. An Advanced Culture Method for Generating Large Quantities of Highly Pure Dendritic Cells from Mouse Bone Marrow. *J. Immunol. Methods* **1999**, *223* (1), 77–92. DOI: 10.1016/S0022-1759(98)00204-X

77. Ochyl, L. J.; Moon, J. J. Whole-Animal Imaging and Flow Cytometric Techniques for Analysis of Antigen-Specific CD8+ T Cell Responses after Nanoparticle Vaccination. *J. Vis. Exp.* **2015**, *98*, e52771. DOI: 10.3791/52771

78. Vasievich, E.; Ramishetti, S.; Zhang, Y.; Huang, L. TRP2 Peptide Vaccine Adjuvanted with (R)-DOTAP Inhibits Tumor Growth in an Advanced Melanoma Model. *Mol. Pharm.* **2012**, *9*, 261–268. DOI: 10.1021/mp200350n

79. Wen, X.; Franses, E. I. Effect of Protonation on the Solution and Phase Behavior of Aqueous Sodium Myristate. *J. Colloid Interface Sci.* **2000**, *231* (1), 42–51. DOI: 10.1006/jcis.2000.7156

80. Lykins, W. R.; Fox, C. B. Practical Considerations for Next-Generation Adjuvant Development and Translation. *Pharmaceutics* **2023**, *15*, 1850. DOI: 10.3390/pharmaceutics15071850

81. Rampado, R.; Peer, D. Design of Experiments in the Optimization of Nanoparticle-Based Drug Delivery Systems. *J. Control. Release* **2023**, *358*, 398–419. DOI: 10.1016/j.jconrel.2023.05.001

82. Ly, H. H.; Daniel, S.; Soriano, S. K. V.; Kis, Z.; Blakney, A. K. Optimization of Lipid Nanoparticles for SaRNA Expression and Cellular Activation Using a Design-of-Experiment Approach. *Mol. Pharm.* **2022**, *19*, 1892−1905. DOI: 10.1021/acs.molpharmaceut.2c00032

83. Hotaling, N. A.; Tang, L.; Irvine, D. J.; Babensee, J. E. Biomaterial Strategies For

Immunomodulation. *Annu. Rev. Biomed. Eng.* **2015**, *17*, 317–349. DOI: 10.1146/annurev-bioeng-071813-104814

84. Yokoyama, A.; Srinivasan, K. R.; Fogler, H. S. Stabilization Mechanism of Colloidal Suspensions by Gum Tragacanth: The Influence of PH on Stability. *J. Colloid Interface Sci.* **1988**, *126* (1), 141–149. DOI: 10.1016/0021-9797(88) 90108-7

85. Hauser, H. Mechanism of Spontaneous Vesiculation. *Proc. Natl. Acad. Sci. U. S. A.* **1989**, *86* (14), 5351–5355. DOI: 10.1073/pnas.86.14.5351

86. Pichot, R.; Watson, R.; Norton, I. Phospholipids at the Interface: Current Trends and Challenges. *Int. J. Mol. Sci.* **2013**, *14* (6), 11767–11794. DOI: 10.3390/ijms 140611767

87. Wang, D.; Sha, L.; Xu, C.; Huang, Y.; Tang, C.; Xu, T.; Li, X.; Di, D.; Liu, J.; Yang, L. Natural Saponin and Cholesterol Assembled Nanostructures as the Promising Delivery Method for Saponin. *Colloids Surfaces B Biointerfaces* **2022**, *214*, 112448. DOI: 10.1016/j.colsurfb.2022.112448

88. Alsaadi, M. M.; Carter, K. C.; Mullen, A. B. High Performance Liquid Chro-Matography with Evaporative Light Scattering Detection for the Characterisationof a Vesicular Delivery System during Stability Studies,. *J. Chromatogr. A* **2013**, *1320*, 80–85. DOI: 10.1016/j.chroma.2013.10.054

89. Thakur, D.; Dubey, N. P.; Singh, R. A Review on Spike and Recovery Method in Analytical Method Development and Validation. *Crit. Rev. Anal. Chem.* **2022**, *4*, 1–19. DOI: 10.1080/10408347.2022.2152275

90. van der Burg, S. H.; Arens, R.; Ossendorp, F.; van Hall, T.; Melief, C. J. M. Vaccines for Established Cancer: Overcoming the Challenges Posed by Immune Evasion. *Nat. Rev. Cancer* **2016**, *16*, 219–233. DOI: 10.1038/nrc.2016.16

91. Nam, J.; Son, S.; Park, K. S.; Moon, J. J. Modularly Programmable Nanoparticle Vaccine Based on Polyethyleneimine for Personalized Cancer Immunotherapy. *Adv. Sci.* **2021**, *8*, 2002577. DOI: 10.1002/advs.202002577

92. Norbury, C. C.; Malide, D.; Gibbs, J. S.; Bennink, J. R.; Yewdell, J. W. Visualizing Priming of Virus-Specific CD8+ T Cells by Infected Dendritic Cells in Vivo. *Nat. Immunol.* **2002**, *3*, 265–271. DOI: 10.1038/ni762

93. Bachem Peptide. https://www.bachem.com/knowledge-center/peptide-calculator/ (accessed 2024-04-08).

94. Pustulka, S. M.; Ling, K.; Pish, S. L.; Champion, J. A. Protein Nanoparticle Charge and Hydrophobicity Govern Protein Corona and Macrophage Uptake. *ACS Appl. Mater. Interfaces* **2020**, *12*, 48284–48295. DOI: 10.1021/acsami.0c12341

95. Roth, G. A.; Gale, E. C.; Alcántara-Hernández, M.; Luo, W.; Axpe, E.; Verma, R.; Yin, Q.; Yu, A. C.; Hector Lopez Hernandez; Maikawa, C. L.; Smith, A. A. A.; Davis, M. M.; Pulendran, B.; Idoyaga, J.; Appel, E. A. Injectable Hydrogels for Sustained Codelivery of Subunit Vaccines Enhance Humoral Immunity. *ACS Cent. Sci.* **2020**, *6* (10), 1800–1812. DOI: 10.1021/acscentsci.0c00732

96. Sun, X.; Zhang, Y.; Li, J.; Park, K. S.; Han, K.; Zhou, X.; Xu, Y.; Nam, J.; Xu, J.; Shi, X.; Wei, L.; Lei, Y. L.; Moon, J. J. Amplifying STING Activation by Cyclic Dinucleotide–Manganese Particles for Local and Systemic Cancer Metalloimmunotherapy. *Nat. Nanotechnol.* **2021**, *16*, 1260–1270. DOI: 10.1038/s41565-021-00962-9

97. Mosquera, J.; García, I.; Liz-Marzán, L. M. Cellular Uptake of Nanoparticles versus Small Molecules: A Matter of Size. *Acc. Chem. Res.* **2018**, *51* (9), 2305–2313. DOI: 10.1021/acs.accounts.8b00292

98. Parambath, J. B. M.; Gayathri, A. K.; Odeh, R. O. A.; Kim, S.; Han, C.; Mohamed, A. A. Single-Stranded DNA Recognition over Fluorescent Gold-Aryl Nanoparticles. *Colloids Interfaces* **2022**, *6*, 42. DOI: 10.3390/colloids6030042

99. Van Den Eeckhout, B.; Tavernier, J.; Gerlo, S. Interleukin-1 as Innate Mediator of T Cell Immunity. *Front. Immunol.* **2021**, *11*, 621931. DOI: 10.3389/fimmu.2020.621931

100. Bourquin, C.; Pommier, A.; Hotz, C. Harnessing the Immune System to Fight Cancer with Toll-Like Receptor and Rig-I-Like Receptor Agonists. *Pharm. Res.* **2020**, *154*, 104192. DOI: 10.1016/j.phrs.2019.03.001

101. Banchereau, J.; Briere, F.; Caux, C.; Davoust, J.; Lebecque, S.; Liu, Y. J.; Pulendran, B.; Palucka, K. Immunobiology of Dendritic Cells. *Annu. Rev. Immunol.* **2000**, *18*, 767. DOI: 10.1146/annurev.immunol.18.1.767

102. Mbongue, J.; Nieves, H.; Torrez, T.; Langridge, W. The Role of Dendritic Cell

Maturation in the Induction of Insulin-Dependent Diabetes Mellitus. *Front. Immunol.* **2017**, *8*, 327. DOI: 10.3389/fimmu.2017.00327

103. Tanaka, T.; Narazaki, M.; Kishimoto, T. IL-6 in Inflammation, Immunity, and Disease. *Cold Spring Harb Perspect Biol.* **2014**, *6* (10), a016295. DOI: 10.1101/cshperspect.a016295

104. Liu, Q.; Yao, Y.; Zhang, S.; Sheng, Z. Astragalus Polysaccharides Regulate T Cell-Mediated Immunity via CD11c(High)CD45RB(Low) DCs in Vitro. *J. Ethnopharmacol.* **2011**, *136* (3), 457–464. DOI: 10.1016/j.jep.2010.06.041

105. Du, X.; Zhao, B.; Li, J.; Cao, X.; Diao, M.; Feng, H.; Chen, X.; Chen, Z.; Zeng, X. Regulation on Maturation and Function of Dendritic Cells by Astragalus Mongholicus Polysaccharides. *Int. Immunopharmacol.* **2006**, *6* (7), 1161–6. DOI: 10.1007/s12672-023-00798-w

106. Wang, D.; Cui, Q.; Yang, Y.; Liu, A.; Zhang, G.; Yu, J. Application of Dendritic Cells in Tumor Immunotherapy and Progress in the Mechanism of Anti-Tumor Efect of Astragalus Polysaccharide (APS) Modulating Dendritic Cells: A Review. *Biomed. Pharmacother.* **2022**, *155*, 113541. DOI: 10.1016/j.biopha.2022.113541

107. Xu, Q.; Cheng, W.; Wei, J.; Ou, Y.; Xiao, X.; Jia, Y. Synergist for Antitumor Therapy: Astragalus Polysaccharides Acting on Immune Microenvironment. *Discov. Oncol.* **2023**, *14*, 179. DOI: 10.1007/s12672-023-00798-w

108. Hwang, J.; Zhang, W.; Dhananjay, Y.; An, E.-K.; Kwak, M.; You, S.; Lee, P. C.-W.; Jin, J.-O. Astragalus Membranaceus Polysaccharides Potentiate the Growth-Inhibitory Activity of Immune Checkpoint Inhibitors against Pulmonary Metastatic Melanoma in Mice. *Int. J. Biol. Macromol.* **2021**, *182*, 1292–1300. DOI: 10.1016/j.ijbiomac.2021.05.073

109. Wilson, N. S.; Yang, B.; Morelli, A. B.; Koernig, S.; Yang, A.; Loeser, S.; Airey, D.; Provan, L.; Hass, P.; Braley, H.; Couto, S.; Drane, D.; Boyle, J.; Belz, G. T.; Ashkenazi, A.; Maraskovsky, E. ISCOMATRIX Vaccines Mediate CD8+ T-Cell Cross-Priming by a MyD88-Dependent Signaling Pathway. *Immunol. Cell Biol.* **2012**, *90*, 540–552. DOI: 10.1038/icb.2011.71

110. Bullock, T. N. J. CD40 Stimulation as a Molecular Adjuvant for Cancer Vaccines and Other Immunotherapies. *Cell. Mol. Immunol.* **2022**, *19*, 14–22. DOI: 10.1038/s41423-021-00734-4

111. Sag, D.; Cekic, C.; Wu, R.; Linden, J.; Hedrick, C. C. The Cholesterol Transporter ABCG1 Links Cholesterol Homeostasis and Tumour Immunity. *Nat. Commun.* **2015**, *6*, 6354. DOI: 10.1038/ncomms7354

112. Nair, S.; Dhodapkar, M. V. Natural Killer T Cells in Cancer Immunotherapy. *Front. Immunol.* **2017**, *8*, 1178. DOI: 10.3389/fimmu.2017.01178

113. Menees, K. B.; Earls, R. H.; Chung, J.; Jernigan, J.; Filipov, N. M.; Carpenter, J. M.; Lee, J.-K. Sex- and Age-dependent Alterations of Splenic Immune Cell Profile and NK Cell Phenotypes and Function in C57BL/6J Mice. *Immun. Aging* **2021**, *18*, 3. DOI: 10.1186/s12979-021-00214-3

114. Nishikawa, H.; Sakaguchi, S. Regulatory T Cells in Tumor Immunity. *Int J Cancer* **2010**, *127*, 759–767. DOI: 10.1002/ijc.25429

115. Wilson, N. S.; Yang, B.; Morelli, A. B.; Koernig, S.; Yang, A.; Loeser, S.; Airey, D.; Provan, L.; Hass, P.; Braley, H.; Couto, S.; Drane, D.; Boyle, J.; Belz, G. T.; Ashkenazi, A.; Maraskovsky, E. ISCOMATRIX Vaccines Mediate CD8 T-Cell Cross-Priming by a MyD88-Dependent Signaling Pathway. *Immunol. Cell Biol.* **2012**, *90* (5), 540–552. DOI: 10.1038/icb.2011.71

116. Liu, Q.; Yao, Y.; Yu, Y.; Dong, N.; Sheng, Z. Astragalus Polysaccharides Attenuate Postburn Sepsis via Inhibiting Negative Immunoregulation of CD4+ CD25(High) T Cells. *PLoS One* **2011**, *6* (6), e19811. DOI: 10.1371/journal. pone.0019811

117. Xu, Q.; Cheng, W.; Wei, J.; Ou, Y.; Xiao, X.; Jia, Y. Synergist for Antitumor Therapy: Astragalus Polysaccharides Acting on Immune Microenvironment. *Discov. Oncol.* **2023**, *14*, 179. DOI: 10.1007/s12672-023-00798-w

118. Didierlaurent, A. M.; Collignon, C.; Bourguignon, P.; Wouters, S.; Fierens, K.; Fochesato, M.; Dendouga, N.; Langlet, C.; Malissen, B.; Lambrecht, B. N.; Garçon, N.; Van Mechelen, M.; Morel, S. Enhancement of Adaptive Immunity by the Human Vaccine Adjuvant AS01 Depends on Activated Dendritic Cells. *J. Immunol.* **2014**, *193* (4), 1920–1930. DOI: 10.4049/jimmunol.1400948

119. Millington, K.; Innes, J.; Hackforth, S.; Hinks, T.; Deeks, J.; Dosanjh, D.; Guyot-Revol, V.; Gunatheesan, R.; Klenerman, P.; Lalvani, A. Dynamic Relationship between IFN-γ and IL-2 Profile of Mycobacterium Tuberculosis-Specific T Cells and Antigen Load. *J. Immunol.* **2007**, *178* (8), 5217–5226. DOI: 10.4049/ jimmunol.178.8.5217

120. Coccia, M.; Collignon, C.; Hervé, C.; Chalon, A.; Welsby, I.; Detienne, S.; Helden, M. J. Van; Dutta, S.; Genito, C. J.; Waters, N. C.; Deun, K. Van; Smilde, A. K.; Berg, R. A. Van Den; Franco, D.; Bourguignon, P.; Morel, S.; Garçon, N.; Lambrecht, B. N.; Goriely, S.; Most, R.; Didierlaurent, A. M. Cellular and Molecular Synergy in AS01-Adjuvanted Vaccines Results in an Early IFN γ Response Promoting Vaccine Immunogenicity. *npj Vaccines* **2017**, *2*, 25. DOI: 10.1038/s41541-017-0027-3.

121. Zhou, X.; Liu, Z.; Long, T.; Zhou, L.; Bao, Y. Immunomodulatory Effects of Herbal Formula of Astragalus Polysaccharide (APS) and Polysaccharopeptide (PSP) in Mice with Lung Cancer. *Int. J. Biol. Macromol.* **2018**, *106*, 596–601. DOI: 10.1016/j.ijbiomac.2017.08.054

122. Rähni, A.; Jaago, M.; Sadam, H.; Pupina, N.; Pihlak, A.; Tuvikene, J.; Annuk, M.; Mägi, A.; Timmusk, T.; Ghaemmaghami, A. M.; Palm, K. Melanoma-Specific Antigen-Associated Antitumor Antibody Reactivity as an Immune-Related Biomarker for Targeted Immunotherapies. *Commun. Med.* **2022**, *2*, 48. DOI: 10.1038/s43856-022-00114-7

123. Jin, S.; Sun, Y.; Liang, X.; Gu, X.; Ning, J.; Xu, Y.; Chen, S.; Pan, L. Emerging New Therapeutic Antibody Derivatives for Cancer Treatment. *Signal Transduct. Target. Ther.* **2022**, *7*, 39. DOI: 10.1038/s41392-021-00868-x

124. Firacative, C.; Gressler, A. E.; Schubert, K.; Schulze, B.; Müller, U.; Brombacher, F.; Bergen, M. von; Alber, G. Identification of T Helper (Th)1- and Th2-Associated Antigens of Cryptococcus Neoformans in a Murine Model of Pulmonary Infection. *Sci. Reports* **2018**, *8*, 2681. DOI: 10.1038/s41598-018-21039-z

125. Ragupathi, G.; Gardner, J. R.; Livingston, P. O.; Gin, D. Y. Natural and Synthetic Saponin Adjuvant QS-21 for Vaccines against Cancer. *Expert Rev. Vaccines. Vaccines* **2011**, *10*, 463–470. DOI: 10.1586/erv.11.18

126. Ponomarev, A.; Shubina, I.; Sokolova, Z.; Baryshnikova, M.; Kosorukov, V. Transplantable Murine Tumors in the Studies of Peptide Antitumor Vaccines. *Oncol. Rev.* **2024**, *17*, 12189. DOI: 10.3389/or.2023.12189

127. Luo, X.; Song, Z.; Zeng, X.; Ye, Y.; Zheng, H.; Cai, D.; Yuan, Q.; Li, H.; Tong, Y.; Lu, D.; Liu, Y.; Zeng, H.; Yang, Y.; Sun, H.; Zou, Q. Promising Self Nanoemulsifying Adjuvant with Plant Derived Saponin D Boosts Immune Response and Exerts an Anti-Tumor Effect. *Front. Immunol.* **2023**, *14*, 1154836. DOI: 10.3389/fimmu.2023.1154836

128. Llopiz, D.; Ruiz, M.; Silva, L.; Sarobe, P. Enhancement of Antitumor Vaccination by Targeting Dendritic Cell-Related IL-10. *Front. Immunol.* **2018**, *9*, 1923. DOI: 10.3389/fimmu.2018.01923

129. Liu, M.; Guo, S.; Stiles, J. K. The Emerging Role of CXCL10 in Cancer (Review). *Oncol. Lett.* **2011**, *2*, 583–589. DOI: 10.3892/ol.2011.300

130. Raaijmakers, T. K.; van den Bijgaart, R. J. E.; den Brok, M. H.; Wassink, M.; de Graaf, A.; Wagenaars, J. A.; Nierkens, S.; Ansems, M.; Scheffer, G. J.; Adema, G. J. Tumor Ablation plus Co-Administration of CpG and Saponin Adjuvants Affects IL-1 Production and Multifunctional T Cell Numbers in Tumor Draining Lymph Nodes. *J. Immunother. Cancer* **2020**, *8*, e000649. DOI: 10.1136/jitc-2020-000649

131. Klebanoff, C.; Gattinoni, L.; Restifo, N. CD8+ T-Cell Memory in Tumor Immunology and Immunotherapy. *Immunol. Rev.* **2006**, *211*, 214–224. DOI: 10.1111/j.0105-2896.2006.00391.x

132. Wang, L.; Geng, H.; Liu, Y.; Liu, L.; Chen, Y.; Wu, F.; Liu, Z.; Ling, S.; Wang, Y.; Zhou, L. Hot and Cold Tumors: Immunological Features and the Therapeutic Strategies. *Med Comm* **2023**, *4* (5), e343. DOI: 10.1002/mco2.343

133. Silva, A.; Mount, A.; Krstevska, K.; Pejoski, D.; Hardy, M. P.; Owczarek, C.; Scotney, P.; Maraskovsky, E.; Morelli, A. B. The Combination of ISCOMATRIX Adjuvant and TLR Agonists Induces Regression of Established Solid Tumors In Vivo. *J. Imunol.* **2015**, *194* (5), 2199–2207. DOI: 10.4049/jimmunol.1402228

134. Tay, R. E.; Richardson, E. K.; Toh, H. C. Revisiting the Role of CD4+ T Cells in Cancer Immunotherapy-New Insights into Old Paradigms. *Cancer Gene Ther.* **2021**, *28*, 5–17. DOI: 10.1038/s41417-020-0183-x

135. Zheng, H.; Liu, X.; Zhang, J.; Rice, S.; Wagman, M.; Kong, Y.; Zhu, L.; Zhu, J.; Joshi, M.; Belani, C. Expression of PD-1 on CD4+ T Cells in Peripheral Blood Associates with Poor Clinical Outcome in Non-Small Cell Lung Cancer. *Oncotarget* **2016**, *7* (35), 56233–56240. DOI: 10.18632/oncotarget.9316

136. Ahmadzadeh, M.; Johnson, L. A.; Heemskerk, B.; Wunderlich, J. R.; Dudley, M. E.; White, D. E.; Rosenberg, S. A. Tumor Antigen–Specific CD8 T Cells Infiltrating the Tumor Express High Levels of PD-1 and Are Functionally Impaired. *Blood* **2009**, *114* (8), 1537–1544. DOI: 10.1182/blood-2008-12-195792

137. Del Prete, A.; Salvi, V.; Soriani, A. et al. Dendritic Cell Subsets in Cancer Immunity and Tumor Antigen Sensing. *Cell. Mol. Immunol.* **2023**, *20*, 432–447. DOI: 10.1038/s41423-023-00990-6

138. Den Brok, M. H.; Nierkens, S.; Wagenaars, J. A.; Ruers, T. J.; Schrier, C. C.; Rijke, E. O.; Adema, G. J. Saponin-Based Adjuvants Create a Highly Effective Anti-Tumor Vaccine When Combined with in Situ Tumor Destruction. *Vaccine* **2012**, *30* (4), 737–744. DOI: 10.1016/j.vaccine.2011.11.080

139. He, Z.; Jia, H.; Zheng, M.; Wang, H.; Yang, W.; Gao, L.; Zhang, Z.; Xue, J.; Xu, B.; Yang, W.; Xing, G.; Gao, X.; Gao, F. Trp2 Peptide-Assembled Nanoparticles with Intrinsically Self-Chelating 64Cu Properties for PET Imaging Tracking and Dendritic Cell-Based Immunotherapy against Melanoma. *ACS Appl. Bio Mater.* **2021**, *4* (7), 5707–5716. DOI: 10.1021/acsabm.1c00480

140. Singh, V.; Ji, Q.; Feigenbaum, L.; Leighty, R.; Hurwitz, A. Melanoma Progression despite Infiltration by in Vivo-Primed TRP-2-Specific T Cells. *J. Immunother.* **2009**, *32* (2), 129–139. DOI: 10.1097/CJI.0b013e31819144d7

141. Vasievich, E. A.; Ramishetti, S.; Zhang, Y.; Huang, L. Trp2 Peptide Vaccine Adjuvanted with (R)-DOTAP Inhibits Tumor Growth in an Advanced Melanoma Model. *Mol. Pharm.* **2012**, *9* (2), 261–268. DOI: 10.1021/mp200350n

142. Patel, P.; Ottensmeier, C.; Mulatero, C.; Lorigan, P.; Plummer, R.; Pandha, H.; Elsheikh, S.; Hadjimichael, E.; Villasanti, N.; Adams, S.; Cunnell, M.; Metheringham, R.; Brentville, V.; Machado, L.; Daniels, I.; Gijon, M.; Hannaman, D.; Durrant, L. Targeting Gp100 and TRP-2 with a DNA Vaccine: Incorporating T Cell Epitopes with a Human IgG1 Antibody Induces Potent T Cell Responses That Are Associated with Favourable Clinical Outcome in a Phase I/II Trial. *Oncooimmunology* **2018**, *7* (6), e1433516. DOI: 10.1080/2162402X.2018.1433516

143. Xu, Z.; Chokkalingam, N.; Tello-Ruiz, E.; Walker, S.; Kulp, D.; Weiner, D. Incorporation of a Novel CD4+ Helper Epitope Identified from Aquifex Aeolicus Enhances Humoral Responses Induced by DNA and Protein Vaccinations. *iScience* **2020**, *23* (8), 101399. DOI: 10.1016/j.isci.2020.101399

144. Even, M.-P.; Bobbala, S.; Gibson, B.; Hook, S.; Winter, G.; Engert, J. Twin-Screw Extruded Lipid Implants Containing TRP2 Peptide for Tumour Therapy. *Eur. J. Pharm. Biopharm.* **2017**, *114*, 79–87. DOI: 10.1016/j.ejpb.2016.12.033

145. Highton, A. J.; Kojarunchitt, T.; Girardin, A.; Hook, S.; Kemp, R. A. Chitosan

Hydrogel Vaccine Generates Protective CD8 T Cell Memory against Mouse Melanoma. *Immunol. Cell Biol.* **2015**, *93*, 634–640. DOI: 10.1038/icb.2015.14

146. Gerard, C.; Baudson, N.; Ory, T.; Louahed, J. Tumor Mouse Model Confirms MAGE-A3 Cancer Immunotherapeutic As an Efficient Inducer of Long- Lasting Anti-Tumoral Responses. *PLoS One* **2014**, *9* (5), e94883. DOI: 10.1371/journal. pone.0094883

147. Groom, J.; Luster, A. CXCR3 in T Cell Function. *Exp. Cell Res.* **2011**, *317* (5), 620–631. DOI: 10.1016/j.yexcr.2010.12.017

148. Hwang, J.; Zhang, W.; Dhananjay, Y.; An, E.-K.; Kwak, M.; You, S.; Lee, P. C.-W.; Jin, J.-O. Astragalus Membranaceus Polysaccharides Potentiate the Growth-Inhibitory Activity of Immune Checkpoint Inhibitors against Pulmonary Metastatic Melanoma in Mice. *Int. J. Biol. Macromol.* **2021**, *182*, 1292–130. DOI: 10.1016/j.ijbiomac.2021.05.073

149. Zhao, R.; Song, Y.; Wang, Y.; Huang, Y.; Li, Z.; Cui, Y.; Yi, M.; Xia, L.; Zhuang, W.; Wu, X.; Zhou, Y. PD-1/PD-L1 Blockade Rescue Exhausted CD8+ T Cells in Gastrointestinal Stromal Tumours via the PI3K/Akt/MTOR Signalling Pathway. *Cell Prolif.* **2019**, *52* (3), e12571. DOI: 10.1111/cpr.12571

150. Zou, W.; Wolchok, J.; Chen, L. PD-L1 (B7-H1) and PD-1 Pathway Blockade for Cancer Therapy: Mechanisms, Response Biomarkers, and Combinations. *Sci. Transl. Med.* **2016**, *8*, 328rv324. DOI: 10.1126/scitranslmed.aad7118

151. Curran, M. A.; Montalvo, W.; Yagita, H.; Allison, J. P. Pd-1 and Ctla-4 Combination Blockade Expands Infiltrating T Cells and Reduces Regulatory T and Myeloid Cells within B16 Melanoma Tumors. *PNAS* **2010**, *107*, 4275−4280. DOI: 10.1073/pnas.0915174107

152. Gunalp, S.; Helvaci, D.; Oner, A.; Bursalı, A.; Conforte, A.; Güner, H.; Karakülah, G.; Szegezdi, E.; Sag, D. TRAIL Promotes the Polarization of Human Macrophages toward a Proinflammatory M1 Phenotype and Is Associated with Increased Survival in Cancer Patients with High Tumor Macrophage Content. *Front. Immunol.* **2023**, *14*, 1209249. DOI: 10.3389/fimmu.2023.1209249

153. Liu, Q.; Sun, Z.; Chen, L. Memory T Cells: Strategies for Optimizing Tumor Immunotherapy. *Protein Cell* **2020**, *11* (8), 549–564. DOI: 10.1007/s13238-020-00707-9

154. Moon, J. J.; Huang, B.; Irvine, D. J. Engineering Nano- and Microparticles to Tune Immunity. *Adv. Mater.* **2012**, *24*, 3724-46. DOI: 10.1002/adma.201200446

155. Skwarczynski, M.; Toth, I. Peptide-Based Synthetic Vaccines. *Chem. Sci.* **2016**, *7*, 842–854. DOI: 10.1039/c5sc03892h.

156. Irvine, D. J.; Swartz, M. A.; Szeto, G. L. Engineering Synthetic Vaccines Using Cues from Natural Immunity. *Nat. Mater.* **2013**, *12*, 978–990. DOI: 10.1038/ nmat3775

157. Thomas, S. N.; Vokali, E.; Lund, A. W.; Hubbell, J. A.; Swartz, M. A. Targeting the Tumor- Draining Lymph Node with Adjuvanted Nanoparticles Reshapes the Antitumor Immune Response. *Biomaterials* **2014**, *35*, 814–824. DOI: 10.1016/j.biomaterials.2013.10.003

158. Jeanbart, L. et al. Enhancing Efficacy of Anticancer Vaccines by Targeted Delivery to Tumor- Draining Lymph Nodes. *Cancer Immunol. Res.* **2014**, *2*, 436–447. DOI: 10.1158/2326-6066.CIR-14-0019-T

159. Deng, K.; Adams, M. M.; Damani, P.; Livingston, P. O.; Ragupathi, G.; Gin, D. Y. Synthesis of QS-21-Xylose: Establishment of the Immunopotentiating Activity of Synthetic QS-21 Adjuvant with a Melanoma Vaccine. *Angew. Chemie - Int. Ed.* **2008**, *47* (34), 6395–6398. DOI:10.1002/anie.200801885

160. Bachmann, M. F.; Jennings, G. T. Vaccine Delivery: A Matter of Size, Geometry, Kinetics and Molecular Patterns. *Nat. Rev. Immunol.* **2010**, *10*, 787–796. DOI: 10.1038/nri2868

161. Wilson, N. S., B.; Yang, A. B.; Morelli, S.; Koernig, A.; Yang, S. L.; Airey, D.; Provan, L.; Hass, P.; Braley, H.; Couto, S.; Drane, D.; Boyle, J.; Belz, G.T.; Ashkenazi, A.; Maraskovsky, E. ISCOMATRIX Vaccines Mediate CD8+ T-Cell Cross-Priming by a MyD88-Dependent Signaling Pathway. *Immunol. Cell Biol.* **2012**, *90*, 540–552. DOI: 10.1038/icb.2011.71

162. Tsang, Y.; Huang, C.; Yang, K. et al. Improving Immunological Tumor Microenvironment Using Electro-Hyperthermia Followed by Dendritic Cell Immunotherapy. *BMC Cancer* **2015**, *15*, 708. DOI: 10.1186/s12885-015-1690-2

163. Xiao, Z.; Wang, R.; Wang, X.; Yang, H.; Dong, J.; He, X.; Yang, Y.; Guo, J.; Cui, J.; Zhou, Z. Impaired Function of Dendritic Cells within the Tumor Microenvironment. *Front. Immunol.* **2023**, *14*, 1213629. DOI: 10.3389/fimmu.20

164. Mantovani, A.; Marchesi, F.; Malesci, A.; Laghi, L.; Allavena, P. Tumour_associated Macrophages as Treatment Targets in Oncology. *Nat. Rev. Clin. Oncol.* **2017**, *14* (7), 399–416. DOI: 10.1038/nrclinonc.2016.217

VITA

Nilgün YAKUBOĞULLARI ÖZEFE

Education:

2018-2024: PhD, İzmir Institute of Technology, Bioengineering, GPA: 3.93/4.00

2015-2018: MSc, İzmir Institute of Technology, Biotechnology, GPA: 3.64/4.00

2011-2015: BSc, Ege University, Bioengineering, GPA: 3.81/4.00

Research Experiences:

2017- continued: Research Assistant, IZTECH, Department of Bioengineering

2023-2024: Research Fellow, TUBITAK 2214-A (1059B142201226), University of Michigan, College of Pharmacy, USA

2021-2023: Scholar, TUBITAK 1001 Project (120S878)

2020-2022: Scholar, IZTECH BAP (2020IYTE0098)

2015-2016: Scholar, TUBITAK 1002 Project (215S544)

2014-2015: Principle Investigator, TUBITAK 2209-B Project (1139B411402292)

Selected Patents & Publications:

TR Patent: A Method For Obtaining Saponin Molecules And Utilizing Active Molecules as Immunomodulator. (TR 2019 10003 A2) 02/22/2021

Yakubogullari, N.; Cagir, A.; Bedir, E.; Sag, D. 2023. *Astragalus* Saponins, Astragaloside VII and Newly Synthesized Derivatives, Induce Dendritic Cell Maturation and T Cell Activation, **Vaccines**, 11,495.

Yakubogullari, N.; Coven, F.O.; Cebi, N.; Coven F.; Coven, N.; Genc, R.; Bedir, E.; Nalbantsoy, A. 2021. Evaluation of Adjuvant Activity of Astragaloside VII and its Combination with Different Immunostimulating Agents in Newcastle Disease Vaccine, **Biologicals**, 70: 28-37.

Yakuboğulları, N.; Genç, R.; Çöven, F.; Nalbantsoy, A;, Bedir, E. 2019. Development of adjuvant nanocarrier systems for seasonal influenza A (H3N2) vaccine based on Astragaloside VII and gum tragacanth (APS). **Vaccine**, 37, 3638–3645.